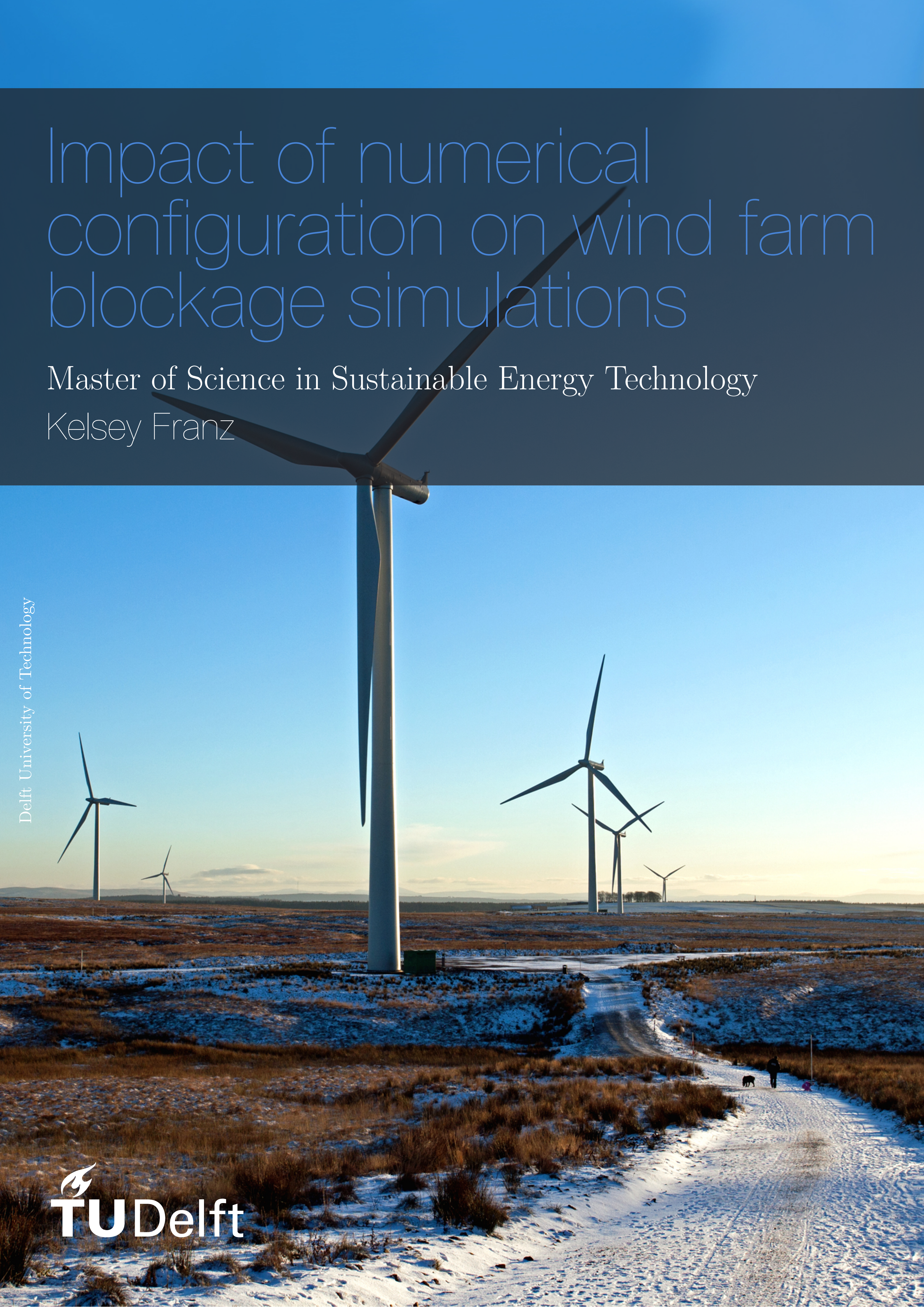

Impact of numerical configuration on wind farm blockage simulations

Master of Science in Sustainable Energy Technology

Kelsey Franz

Delft University of Technology

TUDelft

Impact of numerical configuration on wind farm blockage simulations

by

Kelsey Franz

to obtain the degree of Master of Science in Sustainable Energy Technology at Delft University of Technology, to be defended publicly on Monday, November 14th, 2022 at 13:00.

Project Duration:	November, 2021 - November, 2022
Place:	Faculty of Aerospace Engineering, Delft
Institution:	Delft University of Technology
Thesis Committee:	Dr. S.J. Watson (Chair)
	Dr. Ir. D. Allaerts (Supervisor)
	Dr. Ir. R.P. Dwight (Committee member)
	Ir. M. Khan (Phd supervisor)

Wind Energy Group, Faculty of Aerospace Engineering, Delft University of Technology
Faculty of Electrical Engineering, Mathematics and Computer Science, Delft University of Technology

Cover Image: Whitelee Wind Farm south of Glasgow, Scotland (Fallis, 2010)

Preface

This report is the culmination of research completed as part of my studies to obtain a MSc in Sustainable Energy Technology at Delft University of Technology (TUD). Working on my master's thesis through a global pandemic in a new country pushed me to develop many skills, most importantly it taught me to maintain perspective, preserver, and hold myself accountable. Learning to code, the inner workings of computational fluid dynamics (CFD), and project management were new challenges that I enjoyed facing. Although difficult at times, I am forever grateful for the educational experience I had at TUD and the time I've been able to call the Netherlands home.

I would like to express my sincere gratitude to my supervisors Dr. Dries Allaerts and Mehtab Khan for their support in helping me complete this work. Their insight and feedback were always appreciated and helped me to unravel the complexities of my project. In a sea of new information their input and advice provided stable footing and a sense of direction. Mostly, the patience and kindness extended towards me was greatly appreciated and paramount in helping me succeed in this endeavor. I would also like to thank my committee members for taking the time to review my work and provide feedback.

Additionally, I would like to thank my family and friends, both here and back in the United States, for offering constant support and encouragement throughout my life and in completing my masters programme. No matter the time, day or occasion they were always available to offer reassurance and strengthen my resolve. I would not be able to live the wonderful life I live nor have completed this thesis without their love and belief in me.

Kelsey Franz
Delft, November 2022

Abstract

Wind farm interactions with the surrounding airflow leads to a reduction in velocity greater than the linear sum of single turbine inductions and is known as global or upstream blockage. The mechanisms and magnitude of global blockage effect are not yet fully understood. Models to simulate upstream blockage to improve efficiency estimates and better understand global blockage have thus far not been refined. The aim of this research is to investigate the sensitivity of upstream blockage to the numerical configuration of CFD simulations to improve model accuracy and understanding of global blockage.

RANS simulations are executed under steady state conditions with a $k - \epsilon$ turbulence model. A neutral stability, pressure-driven atmospheric boundary layer is modelled with fully developed uni-directional flow. Wind farms are modelled as actuator discs with 5 rows of turbines on flat terrain. Streamwise and spanwise spacing is set to 7 turbine diameters (D) and 5D respectively. Global blockage is measured against the induction of a single turbine at 2.5D upstream. Variables investigated include the domain height, lateral extent, inlet and outlet distances from the wind farm.

Domain heights ranging from 5D to 25D are investigated for change in magnitude and scale of upstream blockage for a laterally infinite wind farm. A clear trend of increasing blockage with domain height is observed. At domain heights of less than 15D, upstream velocity is increased by a maximum of 0.18%(5D). Larger domain heights produce a maximum velocity reduction of 0.23%(25D). The shape of upstream blockage is independent of domain height.

A finite wind farm of 5 columns and lateral extents ranging from 2.5D to 20D on each side are utilized to investigate the impact on blockage. Wider domains of 5D to 20D display increasing blockage with width, while a domain of 2.5D exhibits behaviour similar to a laterally infinite wind farm. Blockage ranging from 0.13% (10D) to 0.31% (20D) reduction in velocity is shown to be highest at the center column of turbines and decreases toward the outer columns.

Inlet and outlet distances ranging from 15D to 100D are modelled. Upstream blockage for inlet distances of 50D to 100D produce consistent upstream blockage magnitude and extent of 0.22% and 30D respectively. Shorter inlet distances result in decreased upstream blockage with a minimum of 0.12% (15D). The shape of blockage remains consistent through all inlet ranges. Outlet distance have no identifiable impact on upstream blockage magnitude and extent.

Changes to the numerical configuration show a clear correlation of increased blockage with cross sectional area of the domain. Constraining the domain in the vertical and lateral directions constricts flow resulting in reduced blockage. Blockage becomes independent of inlet distances at values of 50D and higher. Outlet distance has no identifiable impact on upstream blockage. Choosing a numerical configuration with adequately sized domain boundaries is pertinent in producing realistic upstream blockage.

Contents

Nomenclature

Abbreviations

Abbreviation	Definition
ABL	Atmospheric Boundary Layer
AEP	Annual Energy Production
AD	Actuator Disc
ADM	Actuator Disc Method
ALM	Actuator Line Method
BC	Boundary Condition
BEM	Blade Element Momentum
CFD	Computational Fluid Dynamics
D	Turbine Diameter
DNS	Direct Numerical Simulation
EVM	Eddy Viscosity Model
IRENA	International Renewable Energy Agency
LES	Large Eddy Simulations
NREL	National Renewable Energy Laboratory
NS	Navier-Stokes
RANS	Reynolds-Averaged Navier-Stokes
RAS	Reynolds-Averaged Simulation
RES	Residual limit
RSM	Reynolds Stress Model
RST	Reynolds Stress Tensor
SIMPLE	Semi-Implicit Method for Pressure-Linked Equations
SST	Shear Stress Transport
TKE	Turbulent Kinetic Energy

Symbols

Symbol	Definition
A	Area
a	Axial induction factor
c	Chord length
CS	Cross sectional area

Symbol	Definition
C_d	Drag coefficient
C_l	Lift coefficient
C_P	Power coefficient
C_T	Thrust coefficient
C_T'	Disc-based thrust coefficient
D	Turbine diameter
D_f	Drag
D_{ij}^P	Pressure dependent diffusion
D_{ij}^v	Viscous diffusion
f	Body forces
F_T	Thrust force
k	turbulent kinetic energy
K_{ij}	Advection
L_f	Lift
$\boldsymbol{n}$	Surface normal vector
P	Power
p	pressure
P_{ij}	Production
P_{loss}	Power loss
R_A	Area Rasio
Re	Reynolds number
SA	Surface area
S_{ij}	Strain rate tensor
T	Temperature
T_{ij}	Turbulent diffusion
t	Time
U	Velocity
U_x	Spanwise velocity
U_y	Streamwise velocity
U_z	Vertical velocity
u_i, u_j, u_k	Velocity components in three dimensions
u_m	Spatial-averaged velocity
u_n	Normal velocity
u_{rel}	Relative velocity
u_t	Tangential velocity
$\overline{u}$	Time averaged variable
u'	Fluctuation of variable in time
u_*	Friction velocity
v	Kinematic viscosity
v_T	Eddy viscosity
w	Actuator line width

Symbol	Definition
x_i, x_j, x_k	Spatial components in three dimensions
z	Height
z_o	Surface roughness length
α	Angle of attack
β	Twist angle
ϵ	Turbulent kinetic energy dissipation rate
Δy	Spanwise spacing
Δx	Streamwise spacing
δ_{ij}	Kronecker delta
κ	von Kármán constant
ω	Specific turbulent dissipation rate
Ω	Potential temperature
ϕ_{ij}	Pressure strain correlation
ρ	Density
τ	Shear stress
τ_{ij}	Reynolds stress tensor

List of Figures

List of Tables

1

Introduction

Energy production through means of renewable resources has become increasingly vital over the past several decades as a means to reduce reliance on fossil fuels and fight climate change. Wind turbines are a time withstanding technology that has become an increasingly popular tool to help meet energy needs through a renewable resource. To produce electrical energy, wind turbines extract kinetic energy from the wind and subsequently convert it into electrical energy through electromagnetic induction.

Over time, installations of wind farms have become more commonplace and thus, planning and design of such installations have become more sophisticated. One of the most important factors in the design process is to determine the potential for energy production given a set of environmental conditions. Over the past several years, to ensure maximum efficiency of wind energy installations, research into the impact of a wind farm on the upstream flow behaviour has been conducted.

This paper aims to build upon this research to provide further insight into the complex and interconnected mechanisms which dictate the flow of kinetic energy through a wind farm. High fidelity computational fluid dynamics (CFD) software will be utilized to investigate how various numerical configurations affect the resultant upstream wind flow.

A brief summary of the history, general trends, and motivations behind the development of wind energy is discussed first in this chapter to provide context to the research topic. This is followed by an overview of the basic theoretical background required to analyse the subject matter. A review of atmospheric conditions, especially as they pertain to wind energy and upstream blockage is completed along with a discussion on the applicable wind farm flow solving methods. Finally, the chapter concludes with an overview of the research questions and sub-questions as well as a synopsis of the layout for the remainder of the paper.

1.1. History and motivations of wind energy development

Technological advancements through the years have resulted in improved turbine energy production and diversification of feasible installation environment characteristics. Over the past 40 years the driving focus of wind turbine engineering has been to create a sustainable, scalable, and economically feasible source of renewable energy generation to replace traditional fossil fuel technologies. Wind turbines are considered *green energy* as the energy input is supplied through renewable wind resources. Over the last few decades, individual wind turbines as well as full scale wind farm installations have become larger and more commonplace. This section will cover the history and observed trends of wind turbine design development along with the motivations for current and future developments.

1.1.1. A brief history of wind turbine development

Harnessing the kinetic energy present in wind through turbine technology has been documented for centuries. The first distinguishable wind driven turbine was designed by Greek engineer Heron of Alexandria in 1 AD (Shahan, 2014). Through the subsequent centuries primitive wind turbines were designed to convert wind energy into mechanical power to run rudimentary machines for simple tasks, such as pumping water and grinding grains (Shahan, 2014). The first wind turbine to successfully convert kinetic wind energy into electricity was built in Denmark in 1891, with a diameter of 22.8 meters (IRENA, 2019).

Through the turn of the century, improvements to wind turbines centered around understanding the aerodynamic loading for optimal rotor design (Shahan, 2014), some common wind turbines can be seen in figure 1.1. Up and into the mid 20th century, wind turbine installations continued to expand, especially in rural areas with limited access to electricity. The first vertical axis wind turbine was designed in 1931 by a French engineer but the design, and subsequent variations have remained relatively scarce (Shahan, 2014).

Over the next several decades, design improvements focused on increasing energy output through increasing the wind swept area, i.e. the area covered by the rotor. Standard production capabilities grew from approximately 100 kW of power in 1931 to 2 MW in 1978 (Shahan, 2014). Throughout this time, wind turbine designs were prone to early failure, making them economically infeasible (Zaaijer and Viré, 2020). Engineers in Denmark looked to increase reliability of wind turbines which resulted in three bladed stall controlled turbines that could be more easily produced, commonly referred to as the *the Danish Concept* (Zaaijer and Viré, 2020).

Figure 1.1 shows a schematic of several wind turbine designs, the Danish Concept constitutes a 3-bladed horizontal axis fast rotation turbine. Most design deviations from the Danish Concept were unfruitful, solidifying the 3-bladed design as superior (Zaaijer and Viré, 2020). This holds true for present day, as the most widely used design is the 3-bladed, pitch control turbine which allows for optimum energy conversion and controllability.

A massive increase in interest and investment in wind turbine development occurred through the late 20th century as a result of the oil crisis increasing interest in non fossil fuel technologies

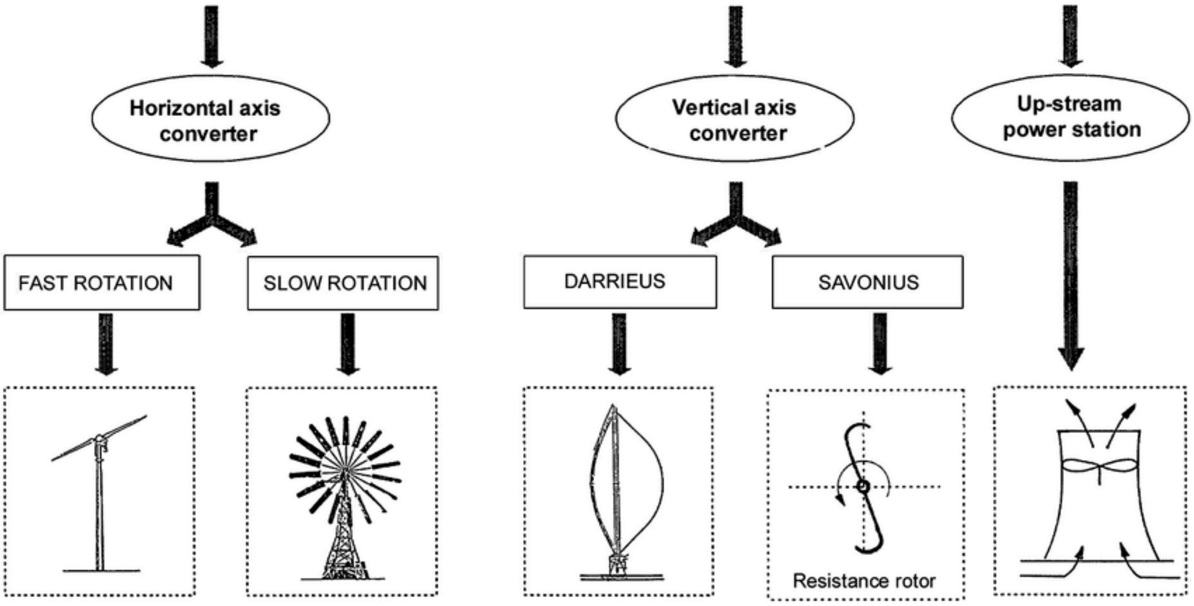

Figure 1.1: Various categories of wind turbine designs (Wagner, 2013).

(Zaaijer and Viré, 2020). With a semi-unified and standard turbine design, concentrated developmental resources have facilitated the production of larger and more powerful wind turbines. As of 2022, the largest operating turbine, with a diameter of 220 meters and capacity of 14 MW, the Haliade-X is currently installed in the port of Rotterdam in The Netherlands (Venditti, 2022).

Further design improvements and upscaling have been and continue to be incentivized by legislative acts in the United States and Europe (Shahan, 2014). Over the past several decades (2000-2020s), wind energy capacity has increased by a factor of approximately 75 fold (IRENA, 2019), party due to a boom in installations full scale wind farms (Shahan, 2014). Figure 1.2 demonstrates the steep increase in installed wind power capacity experienced over the past decade. Global wind power capacity shows growth from approximately 220 GW in 2011 to 1,600 GW in 2021, an increase of almost 630% (IRENA, 2019). Growth is expected to continue as demand for renewable energy increases. Presently, the largest planned wind farm installation is the Gansu Wind Farm consisting of 7,000 turbines with a combined capacity of 20 GW in the Gansu province of China (Besta, 2019).These large installations allow for maximum power output when the available resources are conducive to the design of the turbines.

As can be seen from figure 1.2, onshore wind capacity makes up the vast majority of installed wind generation capacity. However, the market share of installed offshore wind capacity has steadily increased from 5% in 2011 to 6.25% in 2021, with an expected market share of 16% by 2050 (IRENA, 2019). In total, according to the International Renewable Energy Agency (IRENA), to meet climate goals, installed wind capacity must increase to approximately 6,000 GW by 2050 (IRENA, 2019).

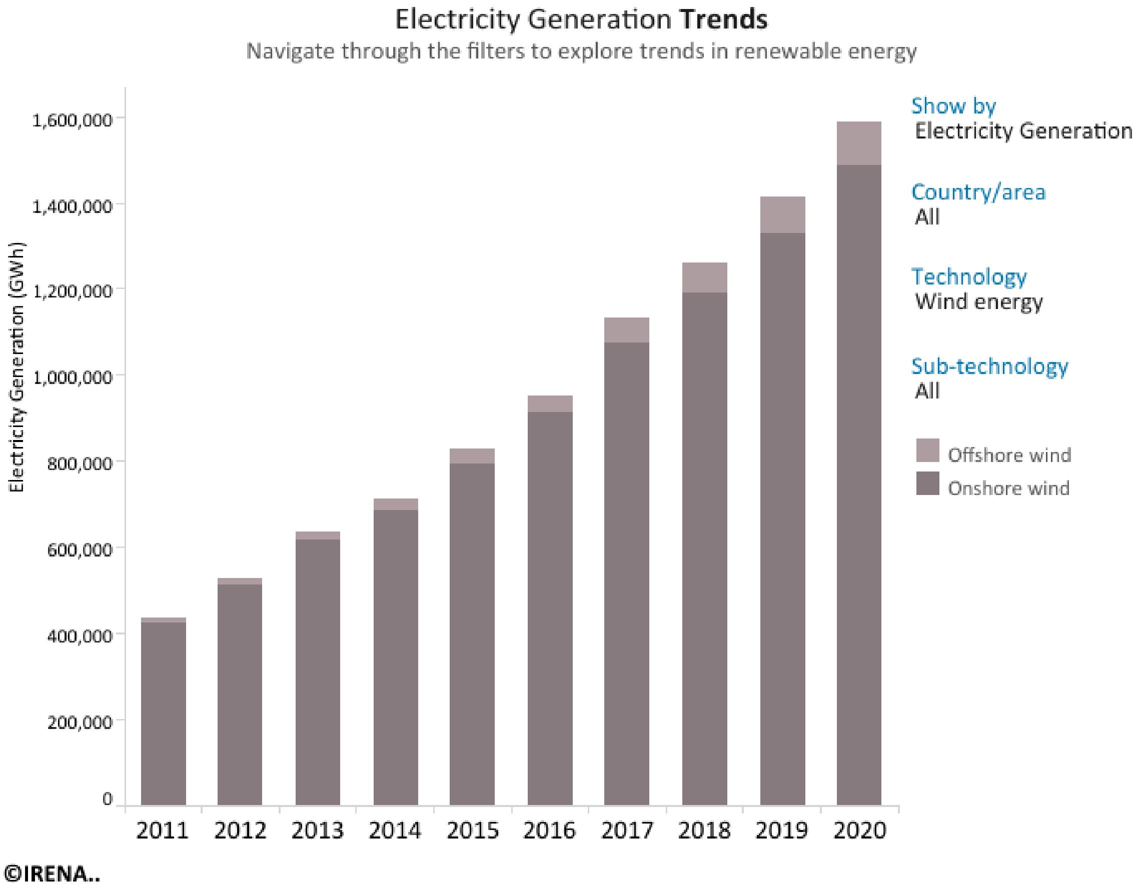

Figure 1.2: Global cumulative installed wind power capacity from 2011 to 2021 for both onshore and offshore wind turbines (IRENA, 2019).

1.1.2. Industry motivation for improved feasibility models

As wind turbines and farms grow in size and power output, the consequences of their installation on the surrounding area becomes increasingly severe. Several methods exist to assist in predicting the optimal layout, sizing, and location of wind farms. These methods can include the collection of empirical data on the frequency of wind speeds and directions, calculating theoretical sizing and layouts, and using CFD software to simulate the flow field of prospective wind farms. These methods are able to visualize and analyse the wind velocity flow field to better assess how a certain wind farm configuration will perform under the specified environmental considerations.

Expected changes in the flow field include the well documented wakes which will impact flow downstream, as well as an induction zone immediately upstream of each individual turbine. Recently, a physical phenomena of upstream flow blockage also known as global blockage has been observed both empirically and in CFD simulations. It should be noted that throughout this paper, global blockage, wind farm blockage, and upstream blockage will be used interchangeably. This upstream flow blockage causes the inflow wind speeds to decrease more than what is expected from the induction factor alone (Centurelli et al., 2021); resulting in less energy generation output from the entire wind farm. Incorrect estimation of global blockage can result in incorrect design of wind farms, such as too small inter-turbine spacing to incorrect sizing as found in Bleeg et al., 2018 and Nygaard et al., 2020. Additionally, the global blockage phenomena is generally unaccounted for in estimates of wind farm potential annual energy production (AEP), an important design component. Upstream blockage due to wind farms has been observed to cause about 6.5% reduction in AEP in some CFD simulations (Allaerts et al., 2018).

For wind energy installation to continue, it must be economically feasible for companies and governments to proceed with investments. An expected annual investment of 311 billion USD is required by 2050 to meet estimates for both onshore and offshore wind development (IRENA, 2019). Such a large investment increases the need for reliable energy estimates to ensure viable payoff. AEP is an important economic factor in the design of wind farms. Often, this estimate is done by taking into account the velocity field of the location, the chosen turbines operating scheme, the induction factor and downstream turbulence production. Net AEP calculations cover the wake, availability, performance, electrical, environmental, and curtailment losses through various estimation tools and hind cast data (Barber, 2017). However, the influence of turbines on the upstream velocity field appears to have a larger than expected impact on the AEP due to global blockage. This study visualizes and analyses the upstream global blockage of simulated wind farms to better understand and quantify the importance of choosing adequate modelling parameters. Additionally, the importance of including upstream flow blockage in power loss calculations for a wind farm is explored.

1.2. Required theoretical background

In order to understand the inner workings of this research paper and research questions some basic theoretical topics need to be discussed. The relevant theoretical knowledge to assess the problem is divided into two categories: large scale flow physics and computational simulations. Large scale flow physics pertains to general fluid flow behaviour and relevant environmental considerations. A general outline of available tools and methods used for wind farm simulations and estimates are covered to set the stage for CFD simulations carried out in this paper. The following sub-sections will outline the basics of each as they pertain to the research.

1.2.1. Flow behaviour through a wind farm

Flow physics through and around wind farms is complex and largely dependent on farm characteristics such as layout, size, and number of turbines. The principle flow physics around a single turbine in isolation will be discussed first to provide insight into the larger mechanisms involved through a wind farm.

A wind turbine is often approximated as an actuator disc (AD) through an inviscid extension of the blade element momentum theory (BEM), with an even distribution of forces across the disc (Mikkelsen, 2004). A more detailed analysis of the implementation of AD theory is covered in detail in chapter 2. The impact of the turbine tower is often considered negligible as it is much smaller and has a shorter life span in comparison to the rotor mechanisms. A simplified cross sectional diagram of the flow around a wind turbine is shown in figure 1.3.

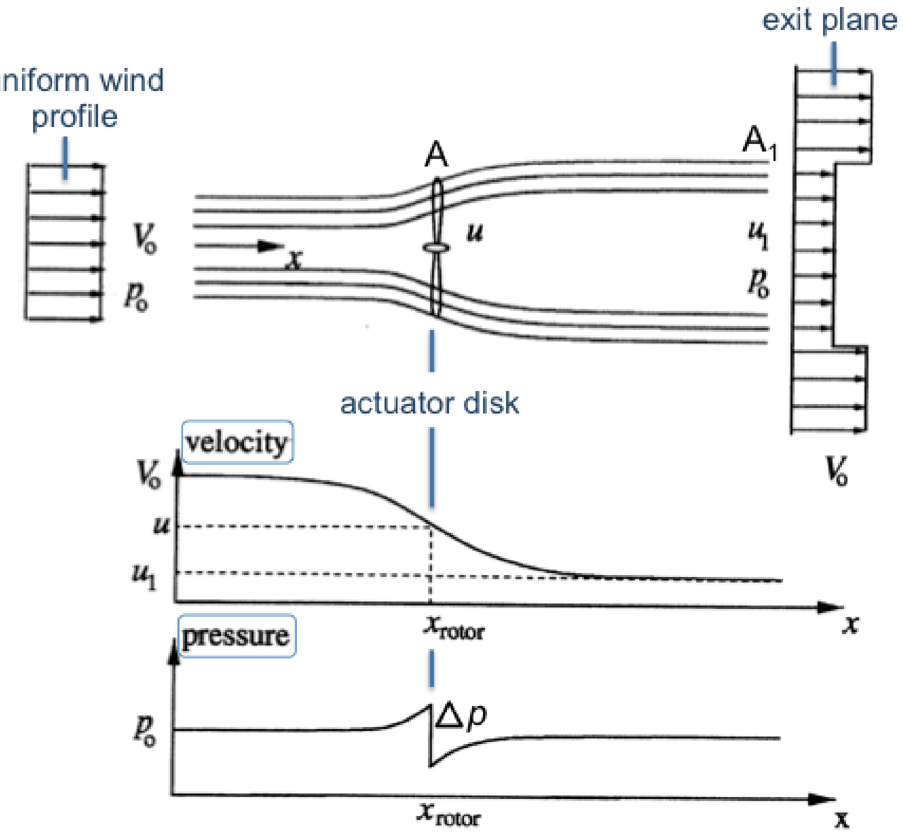

Figure 1.3: Streamlines around single turbine approximated as AD and streamwise velocity and pressure through the domain (Hansen, 2000).

Under the presence of a wind turbine, incoming wind profiles is impeded by the thrust exhibited on the air flow by the rotor. The thrust exerted on the AD results in an induction zone immediately prior to the rotor, characterized by a decreased velocity and increased pressure. As kinetic energy is extracted from the wind at the turbine, immediately after the rotor, there is a pressure drop and continual decrease in velocity.

The theoretical power available (P) through this interaction can be estimated using equation 1.1. Where U is the resultant velocity at the disc, A is the surface area of the disc normal to the flow, and ρ is the density of air.

$$P = \frac{1}{2}\rho A U^3 \tag{1.1}$$

Further downstream, the chaotic and turbulent wake of a turbine travels and meanders, interacting with the surrounding flow. The turbulent energy is dissipated through an energy cascade and the flow field will eventually return to pre-turbine conditions if there are no other external factors influencing the flow. This wake effect of a single turbine is expected to last between 10D to 20D downstream (Allaerts, 2016).

The flow through and around a wind farm is more complex than a single turbine as there are interactions among the wakes of the turbines. Simulated flow through a wind farm are visualized in figure 1.4. As with the single turbine, there is an induction zone created immediately upstream of each rotor. Global upstream blockage is observed in the figure as between 0-5% loss in upstream velocity and extends much further than the induction zone.

Wake effects in a wind farm grow and expand with subsequent turbine rows. As shown in figure 1.4, the wakes of successive turbines interact and merge to form larger, stronger wakes. Wind farm wakes are characterized by higher turbulence, larger flow areas, and decreased velocity. They are theorized to be highly coupled with global blockage and could possibly account for the redistribution of energy across the wind farm.

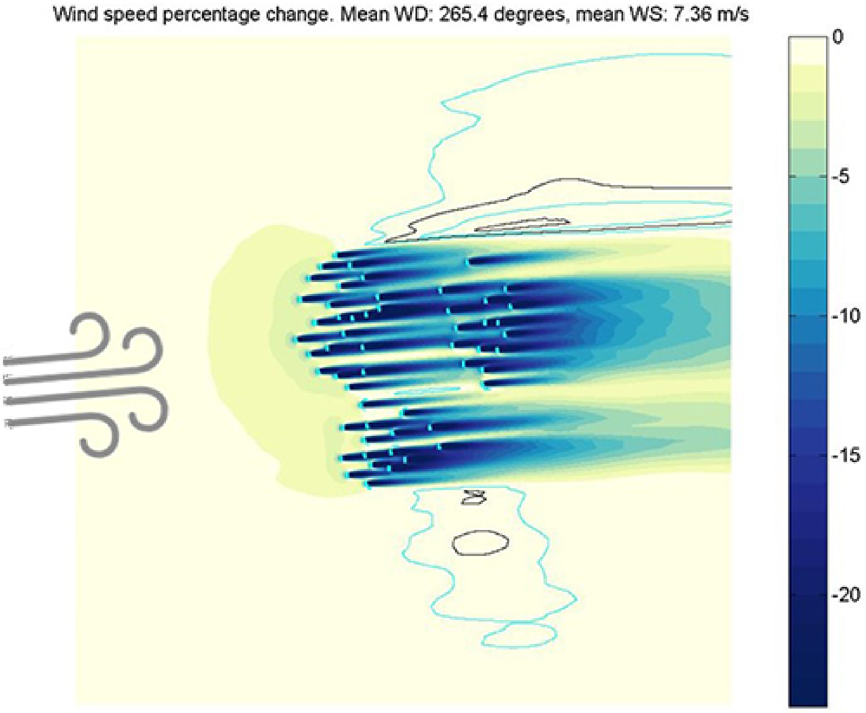

Figure 1.4: Upstream global flow blockage (yellow shading) and velocity changes (blue) (Montavon, 2022).

There is empirical and theoretical evidence to support the claim that there is upstream flow blockage which is larger than the linear sum of induction zones for each turbine. Centurelli et al., 2021 carried out a simulation to linearly superimpose the induction effects of turbines in a wind farm to determine if it was comparable to the global blockage effect. The results of their research concluded that global blockage effect was not adequately accounted for in the linearized models and the gap in results increased with wind farm scale (Centurelli et al., 2021).

The existence of global blockage effect indicates interactions among turbine wakes impacting the flow further upstream. Several simulations and experiments have deduced that global blockage of a wind farm can reach far upstream. Ebenhoch et al., 2017 and Segalini and Dahlberg, 2020 both found that upstream flow characteristics were impacted by the wind farm up to 30D upstream. Sanchez Gomez et al., 2021 conversely found that global blockage extended up to 80D upstream and can cause as much as a 10% velocity deficit in velocity near the turbines. Meanwhile, Meyer Forsting et al., 2017 found global blockage extending only 3D upstream from a single row of turbines.

Interactions between turbine flow fields have led to a discussion on the theory that global blockage is more so a redistribution of energy, rather than a global decrease. The expansion of diverted flow around a turbine may potentially lead to increased velocities for successive rows of turbines if configured correctly. Segalini and Dahlberg, 2020 hypothesizes that turbines with a lateral spacing of greater than 3D should not have an impact on the global blockage effect due to limited turbine flow interactions. This paper will also explore the existence of upstream blockage and potential increase in velocity through the wind farm through CFD simulations to determine if the global blockage effect is indeed energy redistribution as opposed to energy reduction.

1.2.2. Atmospheric conditions

Airflow characteristics through and around wind farms are largely influenced by the surrounding atmospheric conditions. The first layer of Earth's atmosphere, the troposphere, can be divided into the atmospheric boundary layer (ABL) and free atmosphere, which are separated by a thin capping inversion or entrainment zone layer (Stull, 2011). Figure 1.5 shows a simple schematic of a typical atmospheric layout through a single diurnal cycle. Development of the ABL is a result of the drag force exerted on the flow by the topographical roughness and the static stability of the atmosphere (Stull, 2011). The height of the ABL is often assumed to be around 1 km although typical heights can range from a few dozen meters to around 2 kilometers. As typical wind turbine hub heights are around 100 m, turbines can be analysed under the conditions present in the surface layer, which is commonly estimated as the bottom 5-10% of the ABL in direct contact with the ground (Brune, 2020). The surface layer is largely defined by a relatively uniform turbulent flux with height and variable wind speeds, temperatures, and humidity (Stull, 2011).

The ABL is characterized by its turbulent nature and in turn its thermal stability. Development of the ABL varies throughout the day due to radiation from the sun. During the day a convective mixing layer forms as the Earth is heated and causes warm air closer to the ground to rise and displace cooler air, a statically unstable process (Brune, 2020). The entrainment zone has limited turbulence and is considered very stable (Stull, 2011). At night, this mixing layer devolves into a neutral residual layer and stable boundary layer due to the cooling of the Earth. The residual layer is considered neutral as it is relatively homogeneous due to the turbulent mixing of the convective layer, but without the heat flux into the system the turbulence is allowed to dissipate and instability ceases (Brune, 2020). The capping inversion layer is less turbulent than the entertainment zone, however it remains strongly stable. Generally, the structure of the ABL is coupled with the degree of turbulence, as the turbulence results in the energy transfer between different air parcels, and therefore dictates the thermal stability.

Production of turbulence is reliant on the status of the thermal stability of the surrounding

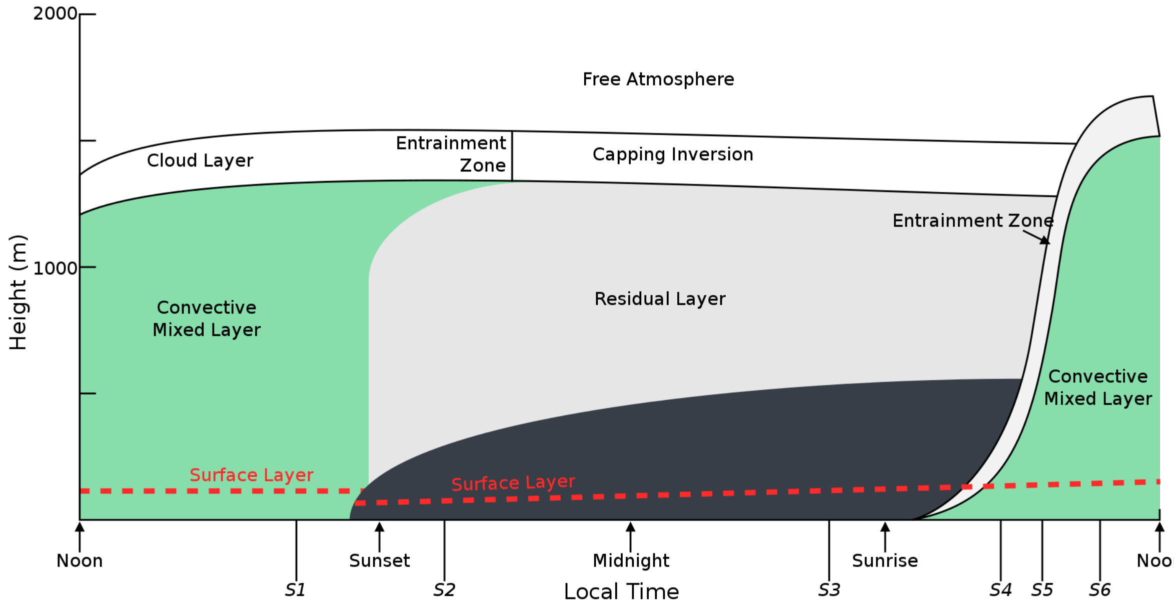

Figure 1.5: Schematic of atmosphere development through one diurnal cycle (Brune, 2020).

area (Stull, 2011). Thermal stability can be generally defined as either neutral, unstable, or stable. As the capping layer of the troposphere creates a barrier to heat flow, any cooling or warming cycles will be experienced within the ABL as a generalized closed boundary (Stull, 2011). Buoyancy and wind shear are the driving forces dictating stability. Each parcel of air is in itself immersed in a fluid (surrounding air), and therefore has a buoyancy force exerted upon it (Stull, 2011). Velocity profiles with height are dependent on the stability of the atmosphere but generally increase with height due to the shear force interaction at the ground. As the velocity increases with height, particles interact and exert shear forces upon each other. Only, buoyancy will be considered in defining the thermal stability of the domain for this research. In figure 1.6, the buoyant forces are represented by F_b and show that under unstable and stable conditions, buoyancy can respectively increase or decrease displacement of a parcel of air. Under neutral conditions, no buoyancy forces are acting upon the parcel as the change in temperature with height is exactly equal to the adiabatic lapse rate (Allaerts, 2016). In this case, the idealized potential temperature profile (θ) is strictly vertical due to the turbulent mixing in the ABL which homogenizes the fluid (Stull, 2011).

Stable conditions are characterized as having a positive potential temperature profile with respect to height, whereas unstable conditions have a negative slope. With stable conditions suppressing the production of turbulence, this often results in longer wake deficit regions as there is less mixing available. Unstable conditions will result in increased mixing and shorter wake regions, in turn resulting in less wind farm energy deficits as the flow returns to pre-disturbed conditions quicker (Allaerts, 2016). A potential temperature with a strictly vertical slope is used to characterize a neutral ABL and is often used in simulations to simplify the physical phenomena.

Although a truly neutral ABL is rare, this research will model such a case, in order to simplify the physical phenomena. Neutral stratification of the ABL occurs when heat flux of near the

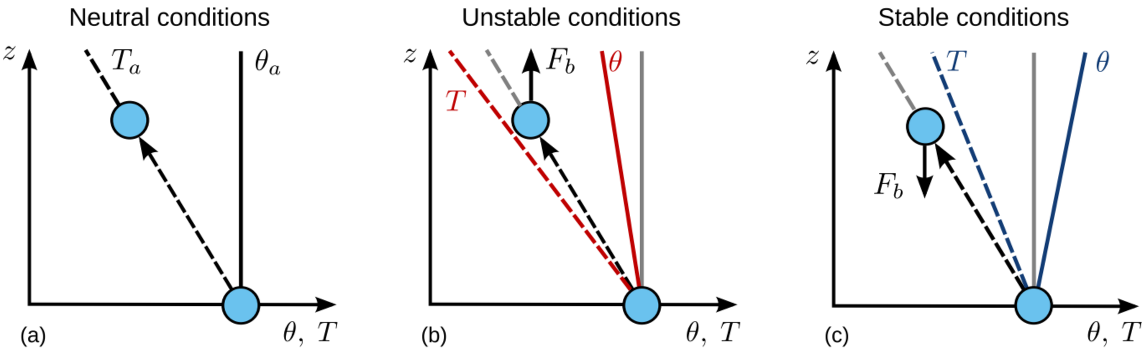

Figure 1.6: Thermal stability temperature (T) and potential temperature (θ) profiles for neutral(a), unstable(b), and stable static conditions(c) (Allaerts, 2016).

ground is relatively weak and temperature influences can be neglected (Zhang, 2009). The velocity profile ($U(z)$) of the neutral atmosphere can be approximated by equation 1.2, often referred to as the log-law profile.

$$U(z) = \frac{u_*}{\kappa} \ln\left(\frac{z}{z_o}\right) \tag{1.2}$$

Here, z is the height at which wind speed is being calculated, z_o is the surface roughness, u_* is the friction velocity calculated from equation 1.3, and k is the von Kármán constant usually set to 0.4. Where U_{ref} is the velocity at the reference height z_{ref}.

$$u_* = \frac{\kappa U_{ref}}{\ln\left(\frac{z_{ref}+z_o}{z_o}\right)} \tag{1.3}$$

A perfectly neutral ABL with flat topographical surface will have a logarithmic wind profile and the shape of the profile will be dependent on the surface roughness of the topology. Surface roughness is often gathered using empirically determined values from categories based on the best landscape fit. For example, an open ocean will have a surface roughness of approximately 0.002 m while an environment with various forest coverage and fields will have a roughness of 0.5 m (Stull, 2011). The surface roughness dictates the velocity profile as it is a measure of drag and shear present at the surface.

The airflow within the ABL is influenced by many additional factors including the Coriolis effect, humidity, gusts, weather patterns, etc. However, in this paper these factors will be excluded as to simplify the environmental factors influencing blockage to focus on the numerical configuration.

1.2.3. Wind farm turbulent interaction with ABL

Turbulence is a complex physical phenomenon that describes the stochastic, random, variations of wind speed and direction in comparison to the mean wind conditions (Stull, 2011). Turbulence in a neutral ABL is the result of shear stresses imposed on the flow by the velocity profile and viscous effects of the fluid (Zhang, 2009). Turbulent stress and drag have a much larger impact on the flow than the frictional stress and drag (Stull, 2011). Turbulent stress is often called the *Reynolds stress* which is an important component in simulating turbulence in CFD simulations.

In most cases, turbulence is usually anisotropic, with lifetime ranging from seconds to minutes. On its own, turbulence will naturally dissipate and relax to mean wind flow conditions and pull energy from the ABL into the wake of wind turbines. Turbulent bodies start off as larger eddies which interact and mix, causing an energy flow into smaller structures. A wind turbine's turbulent wake meanders and dissipates with time and distance as seen in figure 1.7. A measure of the energy within turbulence structures is the turbulent kinetic energy (TKE). The transfer of TKE from large eddies to the molecular level is referred to as the energy cascade. At the final stage of the energy cascade TKE dissipates into thermal energy.

Figure 1.7: Wind farm wake at Horns Rev offshore wind farm in Denmark (Shah, 2016).

If another turbulent body acts on the turbulent structures and creates TKE, the bodies will travel further and take longer to dissipate. In wind farms, turbines are often spaced close enough together that the turbulent streams are not allowed to fully relax after the initial creation at the first row of turbines. With each additional row, there is a TKE influx which delays the dissipation of TKE back to the mean wind flow. This effect is commonly referred to as the wake effect which has been shown to slow down the surrounding ABL due to the large compounding wake effects by effectively increasing the surface roughness (Frandsen, 1992). Understanding the interactions between wind turbines and the atmosphere is vital to understanding the presence of the global blockage effect.

1.2.4. Wind farm flow solving methods

Flow in and around wind farms is complex and stochastic, which leads to difficulty in making valid estimates of flow characteristics for wind farms. There are several methods and tools used to investigate the physical behaviour of a flow field. Empirical measurements, analytical models, and complex simulations are often used in combination to create a thorough description of the problem. One such investigation, Sebastiani et al., 2021 utilized SCADA data over a 10 year period along with numerical methods and various simulation tools to analyse the efficiency of farm configurations and the validity between the different models. The research found different results in regard to wind farm blockage between the various modelling methods.

Real world analysis methods involve gathering site data using specially designed wind measurement tools over long periods of time. Wind direction, speed, and frequency at several heights are usually gathered to determine the feasibility of the site for a specific wind installation. Having real data can help improve the validity of a design. However, the length of time from which to gather usable data often spans several decades, which is often not feasible. Empirical data gathering is more commonly used to gather initial site data, as well as information on post construction behaviour to analyse how the wind turbine(s) are operating for future cases. Both Sebastiani et al., 2021 and Schneemann et al., 2021 utilized databases of real world wind data to assist in investigations of wind farm blockage.

Analytical calculations, or engineering models, consist of sets of equations to simplify the physical problem in order to make design decisions. The models created such as the vortex dipole model and vortex cylinder model used in Branlard et al., 2020 or the self-similar model from Troldborg and Meyer Forsting, 2017 use generalized physical assumptions and physical laws to produce velocity fields without the use of empirical data. Additionally, Ebenhoch et al., 2017 created a linearized model to predict wind farm flow behaviour based on the Navier-Stokes equations which were verified against wind tunnel experiments. These models are useful in gaining an understanding of the physical state but are not as accurate as CFD simulations or empirical data. For example, Sebastiani et al., 2021 found that analytical models over predicted wake effects by 8-10%. However, they are computationally inexpensive and therefore can be useful tools in both wind farm flow fields and wind farm design.

Complex CFD simulations are becoming more commonplace in the design process of wind turbine installations. As touched on in section 1.1, turbines and farms are growing in scale and number. This results in larger impacts to the surrounding environment, and a higher investment cost, driving the demand for better design processes. This demand has pushed the development and implementation of CFD simulations for use in wind farm siting. These computer simulations are used to predict and model the behaviour of flow under various assumptions and known flow characteristics. There are 3 main methods used for these simulations: Reynolds-Averaged Navier-Stokes (RANS), Large Eddy Simulations (LES), and Direct

Numerical Simulations (DNS). LES and DNS are more accurate and thorough but much more computationally expensive than RANS. However, it has been shown that RANS can provide adequate results for a simulation with a fixed ABL height (Sommer, 2021). Further details on the modelling techniques are discussed in 2. This research will utilize RANS techniques to minimize computational and temporal costs while still maintaining relatively good results under the specified simulation configurations.

1.3. Goals and objectives

Using CFD simulations involves inherently complex and interconnected variables which can drastically alter the validity of the results. As the magnitude of global blockage has been estimated to be around 1%, ensuring quality simulations is vital to understanding the phenomenon. To ascertain the quality of results, understanding the impact that simulation design configurations have on the flow field is paramount. To this end, this research aims to answer the question:

"How does the numerical configuration of RANS simulations impact the upstream flow blockage of a theoretical wind farm?"

In pursuit of analyzing this question, several sub questions will be investigated and addressed:

- What is the impact of domain height on the magnitude and shape of upstream flow blockage and how does it alter the wind farm flow field?
- In what ways does the extent between a finite wind farm and lateral boundary affect the upstream blockage and flow field within the domain?
- How do the inlet and outlet distances change the resultant upstream flow blockage magnitude and extent?
- To what extent does wind farm flow blockage impact potential power production for various domain sizing?

1.3.1. Report structure

This paper has thus far covered the basic information and theory to set the stage for the research. The remainder of this report will be dedicated to providing deeper insight into the theoretical knowledge, set up of CFD simulations and then work to answer the research questions. Chapter 2 will largely focus on the inner workings of CFD simulations and the specific numerical configurations pertinent to the research. In chapter 3, the methodology for the simulations and analysis will be laid out. Followed by the results and discussion of the simulations in chapter 4. Finally, chapter 5 provides a summary of the preceding findings as well as recommendations for future work.

2

Background

When designing a simulation, the characteristics of the numerical experiment must be defined as well from which an appropriate numerical configuration can be created. Innumerous methods, configurations, and characteristic decisions are available to simulate the flow in and around wind farms. These decisions impact the behaviour and validity of the modelling and are prone to affect one another. When modelling a wind farm, it is important to make realistic and deliberate assumptions to ensure a valid result is obtained, from which results and conclusions can be drawn.The effect of the design decisions on simulation results have been widely studied through various research methods. This chapter will discuss various simulation design components implemented in research and offer some insight on the relative impacts of these decisions in regards to simulating the flow in and around wind farms.

2.1. DNS vs. LES vs. RANS

As briefly touched in section 1.2.4, there are three main options to solve CFD simulations: DNS, LES, and RANS. DNS directly captures all length and time scales for turbulent flows and solves their evolution over time. It is inherently a computationally and temporally expensive option for CFD and is thus usually reserved when conducting fundamental turbulence research. To put the cost into perspective, the total computational cost of a DNS simulation is approximately equal to the cube of the Reynolds number (Re), this usually limits the research to lower Re and small scales. In regards to the simulation scale required for a wind farm, a typical magnitude of 10^7 can be expected for the Re and therefore a DNS cost of 10^{21} exceeds the limit of realistic simulation costs (Allaerts, 2016).

LES is a less computationally expensive simulation methodology which still captures the flow behaviour well. The main operating principle behind LES is to divide the turbulence into resolve and unresolved scales. The larger resolved scales are directly computed and require a moderate effort. Unresolved smaller scales are modeled through an LES model which aim to simplify and estimate the sub-grid scale turbulent behaviour. The results of the model is then imposed on the resolved scales. LES in inherently three dimensional and unsteady.

It is a popular choice for CFD simulations which aim to investigate temporally dependent turbulent phenomena like atmospheric gravity waves such as in Allaerts, 2016. As the ABL conditions also vary with time, LES is oftentimes used when development and stratification of the ABL is considered such as in Centurelli et al., 2021. Wu and Porté-Agel, 2017 also utilized LES to study the interactions of a finite wind farm in a differently stratified free-atmospheres to analyse the temporal interactions between a wind farm and the ABL. LES can also be used as a tool to validate less costly computational methods such as in Sommer, 2021, which utilized RANS simulations for the bulk of their investigations which were then checked against a similar LES simulation. For the purposes of this research, the added complexity and computational time in comparison to RANS simulations is superfluous.

RANS is a time-averaged system of equations used to model the turbulent physical flow phenomena through a domain. These simulations are relatively cost effective while still providing valuable insight into expected flow behaviour. The basic principle behind RANS is to decompose a solution u_i into its mean value ($\overline{u_i}$) and fluctuation (u_i') as shown in equation 2.1. Further detail into the governing equations dictating the RANS simulation methodology are given in chapter 3.

$$u_i = \overline{u_i} + u_i' \tag{2.1}$$

RANS is a popular choice for CFD wind farm simulations due to its simplicity and cost effective nature. It is used for a variety of scales and functions as a relatively inexpensive tool to study flow fields. RANS was used by Bleeg et al., 2018 and Bleeg and Montavon, 2022, Nishino and Draper, 2015,Popescu and Flåtten, 2021, Meyer Forsting et al., 2017, and Forsting et al., 2021 to study the impact of wind turbines, from single turbines to single rows, to a full scale farm, on the power production. These simulations investigated various numerical configuration effects. Similarly, Sommer, 2021 investigated the impact of upstream blockage using various RANS configurations, however, the link between blockage and the atmosphere was the driving aim of the research.

Additionally, RANS is also a common CFD method to check analytical models and real world data against, similarly to LES. Branlard et al., 2020 compared various engineering models and utilized RANS simulations to check the validity of the models. Sebastiani et al., 2021 used RANS as a part of an analysis of the Lillgrund wind farm in conjunction with SCADA data to investigate blockage and flow fields. Meanwhile, Troldborg and Meyer Forsting, 2017 used RANS on a much smaller scale, studying a single turbine to create an analytical model.

Figure 2.1 visually demonstrates the difference in results between the three CFD methods discussed. The more computationally intensive the more detail is given in the results. As this research is not interested in the temporal evolution of the turbulence, and rather the bulk effect of upstream blockage, the steady-state mean solution produced through a RANS simulation is adequate to investigate the research questions. An appropriate numerical configuration must be chosen for the RANS simulation to provide quality simulation results. Many such numerical studies have worked to determine which conditions provide quality results, such as Avila et al.,

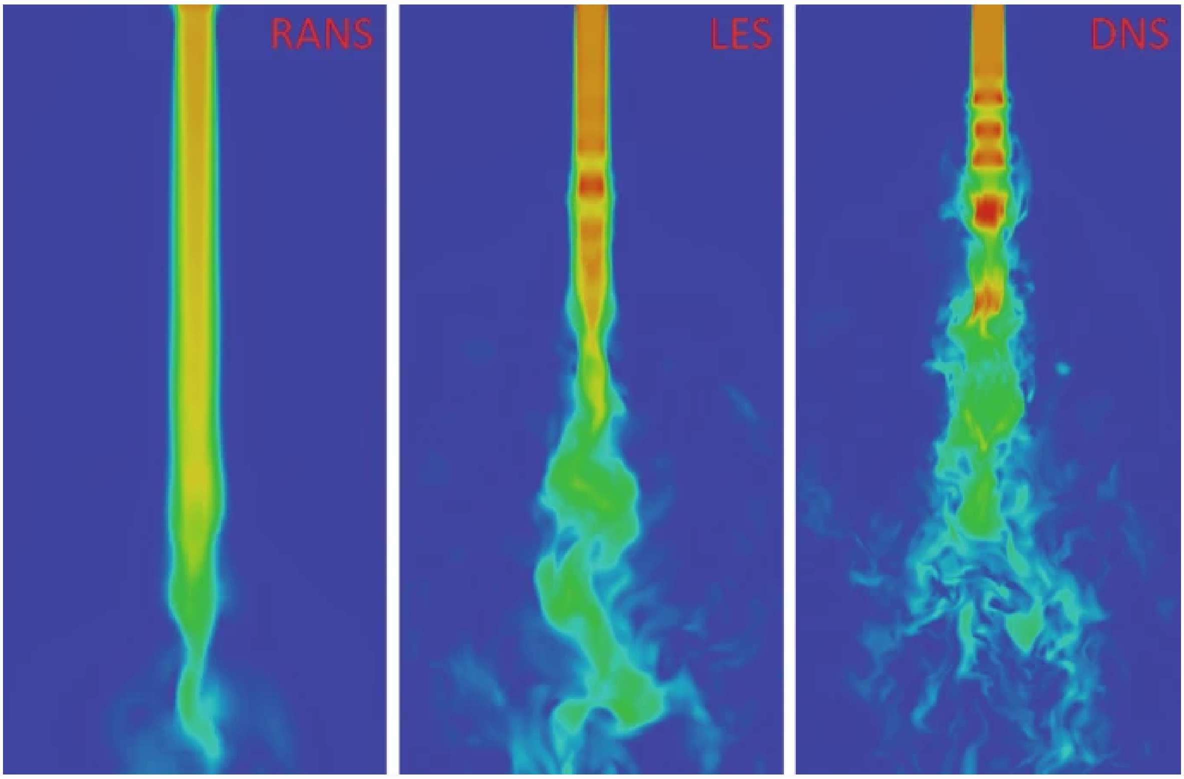

Figure 2.1: Turbulent wakes modeled with RANS, LES, and DNS (Rodriguez, 2019)

2017. However, due to the intrinsically complicated and nuanced makeup of CFD simulations, there is much discussion on which numerical configurations are superior.

2.2. Numerical configuration

The numerical configuration of a CFD simulation must reflect the present physical conditions and turbine set up. The following subsections will review the most pertinent aspects of this numerical setup and discuss their relative impacts on fluid flow behaviour, specifically as it relates to upstream blockage. It is important to note, as CFD simulations are complex and sensitive, each aspect of the simulation design is intrinsically linked to the other chosen design characteristics. Therefore, when comparing and testing various configurations it is important to maintain perspective that the numerous differences between numerical setups are intertwined with final results.

2.2.1. Domain sizing

The domain of a wind farm simulation must be set to adequately represent the flow field while also aiming to reduce unnecessary computational cost and time. In order to suitably represent the flow field, domains must be large enough to avoid distortion of results due to the domain constraints. These boundaries are defined in this paper as the inlet, outlet, lateral, top, and ground boundaries. As domain sizing is highly linked to wind turbine and farm size and configuration, domain sizing will usually be referred to in terms of turbine diameters (D) to allow for a more general analysis. A generalized schematic of the location and distances referred to in this paper is seen in figure 2.2. Domain height is defined as the total distance from the ground to the top of the domain. The lateral, inlet, and outlet distances are defined as the length between respective boundary to the outside wind farm boundary.

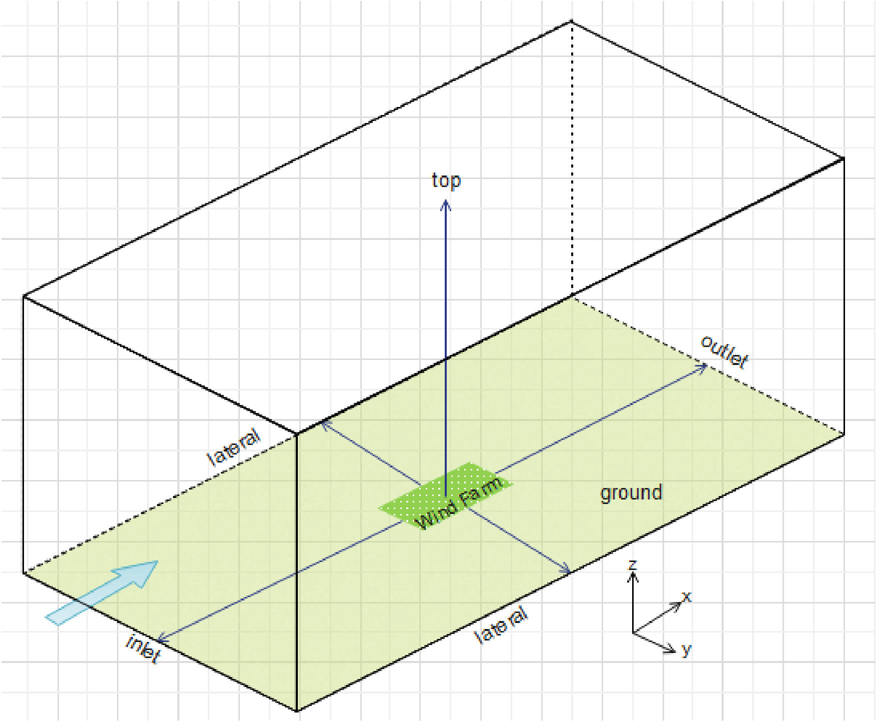

Figure 2.2: Diagram of domain boundaries and flow direction (blue arrow). Corresponding coordinate axis shown as height (z), lateral distance (y), and streamwise direction (x).

The vertical domain height is often chosen in regards to the height of the ABL, especially in the case of a neutral stability. Interest in the importance of a sufficiently high domain height in modelling global blockage has increased the number of experiments and simulations over the past several years. In literature, the height can range from as little as a few hundred meters or several turbine diameters, as in Centurelli et al., 2021 to high as 25km or over 200D in Allaerts et al., 2018. Ebenhoch et al., 2017 argues that there is a large momentum transfer between the ABL and wind farm, and through a wind tunnel experiment concluded that a domain height of approximately 2D to 8D resulted in blockage up to 30D upstream of the first row of turbines. Meanwhile, Centurelli et al., 2021 determined that as the ABL is decreased the inflow velocity deficit is strongly impacted and thus the error of numerical estimates increases due to an under representation of upstream blockage in typical estimates. Bleeg and Montavon, 2022 found that as domain height is decreased, from 125D to 7.4D, the power production is increased i.e. the inflow velocity is increased near the first row of wind turbines. Conversely, Sommer, 2021 determined blockage effect decreases as the ABL is increased, with a base domain height of 100D.

Lateral distances from the wind farm may have an influence on the flow field as a narrow domain can feasibly restrict the flow around the wind farm. The narrowest simulations set the lateral distance equal to that of the wind farm such as in Allaerts, 2016 and Allaerts et al., 2018. However, these simulations also implement cyclic lateral boundary conditions which results in a pseudo infinite wind farms. In simulations with a finite wind farm, the lateral extents range from 8D Popescu and Flåtten, 2021 to 110D Bleeg and Montavon, 2022. Constricting lateral extents may be linked to the discourse between whether global blockage is indeed blockage or more so a redistribution of energy. With the flow being confined to a smaller domain, the energy in the wind may be forced through the wind farm, particularly on the outside lateral column of turbines. Bleeg et al., 2018 investigated a power production along an isolated row and full wind farm, with spacing of at least 8D from wind turbines to the lateral bound, found that there was an increase in energy production on the outer turbines. Similarly, Bleeg and Montavon, 2022 investigated the lateral interactions between turbines in a finite wind farm with relatively large lateral extents and found that under idealised conditions there was a production gain; these gains were more apparent when the domain is constrained further. Conversely, Sommer, 2021, with large lateral extents of approximately 220D found no evidence of improved efficiency on the column of turbines closest to the lateral bounds.

The inlet distance shall be set as to provide enough space to convey the upstream impacts of a wind farm on the upstream flow field. In literature, this distance generally ranges from as little as a 6D, as in Popescu and Flåtten, 2021 to several hundred D as in Sommer, 2021. As this paper is specifically interested in the upstream blockage impacts, inlet distance is of particular interest as an inadequate inlet distance could hinder the interpretation of the extant to which upstream blockage can be observed. The distance upstream blockage extends is not yet fully quite defined. A wind tunnel experiment conducted by Segalini and Dahlberg, 2020 hypothesizes that a row of turbines will be independent from subsequent rows after approximately 15D of space, i.e. that the global blockage of a rows does not extend past 15D. Similarly, Sanchez Gomez et al., 2021 conducted CFD simulations with an inlet distance of 54D, which determined upstream decrease in velocity only extends up to 15D. Meanwhile Sommer, 2021 argues that blockage extends at minimum of 15D upstream of wind farms.

As it is currently theorized that turbulent wake interactions are intrinsically coupled with upstream blockage, wakes must be correctly simulated when investigating upstream blockage. Outlet distance from a wind farm must be long enough to allow for the dissipation of turbulent kinetic energy after the flow through a wind farm. Distance from the last row of turbines to the outlet generally range from 8D to over 200D in Popescu and Flåtten, 2021 and Sommer, 2021, respectively. The estimated distance for a wake to fully recover from interactions with wind turbines is thought to be approximately 10D downstream (Ammara et al., 2002). However, it is possible that wake region lasts much further, possibly up to 20D downstream (Chamorro and Porté-Agel, 2011). Constriction of the outlet distance may alter the wake behaviour and subsequently the upstream flow blockage through the assumed two-way interactions.

2.2.2. Mesh refinement methods

Domains must be refined to a high enough level to capture fluid behaviour but it is also desired to have a coarse as possible mesh to reduce computing and time costs. The most simplistic method is to have constant refinement cell dimensions of the entire domain. However, in order to provide better modelling of areas of specific interest, refinement patterns are often implemented. A common method is to refine the width and length of the wind farm across both horizontal axes to create a plus like pattern. The rational behind this method is to refine the wind farm as well as outer areas of interest while avoiding unnecessary refinement of areas of less concern. Experiments such as those conducted in Simisiroglou et al., 2019 and Sebastiani et al., 2021 both employee this refinement methodology. The level of refinement reached in the coarse area for Sebastiani et al., 2021 is a grid resolution of 1.3D horizontally and 0.5D in the vertical direction, and 0.1D in all directions in the refined area. Simisiroglou et al., 2019 has a grid resolution of 0.16D in the most refined region.

Another commonly refined area is around each individual wind turbine. To refine the areas around a turbine, cylinders, spheres, and blocks are often used and extend further upstream and downstream if increased refinement is desired for the flow interactions. Sebastiani et al., 2021 also employed this method and reached a grid resolution of 0.05D around the turbines with expanding layers of refinement out to a coarse mesh with a grid resolution of 0.3D; the refinement ratio between layers are 1:2. Similarly, Troldborg and Meyer Forsting, 2017 used a grid resolution of 0.3D around the turbines with a gradual stretching of cells towards the outer bounds of the domain. Stergiannis et al., 2016 employed a similar across two turbines method to closely study the flow interactions between turbines.

Additionally, to capture the fluid near to the ground, refinement at the ground with growth in cell size in the z direction is often implemented. This growth ratio allows for greater refinement near the ground which gradually expands in the vertical direction. Allaerts and Meyers, 2018, Sommer, 2021, Wu and Porté-Agel, 2017, Yan et al., 2016, Simisiroglou et al., 2019, and Parente et al., 2011 utilize gradual stretching of cell size in the vertical direction from the ground to the top boundary. Growth can be either gradual or step-wise, such as a growth-ratio of 1.05 used in Porté-Agel et al., 2020, or step up method used in Allaerts and Meyers, 2018.

There are several approaches to refining the mesh of a particular domain. The quality of a mesh can be greatly impacted by the refinement implementation. Any changes in refinement should not influence the flow behaviour. As such, grid sensitivity studies are often carried out to measure the impact of refinement against the simulation results.

2.2.3. Boundary conditions for various atmospheric conditions

The boundary conditions (BC) imposed on the model will set the physical characteristics of the flow and shall adequately represent the atmosphere and topology of the given site. As most domains are rectangular prisms, there is an inlet, outlet, two lateral sides, ground, and top to define BCs as described in figure 2.2. These BCs can be the imposition of a variable (Dirichlet), a gradient of a variable (Neumann), combination of Dirichlet and Neumann (Robin), or a Periodic BC which sets the variable values to be equal on two opposite boundaries. in 1993 Richards and Hoxey, 1993 developed BCs to create horizontally homogeneous flow conditions within the atmospheric surface layer. This work is often the basis for BCs used in CFD simulations, especially in the case of a neutral ABL with a $k - \epsilon$ turbulence model. Various adjustments and changes to the BCs put forth by Richards and Hoxey, 1993 have been made to better fit simulation conditions or work to improve upon the model. The BCs chosen must be in accordance with each other, to properly balance the physical mass, momentum, and energy flow through the domain.

Inlet

It is fairly well established in literature to set the velocity(U), TKE (k), and the turbulent kinetic energy dissipation rate (ϵ) as Dirichlet BCs, as well as a Neumann condition for pressure. These BCs are chosen to describe the commonly refereed to log-law ground-normal BC present in a neutral ABL as described in chapter 1 and in equation 1.2. Richards and Hoxey, 1993 describes these BCs for inlet flow through a single side of a rectangular prism using equations 2.2 through 2.4.

$$U(z) = \frac{u_*}{\kappa} \ln\left(\frac{z + z_o}{z_o}\right) \tag{2.2}$$

$$k = \frac{u_*^2}{\sqrt{C_\mu}} \tag{2.3}$$

$$\epsilon(z) = \frac{u_*^3}{\kappa(z + z_o)} \tag{2.4}$$

Where z_o is the surface roughness, z is the height, and C_μ is a model constant. Bleeg and Montavon, 2022 utilized these conditions to study blockage in a neutral ABL. Meanwhile, Yan et al., 2016 and Parente et al., 2011 found that k in Richards and Hoxey, 1993 fails to account for changes with height and developed equations to account for this change. Equation 2.5 gives the recommended adjustment by Parente et al., 2011 to account for changes in TKE as a function of height, where C_1 and C_2 are model constants.

$$k(z) = C_1 \ln(z + z_o) + C_2 \tag{2.5}$$

Another method to produce quality inlet profiles is to utilize a precursor domain or simulation to produce equilibrium values for the inlet BC. Sivanandan, 2021 developed a conventionally neutral boundary layer through a single column precursor simulation to set inflow conditions as a fully developed ABL. Similarly, Avila et al., 2017 used an empty domain to produce inflow conditions to be imposed on a wind farm. The inlet BCs are responsible for setting correct atmospheric conditions and are highly coupled with the top and ground BCs.

Ground

The ground BC is commonly set as a no-slip wall function to account for interactions between the ground and fluid. Wall functions play an important role in the balance of energy in the simulated domain. The shear stress between the immobile topology and fluid are what creates the initial boundary layer and helps to maintain the log-law velocity profile. Richards and Hoxey, 1993 suggests imposing equations 2.2, 2.3 and 2.4 calculated near the ground to serve as the wall function for the surface layer.

Simisiroglou et al., 2019, Bleeg et al., 2018, Wu and Porté-Agel, 2017 utilized this standard wall function based on the log-law velocity profile, with slight alterations to better fit their models. Blocken et al., 2007 adjusted the wall function to produce better velocity profiles. Meanwhile, Parente et al., 2011 developed a method to calculate the production of TKE at the center of the first cell nearest the ground as opposed to integrating the value over the entire cell as done in Richards and Hoxey, 1993. There are many alterations and empirically derived wall functions which can be defined at the ground BC. Other common changes are to adjust the model constants to better balance the domain interactions.

Top

The top BC suggested by Richards and Hoxey, 1993 is a constant sheer stress (τ) as described in equation 2.6, with ρ equal to the density of air. This BC serves to mimic the real world interactions the ABL has with higher levels in the atmosphere.

$$\tau = \rho u_*^2 \tag{2.6}$$

Parente et al., 2011 imposed this constant sheer stress method to develop a modelling approach for a neutral ABL. Many experiments do not follow this suggestion of Richards and Hoxey, 1993. Zero-gradient, symmetry, and free slip walls are common BCs which generally define the top boundary as a friction-less, impassable boundary with zero gradients. Avila et al., 2017 imposed a symmetry BC at the top boundary in their work on creating a CFD framework for wind farm simulations. Bleeg et al., 2018 investigated the consequence of wind farm blockage on energy production estimates using a slip wall top BC. Yan et al., 2016 used a method of specifying the velocity, TKE, and ϵ values at the top boundary, along with a zero-gradient condition together with the appropriate ground BC to remove inconsistencies often found with an improper top BC.

Outlet

At the outlet, flow is considered to be fully developed and therefore zero gradient Neumann conditions are imposed for velocity, k, and ϵ. Under incompressible subsonic flow exactly one Dirichlet boundary condition is imposed, usually chosen to be static pressure. Popescu and Flåtten, 2021 studied the blockage effects at wind farm scales with zero gradient and fixed pressure outlet BCs. Bleeg and Montavon, 2022 studied the blockage of a single row of turbines under varying numerical configurations with a maintained outlet BC of a fixed pressure and zero-gradient turbulence, velocity, and potential temperature. Sommer, 2021 also investigated the blockage at various domain heights assuming a fully developed outlet flow.

Lateral

For an infinite wind farm simulation, periodic BCs must be imposed on the lateral boundaries. Periodic BCs function through a simulated physical connection of two sides of similar size. To study wind farm efficiency under varying atmospheric conditions Allaerts and Meyers, 2018 imposed a periodic BC on the lateral sides to create an infinitely large wind farm. Another simulation, Wu and Porté-Agel, 2017 utilized periodic lateral boundaries to create an infinite wind farm for comparison against a finite sized wind farm to better understand the flow inside and around a finite wind farm. Periodic BCs can also be defined on lateral sides to produce the equilibrium values for a precursor simulation as discussed in subsection 2.2.3.

A free slip BC is also used for the lateral bounds in wind farm simulations. As this condition sets a zero-gradient impermeable boundary, the domain must be sufficiently far from any obstacles to ensure there is no artificial constriction of flow into the wind farm. One such experiment, Bleeg and Montavon, 2022, imposed lateral free slip BCs to study the upstream blockage of a finite wind farm under changing numerical configurations. Similarly, Parente et al., 2011 set the lateral extents to be free slip walls for a neutral ABL while Simisiroglou et al., 2019 defined the sides to be impermeable and frictionless.

2.2.4. Turbulence models

While the BCs define flow on the outer limits of the domain, the turbulence model largely dictates the flow within the domain. The RANS methodology approximates the turbulence through the Reynolds stress tensor (RST). Various approximation methods are available in varying complexity to characterize the turbulence as there are more unknowns than than equations for the RST. Each model describes the turbulence by applying simplifications to the RST to solve the closure problem. Turbulence models are generally characterized by the number of transport models required and classified as either Eddy Viscosity Models (EVM) or Reynolds Stress Models (RSM). EVMs assumes proportionality between the mean strain rate and Reynolds stress while RSM directly solves simplified model transport equations. RSMs are generally more expensive than EVMs as they require approximately six to seven transport equations while EVMs require approximately one to two. The two most commonly used turbulence models in wind farm simulations are the *Jones & Launder 2-equation model* ($k-\epsilon$) and the *$k-\omega$ Shear Stress Transport (SST) model*, both of which are two-equation EVMs. The application of turbulence models in RANS simulations is discussed further in section 3.1.

k-epsilon

Compared to other models $k-\epsilon$ has low computational costs and performs well with external flows. It should be used for homogeneous flows with small pressure gradients. $k-\epsilon$ is a valuable turbulence model for wind farms in neutral atmosphere which does not have a strong pressure gradient and the area of interest is not concerned with fluid flow along turbine blades. The $k-\epsilon$ model assumes isotropic turbulent viscosity which constitutes equal ratio between Reynolds stress and mean rate of deformation in all directions (Alfonsi, 2009).

The partial differential equations 2.7 for TKE and 2.8 for ϵ model the Reynolds stresses ($\tau_{ij} = \overline{u_i' u_j'}$) through Boussineq hypothesis given in equation 2.9 (Alfonsi, 2009).

$$\frac{\partial k}{dt} + \overline{u_i}\frac{\partial k}{\partial x_i} = -\tau_{ij}\frac{\partial \overline{u_i}}{\partial x_j} - \epsilon + \frac{\partial}{\partial x_i}\left(\frac{v_T}{\sigma_k}\frac{\partial k}{\partial x_i}\right) + v\frac{\partial^2 k}{\partial x_i \partial x_i} \tag{2.7}$$

$$\frac{\partial \epsilon}{dt} + \overline{u_i}\frac{\partial \epsilon}{\partial x_i} = -C_1\frac{\epsilon}{k}\tau_{ij}\frac{\partial \overline{u_i}}{\partial x_j} + \frac{\partial}{\partial x_i}\left(\frac{v_T}{\sigma_\epsilon}\frac{\partial \epsilon}{\partial x_i}\right) - C_2\frac{\epsilon^2}{k} + v\frac{\partial^2 \epsilon}{\partial x_i \partial x_i} \tag{2.8}$$

$$\overline{u_i'u_j'} = \frac{2}{3}k\delta_{ij} - 2v_T S_{ij} \tag{2.9}$$

with kinematic viscosity (v), eddy viscosity (v_T) given by equation 2.10, Kronecker delta (δ_{ij}), and strain rate tensor (S_{ij}) given by equation 2.11.

$$v_T = C_\mu \frac{k^2}{\epsilon} \tag{2.10}$$

$$S_{ij} = \frac{1}{2}\left(\frac{\partial \overline{u_i}}{\partial x_j} + \frac{\partial \overline{u_j}}{\partial x_i}\right) \tag{2.11}$$

Model constants σ_k and σ_ϵ along with constants C_1 and C_2 in the turbulence dissipation rate ensure the model agrees with the log-law through equation 2.12.

$$C_1 = C_2 - \frac{k^2}{\sigma_\epsilon \sqrt{C_\mu}} \tag{2.12}$$

Standard constant values, described by Launder and Spalding, 1974 for the turbulence coefficients are given in table 2.1. Additionally, work has been conducted in the aim of increasing the efficacy of the turbulence model with improved coefficients. Sommer, 2021 uses an additional set of coefficient values aimed at a neutral surface layer. Similarly, Hargreaves and Wright, 2007 expanded on the work of Richards and Hoxey, 1993 to ensure a sustained velocity profile along the span of the domain through different turbulence model coefficients.

	C_μ	C_1	C_2	σ_k	σ_ϵ
Launder and Spalding, 1974	0.09	1.44	1.92	1.0	1.3
Sommer, 2021	0.03	1.21	1.92	1.0	1.3
Hargreaves and Wright, 2007	0.09	1.44	1.92	1.0	1.11

Table 2.1: Sets of $k-\epsilon$ turbulence model coefficients

The $k-\epsilon$ is widely used in research of wind farm flow in CFD simulations such as in Simisiroglou et al., 2019, Sebastiani et al., 2021 and Popescu and Flåtten, 2021. Research done by Bleeg and Montavon, 2022, Stergiannis et al., 2016, and Yan et al., 2016 use the $k-\epsilon$ turbulence model with modified coefficients.

k-omega SST

The $k-\omega$ *SST* model also utilizes transport equations for k and ω, which represents the specific turbulence dissipation rate. It has low computational costs, requires simple wall boundary conditions for ω and performs better with pressure gradients, flow separation, and boundary flows than $k-\epsilon$. Equations 2.13 and 2.14 give the equations for k and ω with SST.

$$\frac{\partial k}{\partial t} + \overline{u_i}\frac{k}{\partial x_i} = \tau_{ij}\frac{\partial \overline{u_i}}{\partial x_j} - \beta^* k\omega + \frac{\partial}{\partial x_i}\left(\sigma_k v_T \frac{\partial k}{\partial x_j}\right) + v\frac{\partial^2 k}{\partial x_i \partial x_i} \tag{2.13}$$

$$\frac{\partial \omega}{\partial t} + \overline{u_i}\frac{\partial \omega}{\partial x_i} = \frac{\lambda}{v_T}\tau_{ij}\frac{\partial \overline{u_i}}{\partial x_j} + \frac{\partial}{\partial x_i}\left(\sigma_\omega v_T \frac{\partial \omega}{\partial x_i}\right) - \beta\omega^2 + v\frac{\partial^2 \omega}{\partial x_i \partial x_i} + 2(1-F_1)\frac{\sigma_{\omega 2}}{\omega}\frac{\partial k}{\partial x_i}\frac{\partial \omega}{\partial x_i} \quad (2.14)$$

And the kinematic eddy viscosity given by equation 2.15.

$$v_T = \frac{a_1 k}{\max(a_1\omega; \Omega F_2)} \quad (2.15)$$

Where β^*, λ, σ_ω, β, F_1, $\sigma_{\omega 2}$, a_1, Ω, and F_2 are model coefficients or auxiliary relations. Further derivation of equations and variables can be found in F. R. Menter, 1993, F. Menter et al., 2003, and Alfonsi, 2009. The $k-\omega$ SST model combines the standard $k-\omega$ turbulence model with $k-\epsilon$ to obtain quality results from within the boundary layer and through the free stream (F. R. Menter, 1993). Both Branlard et al., 2020 and Forsting et al., 2021 utilized the $k-\omega$ SST model for a reference simulation to test various engineering models in their ability to predict wind farm blockage. While Meyer Forsting et al., 2017 compared the results of a $k-\omega$ SST simulation with a numerical model to analyse upstream flow blockage of a row of wind turbines.

2.2.5. Wind farm representation

Defining the wind farm in a simulation involves including the geometry of the wind turbines, configuration of the farm, and including characteristic equations to calculate the impact of the turbine on the surrounding fluids.

Turbine modelling

Although it is possible to model the specific geometry of turbines, it is commonplace to simplify the geometry of the rotor using either the actuator disc method (ADM) or actuator line method (ALM) and to ignore the tower structure as it is considered to have a negligible impact. The ADM works as a non-rotating porous disc that exerts a thrust on the incoming flow. Figure 2.3 visually breaks down the representation of the wind turbine through the ADM method. The Froude ADM offers a simple calculation for the thrust force (F_T) through equation 2.16 (Burton et al., 2011).

$$F_T = 2\rho A |u_m \cdot \boldsymbol{n}|^2 a(1-a) \quad (2.16)$$

Where A is the AD surface area, u_m spatial-averaged inflow velocity taken at a user-prescribed upstream location, $\boldsymbol{n}$ is a surface normal vector oriented upstream, and a the axial induction factor calculated using equation 2.17 which includes the thrust (C_T) and power (C_p) coefficients of the prescribed turbine.

$$a = 1 - \frac{C_p}{C_T} \quad (2.17)$$

The ADM method is relatively simple and easy to implement by setting only a few turbine parameters such as C_p, C_T, and A. While Stergiannis et al., 2016 tested the validity of the model against experimental data and found the the model to under predict the wake deficit the method is still commonly used as it provides adequate results for many experimental setups. One such experiment, Medici et al., 2011, utilized the Froude ADM in a wind tunnel experiment to asses the blockage of a single turbine.

One approach to further refine the AD representation is to utilize a disc-based thrust coefficient (C_T') which aims to account for variability in the flow across the rotor (Sivanandan, 2021). Equation 2.18 is recalculated at each iteration of the simulation along with the resultant thrust in equation 2.19.

$$C_T' = \frac{C_T}{(1-a)^2} \tag{2.18}$$

$$F_T = -\frac{1}{2} C_T' \rho A |u_m \cdot \boldsymbol{n}|^2 \tag{2.19}$$

Through this processes the resulting wind speed and thrust is averaged over the surface area of the AD. Sivanandan, 2021 utilized the disc-based ADM while investigating the link between upstream flow blockage and gravity waves, as the large wind farm resulted in many wind turbine interactions which impact the thrust coefficient at each turbine. Meanwhile, Simisiroglou et al., 2019 compared the standard Froude and disc-based ADMs against power production from Lilligrund wind farm and found the variable-scaling model to provide better results.

The ALM is a more complex, but still simplified approach in comparison to modelling the actual turbine geometry, which represents each blade of the turbine as a rotating line with a specific lift (L_f) and drag (D_f) that exerts a force on the inflow ($\vec{F_T}$). Figure 2.3(b) shows the lines which represent the turbine blades. To calculate this force the localized lift (L_f) and drag (D_f) are first calculated as described in equations 2.20 and 2.21.

$$L_f = \frac{1}{2} C_l(\alpha) \rho u_{rel}^2 c w \tag{2.20}$$

$$D_f = \frac{1}{2} C_d(\alpha) \rho u_{rel}^2 c w \tag{2.21}$$

Using the actuator line width (w), angle of attack (α) as calculated through 2.22, relative fluid velocity (u_{rel}), and chord length of the turbine (c).

$$\alpha = tan^{-1}\left(\frac{u_n}{u_t}\right) - \beta \tag{2.22}$$

Where u_n and u_t are the normal and tangential velocities and β is the twist angle. Finally, the force calculation is applied to the mesh via a Gaussian distribution to provide numerical stability (Popescu and Flåtten, 2021).

$$\vec{F_T} = \frac{\vec{L_f} + \vec{D_f}}{\epsilon^3 \pi^{\frac{3}{2}}} \exp\left[-\left(\frac{r}{\epsilon}\right)^2 \right] \tag{2.23}$$

where r is equal to the distance between the location of the applied force and the center of the actuator element, and ϵ is a proportional constant. Popescu and Flåtten, 2021 applied the ALM to study the blockage effect of wind turbines and wind farms. The ALM model was chosen as it provides more detailed insight into the individual turbine blade impacts.

Figure 2.3 demonstrates a simplified schematic of the ADM and ALM models. As can be seen from the figure, the ADM model is relatively simple and imposes the thrust force equally across the entire surface area of the AD. Meanwhile, the ALM has the thrust force on each individual line modelled as well as a rotational component.

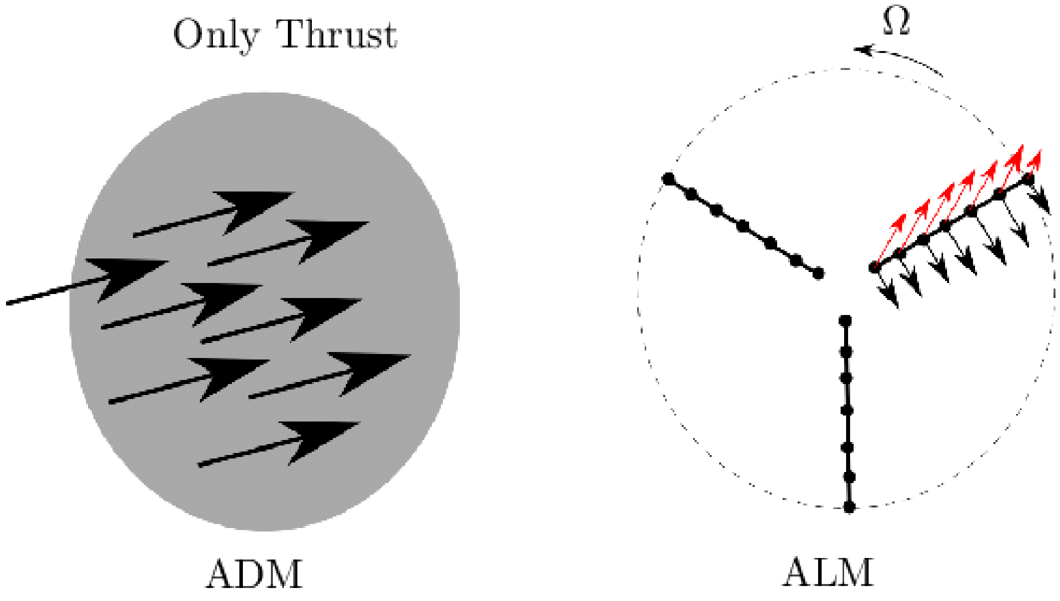

Figure 2.3: ADM vs. ALM representation (Deskos et al., 2017).

The difference in methodology affects the resulting flow behaviour of the turbine wake. Mainly, the wake of the ALM experiences higher turbulence in the near wake zone which can be attributed to the ability of the line model to produce rotational velocity components (Deskos et al., 2017). Conversely, the ADM only consists of a constant momentum sink across the AD which results in relatively uniform wakes in the near wake zone as there are no rotational components.

Although there is an observed discrepancy between produced wake structures, the flow behaviour of the ALM and ADM were both able to adequately describe the wakes when compared to each other (Martínez-Tossas et al., 2015). As such, most simulations have implemented ADM to symbolize the force of the rotor as opposed to the ALM, due to the simplification of modelling. Both models work well with structured grid refinement to convey the flow behaviour while avoiding unnecessary refinement zones.

Wind farm configuration

The configuration of the turbines in a wind farm have a large impact on the flow behaviour of the simulation. Based on the desired investigation, wind farms can range from a single turbine operating in isolation, a single row of turbines, a single column of turbines, finite wind farms, or infinite wind farms.

Single turbines are often modeled as a reference point from which to compare the results of a larger farm, such as in Bleeg and Montavon, 2022. While a single row or column of turbines can be simulated to determine the difference in flow behaviour for each turbine operating in unison. Also in Bleeg and Montavon, 2022, a single row of turbines is modelled and simulated to determine the impact of turbine interactions on power production in comparison to the single turbine modelled.

Finite wind farms vs infinite wind farms are most applicable to the investigation into global blockage as a larger number of turbines is expected to increase turbine wake interactions and therefore upstream blockage. Rows of turbines are often placed either directly behind the preceding row such or in a staggered pattern as in Popescu and Flåtten, 2021. The spacing between the turbines is also an important factor in the resultant turbine interactions and eventual upstream blockage.

Spacing in the spanwise is defined from turbine hub to the adjacent turbine hub with values ranging from 3D in Bleeg et al., 2018 to 10D in Sommer, 2021. The lateral interactions between turbines will be heavily impacted by their proximity. The expected increase in velocity between turbines will theoretically increase as spacing decreases. Streamwise spacing mostly impacts the turbine power production through the wake effect and induction/blockage effect of the turbines. Values range from 3D in Bleeg et al., 2018 in very tight configurations to 10D in Sommer, 2021. The closer the spacing is in the streamwise direction the less power production through the farm is expected, due to the higher velocity deficits in the wakes and possible increased interaction between turbines. Real world wind farms have similar spacing ranges, such as the Lilligrund Wind Farm, with a spanwise spacing of 3.3D and streamwise spacing of 4.3D (Göçmen et al., 2016).

2.3. Summary

This chapter covered the CFD simulation methods available to model a fluid flow and the details of the numerical configuration of such a simulation. The numerical configuration and solution methodology of CFD simulations is incredibly complex, interconnected, and sensitive. To obtain quality results and conclusions great care must be taken in the design and execution of the simulation. The simulation domain and geometry shall convey the real world inspiration behind the simulation without causing over determined simulations with unnecessary specificity. A myriad of solver adjustments and alterations can be chosen to better quantify the flow field behaviour. As upstream flow blockage is expected to have a magnitude of approximately 1%, choosing valid numerical configurations for the simulated wind farm is pertinent to correctly discerning any possible trends and conclusions. The next chapter will discuss the methodology of the study in in regards to the chosen CFD setup and numerical configuration.

3

Methodology of CFD simulations

This chapter discusses the methodology and reasoning behind the simulation set up. In order to investigate the impact of the numerical configuration on the upstream global blockage of a simulated wind farm, multiple sets of simulations are carried out, each set focusing on one variable. Simple domain characteristics are chosen to remove possible sources for error or distortion of results. In this regard, RANS simulations are run for a neutral ABL with a simple structured mesh, flat unchanging terrain, both infinite and finite number of wind turbines, and homogeneous unidirectional inflow.

In the first section of this chapter governing equations for RANS are derived and discussed as they relate to the execution of the CFD simulations. The following section details and elaborates upon the simulation characteristics. Additionally, the layout of the various variable inputs is covered. All parameters shall be assumed consistent through each simulation unless otherwise stated. The final section details the setup of the numerical configuration investigation to achieve the aims and objectives of the research.

3.1. Governing equations

RANS is used to reduce computing time and costs associated with time dependant simulations (i.e. LES or DNS) as discussed in chapter 2. The open source CFD software OpenFOAM version 6 semi-implicit method for pressure-linked equations (SIMPLE) algorithm based on the work of Caretto et al., 1973 is used to define and run the Reynolds-average simulation (RAS) turbulence model. The SIMPLE solver inherits the governing equations of RANS as described in this section. The RAS models are initialized with mean estimates of field values to ensure stability and physical results.

RANS simulations rely on a set of governing equations to simulate the development of flow through a specified domain under the prescribed characteristics. In order to correctly model the flow for this research, two conservation laws must be satisfied: conservation of mass, otherwise known as the continuity equation (3.1) and conservation of momentum (3.2).

Assuming the mass of all the elements is constant and the flow is incompressible, i.e. constant density and viscosity, the continuity equation can be given as equation 3.1. While equation 3.2 can be seen as the temporal change of momentum of a fluid due to the sum of surface and volume forces acting upon it. Where the first term is the time change in velocity and second term is momentum transport over boundaries. The force terms are on the right hand side of equation 3.2 as pressure forces, viscous forces, and all remaining forces specific to the scenario, respectively.

$$\frac{\partial u_i}{\partial x_i} = 0 \tag{3.1}$$

$$\frac{\partial u_i}{\partial t} + \frac{\partial (u_i u_j)}{\partial x_j} = -\frac{1}{\rho}\frac{\partial p}{\partial x_i} + v\frac{\partial^2 u_i}{\partial x_j \partial x_j} + f_j \tag{3.2}$$

Applying Reynolds-averaging first discussed in section 2.1 involves the decomposition of a variable (u_i) into it's mean value ($\overline{u_i}$) and fluctuation(u'_i). The sum of the decomposition is inserted into the Navier-Stokes equations and Reynolds averaged based on the rules shown in table 3.1. Where a is equal to an arbitrary constant.

$\overline{u'_i} = 0$	$\overline{\frac{\partial u_i}{\partial x_i}} = \frac{\partial \overline{u_i}}{\partial x_i}$
$\overline{\overline{u_i} u'_j} = 0$	
$\overline{\overline{u_i} u_j} = \overline{u_i}\;\overline{u_j}$	$\overline{u_i u_j} = \overline{u_i}\;\overline{u_j} + \overline{u'_i u'_j}$
$\overline{a u_i} = a\overline{u_i}$	$\overline{u_i + u_j} = \overline{u_i} + \overline{u_j}$

Table 3.1: Reynolds averaging rules

The resulting RANS simplified equations for incompressible flow are shown in equations 3.3 and 3.4. The body forces term f_i is removed as there are no outside forces being considered.

$$\frac{\partial \overline{u_i}}{\partial x_i} = 0 \tag{3.3}$$

$$\frac{\partial \overline{u_i}}{\partial t} + \overline{u_j}\frac{\partial \overline{u_i}}{\partial x_j} = -\frac{1}{\rho}\frac{\partial \overline{p}}{\partial x_i} + v\frac{\partial^2 \overline{u_i}}{\partial x_j \partial x_j} - \frac{\partial \tau_{ij}}{\partial x_j} \tag{3.4}$$

The final term of equation 3.4 is the Reynolds stress tensor which can be written in index notation as $\tau_{ij} = -\overline{u'_i u'_j}$. The general form of the RST transport equation is given in equation 3.5 and whose terms include the change in RST over time ($\frac{\partial \overline{u'_i u'_j}}{\partial t}$), advection ($K_{ij}$), production ($P_{ij}$), diffusion (turbulent (T_{ij}), viscous (D^v_{ij}), and pressure dependent (D^P_{ij})), pressure strain correlation(ϕ_{ij}), and dissipation (ϵ_{ij}). Each term includes additional unknowns and therefore cannot be solved mathematically. Turbulence closure models are used to solve this problem with empirical approximations.

$$\frac{\partial \overline{u_i' u_j'}}{\partial t} + K_{ij} = P_{ij} + (T_{ij} + D_{ij}^{v} + D_{ij}^{p}) + \phi_{ij} - \epsilon_{ij} \tag{3.5}$$

As discussed in section 2.2.4 EVMs are used to approximate the RST transport equation as shown in equation 3.5. The standard $k - \epsilon$ turbulence model laid out in 2.2.4 is used to satisfy the turbulence closure problem of the RST. The two additional transport equations for TKE (equation 2.7) and ϵ (equation 2.8) along with the RANS equations 3.3 and 3.4 for the three velocity components result in six unknown variables ($u_{i,j,k}$, p k, and ϵ) with six partial differential equations (Alfonsi, 2009). The system can then be solved as there is an equal number of known equations to unknown variables.

Within OpenFOAM, the $k - \epsilon$ turbulence model has several controllable inputs within the *turbulenceProperties* dictionary to specify the desired turbulence behaviour as described in equations 2.7 to 2.11. The default implementation values for OpenFOAM are based on Launder and Spalding, 1974 and as such, the standard model coefficients are set as: $C_\mu = 0.09$, $C_1 = 1.44$, $C_2 = 1.92$, $\sigma_k = 1.0$, and $\sigma_\epsilon = 1.3$. However, the work of Hargreaves and Wright, 2007 found that for neutral ABLs, $\sigma_\epsilon = 1.11$ produced better results and thus is used in the subsequent simulations.

The SIMPLE algorithm solves the RANS equations through an iterative process which uses current values to obtain new values for velocity and pressure through momentum and pressure equations and corrects for flux (Caretto et al., 1973). The process is repeated until the simulation is converged or specified run time is met.

3.2. Simulation

The numerical configuration of the RANS simulation serves two purposes: correctly modelling the prescribed environmental conditions and providing an ability to alter the configuration setup to determine results and trends. To simulate the chosen scenario, the simulation is set up to produce a neutral ABL, flat terrain, unidirectional horizontally homogeneous flow, and a velocity profile that prescribes to the log-law equation 1.2. Initialization through an initial estimation of variable values is done to aid in stabilizing the simulation and reduce the time for flow to develop and the simulation to converge. The domain sizing is chosen to ensure minimal interference in results from extents not investigated under the specified simulation batch. Studies to determine convergence criteria and adequate mesh resolution based on preliminary results are carried out to instill confidence in the results.

3.2.1. Actuator disc model of reference turbine

The actuator disc model discussed in section 2.2.5 is implemented in the simulation configuration as it provides a reasonable approximation of the flow around a wind turbine while maintaining simplicity of the model. The National Renewable Energy Laboratory (NREL) 5MW reference turbine is the chosen reference turbine used to obtain dimensions and power characteristics. This turbine is chosen for its standard design characteristics as well as being frequently used in CFD simulations such as in Troldborg and Meyer Forsting, 2017 and Sanchez

Gomez et al., 2021. The ADs are defined to represent the general geometry and characteristics of the NREL 5MW reference turbine (Jonkman et al., 2009).

The NREL 5MW turbine has a hub height of 90 meters and diameter of 126 meters, a rated wind speed of 11.4 m/s, and cut-in and cut-out wind speed of 3 and 25 m/s, respectively. When defining the AD to represent the turbine the Betz defined thrust coefficient of 0.89 is used in order to ensure global blockage is produced at an identifiable scale in the simulations. A similar approach for the thrust coefficient has been used in CFD simulation investigations such as Mikkelsen, 2004.

Each AD was defined within OpenFOAM's *topoSet* dictionary using the *cylinderToCell* and *setToCellZone* functions to orient the discs normal to the direction of the flow at the proper hub height and radius of the 5MW reference turbine. A streamwise thickness slightly larger than the grid meshing for the cylindrical discs is chosen to ensure at least one cell center is be correctly captured by OpenFOAM. A power coefficient of 0.482 is set within *fvOptions* based on the reference turbines technical documents (Jonkman et al., 2009) as well as the corresponding disc area (A) and orientation. *fvOptions* defines the ADs as actuation disc sources with constant momentum (using thrust as a basis) and velocity at the disc (U_1) using equation 2.16 and 3.6, respectively. The upstream velocity (U_o) is user defined by specifying a point upstream of the disc at which to take the velocity during the simulation run.

$$U_1 = (1-a)U_o^2 \tag{3.6}$$

Turbine spacing is set as 5D in the spanwise (Δy) and 7D in the streamwise direction (Δx) as shown in figure 3.6. This is within the range of typical spacing used in simulations, such as in Centurelli et al., 2021. Infinite wind farm simulations consist of 5 turbines in the streamwise direction and infinite number of turbines in the spanwise direction. For finite wind farm simulations, a 5x5 wind farm is used to provide enough turbine wake interactions to produce identifiable trends in upstream blockage, while keeping computational time and cost at reasonable levels. The turbine configuration is a symmetric layout, with each row of turbines appearing exactly 7D downstream of the preceding row of turbines.

In order to properly check and analyze global blockage and separate induction effects, each numerical configuration has a paired simulation of a turbine operating in isolation at the same location within the domain as the center front turbine of the wind farm simulation. As induction is understood to occur between 1D and 4D ahead of the turbine (Segalini and Dahlberg, 2020), there are various points at which it can be compared against blockage. For the purposes of these simulations, 2.5D ahead of the turbine will be defined as the point at which induction is compared to blockage, as is done in Sommer, 2021. As such the upstream velocities and subsequent power loss calculations utilize sample points taken 2.5D upstream of the respective wind turbine.

3.2.2. Modelling neutral ABL with appropriate boundary conditions

To ensure the proper exploration of the research topics, extra care was taken in ensuring the ABL and flow field were properly simulated. Proper modelling of a neutral ABL is reliant on the chosen BCs, particularly the inlet profiles, and initial conditions of the simulation. Therefore several BC groupings were tested to determine the best conditions to simulate a truly neutral ABL.

Many simulations make use of the assumptions and approach described in Richards and Hoxey, 1993 as discussed in chapter 2. However, a specification in the Richards and Hoxey, 1993 approach that is often ignored is the addition of a constant shear stress at the top of the domain. In real atmospheric conditions, the surface layer is usually maintained through the interaction with upper atmospheric levels (Richards and Hoxey, 1993). The imposed shear stress given in equation 2.6 is based on the relationship between kinematic stress and turbulent stress (Stull, 2011). In a fully neutral ABL simulation with either zero gradient or free slip wall conditions, this interaction is absent and can result in a degradation of the velocity profile if not properly addressed.

Figure 3.1 shows sample results at various distances upstream of the center front wind turbine for both empty and finite wind farms at two domain heights; assuming Richards and Hoxey, 1993 BCs but ignoring the shear stress BC. The results show that the velocity in the empty domain deviates from the inlet velocity in both an empty fetch and one containing a finite wind farm. There is a strong correlation shown between the empty domain velocity and the finite domain velocity at their respective heights, which impedes the ability to draw conclusions on upstream blockage. As previously discussed, the horizontal flow of a neutral ABL should be horizontally homogeneous and the streamwise velocity profile should remain constant. This deviation due to the absence of shear stress can cause the results of the simulation to become skewed. Removing the error through simple calculations of subtracting the upstream change in velocity from the inlet velocity gives a better expected result, shown on the right hand side of figure 3.1

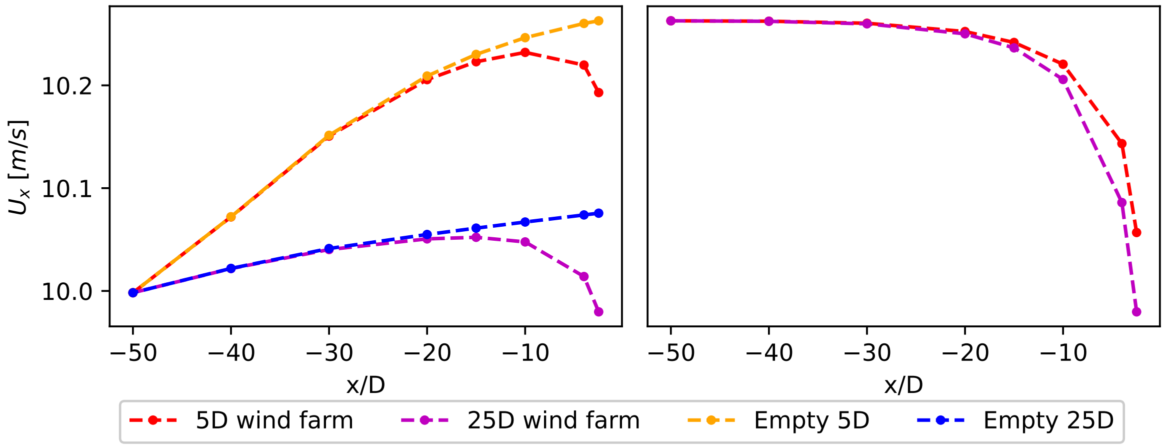

Figure 3.1: Comparison of upstream velocity of empty and finite wind farm domains at two domain heights (5D and 25D) with Richards and Hoxey, 1993 BCs without shear stress(left) and the impact of removing error (right)

As upstream flow blockage is expected to be in the range of 1-3% decrease in flow velocity, the error from ignoring the shear stress recommendation of Richards and Hoxey, 1993 is substantial enough to distort results. There are several approaches that have been suggested to alleviate the velocity profile degradation. The first, and perhaps most obvious, is to include the shear stress at top boundary. Equation 2.6 shows that the magnitude of the shear stress to be imposed on the top boundary is a function of the fluid density and friction velocity.

The impact on velocity profile degradation can be seen in figure 3.2. The figure demonstrates that the velocity profile with an imposed shear stress is indeed kept intact in comparison to when different top boundary conditions are imposed. The degradation is of increased importance at the heights containing the wind farm, from the figure it can be seen the degradation of velocity profiles is drastically improved at these heights with the imposition of a shear stress at the top BC.

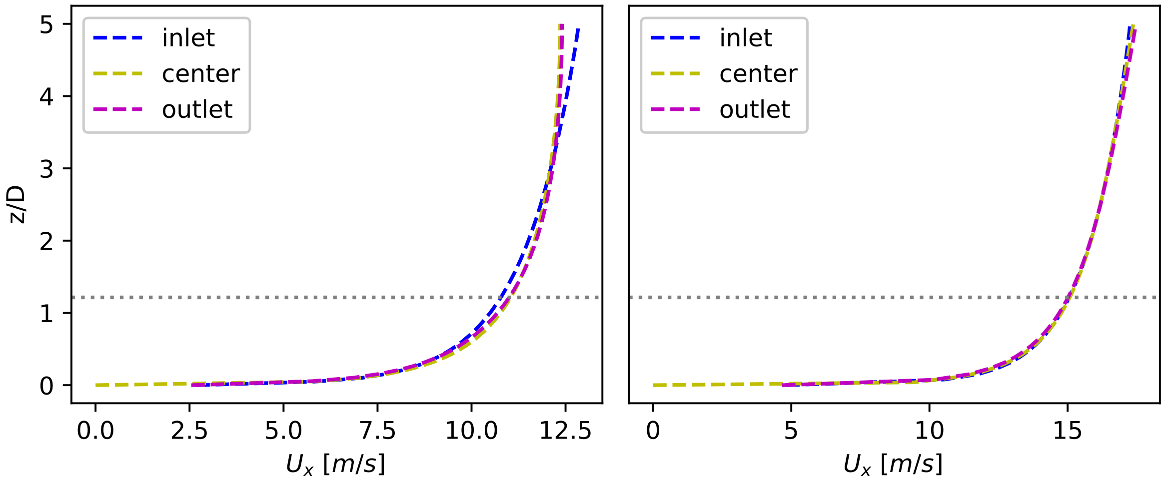

Figure 3.2: U_x profiles against height at positions along x axis, (left) has no shear stress at the top BC, (right) has a constant shear stress at the top BC. Grey line represents top of wind farm.

There is however still a slight error in the deviation of horizontal velocity in the streamwise direction, approximately an order of magnitude smaller than expected blockage values, on the range of 0.02%, and therefore deemed workable to determine blockage trends associated with numerical configuration changes. As the imposed shear stress is not a function of domain height, all simulations will have the same shear stress imposed upon the top boundary condition based on the velocity flow field specified and terrain topology.

The remaining BCs for the simulation follow the Richards and Hoxey, 1993 approach to simulate a neutral ABL as first discussed in 2.2.3. The inlet is set as a log-law velocity profile based on user defined ABL conditions. The log-law values used for these simulations are at a reference height and velocity of 6 meters and 10 m/s, unidirectional streamwise flow, and surface roughness of 0.01 based on Hargreaves and Wright, 2007. The surface roughness is a typical value for a flat open terrain (Anjum, 2014).

The inlet conditions are instituted in OpenFOAM through the *atmBoundaryLayer* class which prescribes the defined ABL conditions for U, k and ϵ. Pressure and turbulent viscosity are set as *zeroGradient* and a uniform value of 0 based on recommendations of Hargreaves and Wright, 2007.

Wall functions discussed in section 2.2.3 are utilized for the ground BC. The velocity at the ground is set to 0 and pressure set to *zeroGradient.* TKE, ϵ, and turbulent viscosity utilize OpenFOAMs suite of wall functions which work to produce a neutral ABL in accordance with Richards and Hoxey, 1993 and Hargreaves and Wright, 2007. These equations integrate the ABL conditions also used for the inlet values, such as surface roughness.

Lateral BCs vary between infinite and finite wind farm simulations. In order to simulate an infinite wind farm, the lateral conditions must be cyclic. Cyclic BCs match a pair of boundaries of similar topology, in this case the two lateral sides, which result in a laterally infinite wind farm simulation. For finite wind farm simulations, a slip condition is imposed to prevent flow through the boundaries and impose a frictionless wall on the lateral sides of the domain.

Finally, the outlet BC assumes a fully developed flow with no reverse flow. As such, U, ϵ, and TKE are set to an *inletOutlet* which does not allow for reverse flow and inherits the internal field values for each variable. Meanwhile, pressure is set to a *uniformFixedValue* of the internal field and turbulent viscosity is set to a uniform value of 0.

3.2.3. Meshing and grid convergence

To ensure proper convergence of the simulations, a simple convergence study is carried out testing several residual ranges. The numerical configuration used for the study is that of a single turbine in a domain with sizing of 25D height, 128D total length, and 41D total width. This domain sizing and single turbine configuration are chosen to reduce unnecessary computing costs while still ensuring a large distance from the turbine to instill confidence in the study. As 10^{-6} is often used in simulations such as Sommer, 2021 and Forsting et al., 2021; simulations are run with a residual (RES) criteria ranging from 10^{-3} to 10^{-7}.

In a similar method to measure convergence is used in Sommer, 2021, where induction results of a single turbine are used to determine the convergence criteria. Velocity probes at hub height for 2.5D ahead of the turbine ($U_{-2.5D}$) are obtained and compared against a reference velocity (U_{ref}) at the same location in an empty domain as can be seen in equation 3.7. The results are plotted against the respective residual values and shown in figure 3.3. The results show that the results are relatively converged for all residual values as the difference in induction results between a residual of 10^{-3} and 10^{-7} is on the order of 0.000122%, which is well below the scale where induction and global blockage are measured. However, due to the trend of the line and convention, simulations are run until residuals reach a value of 10^{-6}.

$$Induction = -\left(\frac{U_{-2.5D} - U_{ref}}{U_{ref}}\right) * 100\% \tag{3.7}$$

Although many simulations, like those discussed in section 2.2.2 use changes in refinement in the horizontal plane, errors in such setups were encountered, such as those shown in figure 3.4. It can be seen that at each location where there is a change in refinement, the largest

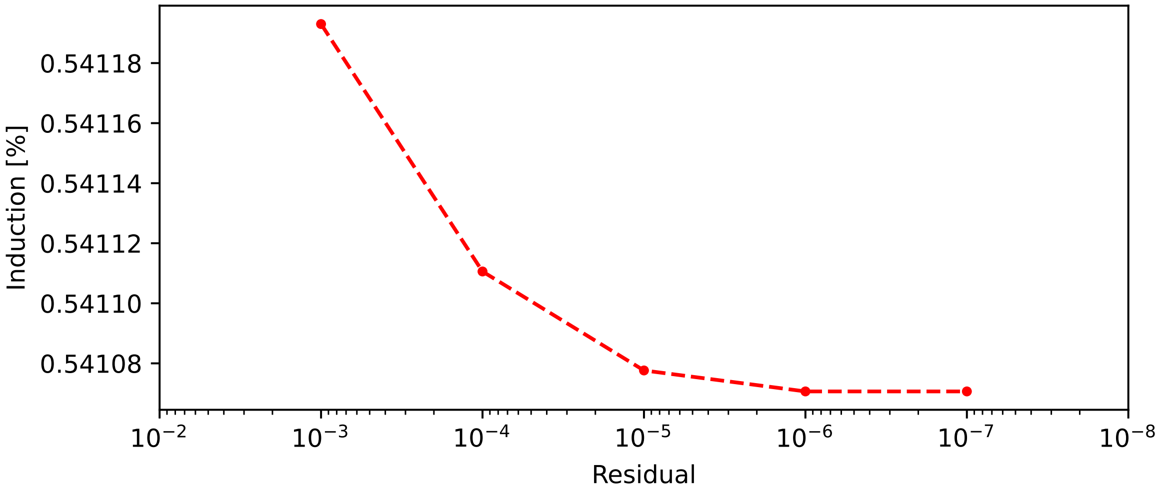

Figure 3.3: Residual plot for convergence study of a domain with a single turbine.

spike is approximately 1% of the wind speed. As global blockage has a an expected magnitude of approximately 1-3%, the magnitude of error due to the grid refinement pattern is deemed infeasible to produce quality results.

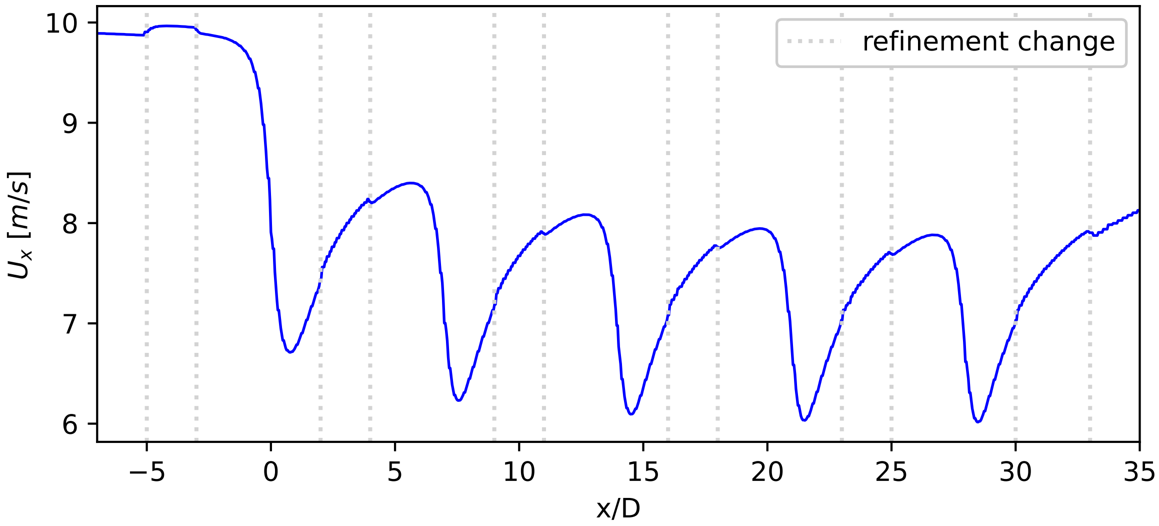

Figure 3.4: Spikes in velocity profile through wind farm at hub height due to changes in mesh refinement. Grey lines show refinement changes, blue line shows velocity profile through a column of wind turbines.

The simulation setup uses a semi unique method of prescribing separate blocks with equal sizing in the horizontal directions, stacked one on top of another, with varying mesh resolution to define the domain. This is done to remove distortion of results due to changes in mesh refinement in the surface layer of the domain in both the streamwise and spanwise directions. Figure 3.6 shows a simple schematic of the domain and the 2:1 refinement across respective blocks.The multi-block system was also used to reduce unnecessary refinement in the upper bounds of the domain to reduce computational time and cost.

Additionally, a simple grid convergence study is completed with a small domain using various degrees of mesh refinement. As mesh refinement generally ranges from 5% to 15% of the turbine diameter, values chosen for the study are 6.25%, 7.5%, 8.75% 10%, and 12.5% of the turbine diameter for the first block, which is associated with the surface layer. Refinement is kept consistent in all directions for each cell. The domain is the same as in the RES study simulations to ensure results are applicable to the experimental simulations without requiring excess computational time or cost. Similarly to the convergence study, the induction is taken at 2.5D upstream of the turbine in isolation and compared against reference velocity for each case. The results of the grid refinement study are shown below in figure 3.5.

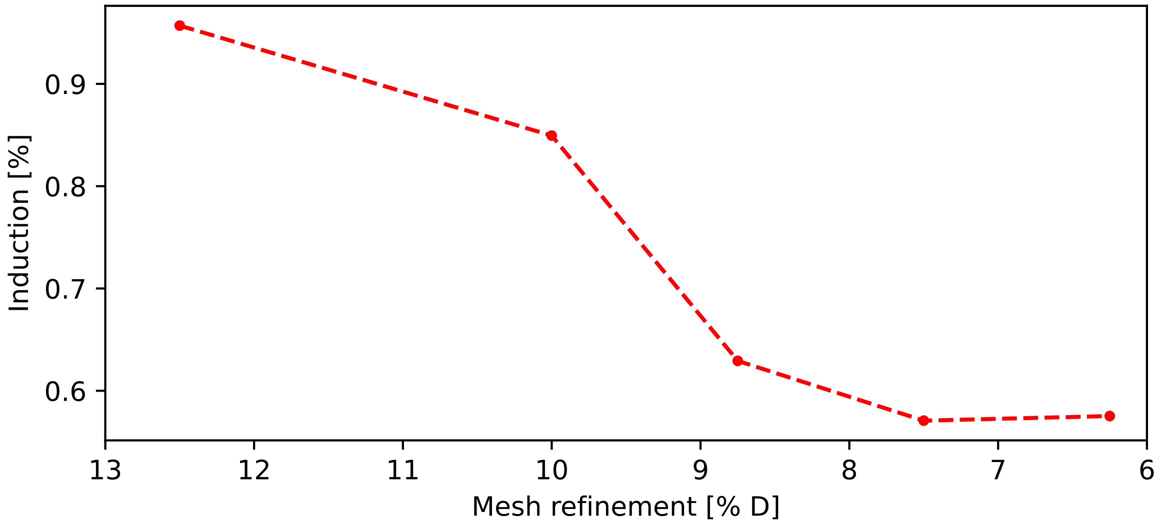

Figure 3.5: Grid study results using various percentages of a turbine diameter spacing in a four stacked block domain. A 2:1 mesh refinement between blocks and a single turbine for induction calculation.

The figure shows that the wind speed begins to converge at around 8.75% mesh refinement with even better results at 7.5% mesh refinement. A final mesh refinement of 7.5% is chosen as it agrees with finer meshes without requiring superfluous number of cells. This refinement level results in a physical size of 9.45 meters in the first block (ground level), 18.9 metes in the second block, 37.8 meters in the third block, and 75.6 meters in the fourth block. A similar meshing and refinement patter is utilized in Sanchez Gomez et al., 2021, with the most refined region having 7 meters in the horizontal directions and 5 meters in the z direction up to a certain height. At specified vertical extents the z refinement level coarsens to 80 meters and then to the coarsest level of 200 meters for Sanchez Gomez et al., 2021. The resolution in the surface layer is in accordance with the required refinement across ADs for grid independent wakes according to work done by van der Laan et al., 2015, which concluded 8 cells per turbine diameter (12.5% of D) is sufficient.

The final setup of the simulations is shown in figure 3.6, including the BCs, mesh resolution changes, and wind farm configuration. The blocking method has constant vertical heights for the blocks of 300 m, 1000 m, 2000 m, and 3150 m at the highest point. In the case that a simulation a domain height is shorter than the starting height of a block, the simulation will not utilize all 4 blocks.

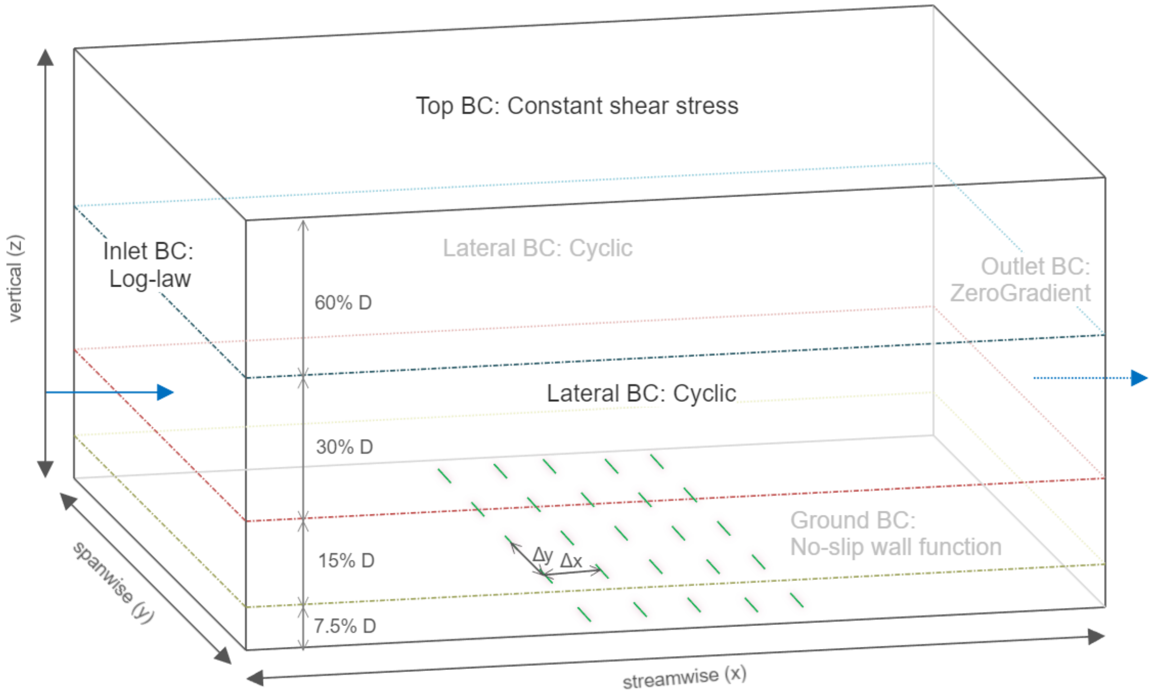

Figure 3.6: Domain setup for simulations using four block method. Green lines represent turbines with Δx streamwise spacing and Δy spanwise spacing between turbines. Setup is for a laterally infinite wind farm and with five rows. Mesh resolution shown as percentage D and 2:1refinement between adjacent blocks.

3.3. Numerical configuration investigations

Variations in the numerical configuration are systematically altered to provide simulation results and to obtain meaningful information to answer the research questions. The variables to be altered are chosen to answer the research questions described in section 1.3. Table 3.2 summarizes the various domain alterations for each numerical configuration investigation. The changes to the numerical configuration are segregated into four categories or *simulation suites*, which are discussed in detail below.

Domain height

As previously mentioned in chapters 1 and 2, the ABL is intrinsically linked with the flow behaviour in the prescribed domain. The domain height is set to convey the physical characteristics of the surrounding atmospheric environment. This can include multiple atmospheric layers, however, for a truly neutral ABL, the height of the domain will be set at the ABL height. Using values from literature, briefly discussed in chapter 1, several simulations are executed with varying domain heights to determine the effect on upstream blockage. Upstream and downstream distances from the wind farm are set at 50D each to ensure no distortion of results from interference with inlet and outlet boundaries. The lateral extend is defined to be 2.5D from the rotor center of the outside column of turbines to coincide with the spanwise spacing of the turbines and simulate an infinite wind farm.

Lateral span sizing

To further investigate the domain sizing impact on upstream blockage, simulations with varying lateral extents are run on a finite wind farm. As global blockage implies, the wind farm may cause a blockage effect on the upstream velocity as the fluid is impeded and the spacing of the lateral extents may provide an outlet for the restricted flow or in the case of narrow spacing, the flow may be forced through or over the wind farm as discussed in section 2.2.1. Variations in spacing between the finite wind farm and lateral boundaries are used to determine the impacts on the resulting global blockage. This is done in a similar fashion to the domain height investigations. The outlet and inlet spacing are kept at 50D preceding and proceeding the wind farm and domain height is set as 25D from the ground boundary to reduce the possibility for interference.

Inlet distance

To test the potential impact of inlet distance from the wind farm on final blockage results, various simulations are run with varying inlet distances on an infinite wind farm. As such, lateral extents are set to 2.5D to induce an infinite wind farm in the spanwise direction. Domain height is set to 25D and outlet distance to 50D to remove opportunity for boundaries to alter the results. As discussed in section 2.2.1, inlet distance is of importance to correctly convey the extent and magnitude at which the upstream blockage impact is observed. As it is not yet understood the distance upstream at which blockage can be measured, inlet distance for proper simulation of upstream blockage is of interest. Values chosen for experimentation test a range that is commonly used in research.

Outlet distance

Outlet distance is simulated in a similar fashion to inlet distances, with an inlet distance of 50D, vertical height of 25D, and lateral extents of 2.5D to create an infinite wind farm. The outlet distance impact on blockage is theorized to be linked to the coupling of wind turbine wakes and upstream blockage as discussed in section 2.2.1. The outlet distances are set to the same range as inlet distances, as simulations are often run under similar sizing for both inlet and outlet distances. As the outlet BC is commonly set under the assumption of a fully developed flow, not setting a proper outlet distance may skew results and distort the resultant upstream blockage.

	Simulation ID	Height	Upstream	Downstream	Lateral	
		z/D	x/D	x/D	y/D	BC
Domain Height	dh - 5	5	50	50	2.5	Cyclic
	dh - 10	10				
	dh - 15	15				
	dh -20	20				
	dh - 25	25				
Lateral Extent	le - 2.5	25	50	50	2.5	Slip
	le - 5				5	
	le - 10				10	
	le - 15				15	
	le - 20				20	
	le - 30				30	
Upstream Distance	up - 15	25	15	50	2.5	Cyclic
	up - 25		25			
	up - 50		50			
	up - 75		75			
	up - 100		100			
Downstream Distance	dw - 15	25	50	15	2.5	Cyclic
	dw- 25			25		
	dw - 50			50		
	dw - 75			75		
	dw - 100			100		

Table 3.2: Domain sizing configuration for upstream flow blockage simulations with distances normalized to a turbine diameter.

3.4. Summary

This chapter discussed the derivation and implementation of the RANS governing equations as they relate to the research. The details of the simulation regarding the actuator disc modelling, adequate simulation of a truly neutral ABL, and meshing and refinement methods were then covered. Finally, the outline and reasoning for the changes in the numerical configuration of the simulation setup were explained.

The simulations utilize incompressible RANS equations with a $k - \epsilon$ turbulence model with coefficients based on the work of Hargreaves and Wright, 2007 through the SIMPLE algorithm available in OpenFOAM. Turbines are modelled with a standard Froude ADM tailored to the NREL 5MW reference turbine specifications with a C_T based on the Betz limit. Spanwise and streamwise spacing between turbines is set to 5D and 7D respectively, with 5 rows of turbines modelled directly behind the preceding row. The neutral ABL with homogeneous horizontal flow is modelled based on the boundary conditions set forth in Richards and Hoxey, 1993, including the shear stress as the top BC. The domain is meshed as four stacked blocks with mesh refinement of 2:1 between lower and upper blocks. The degree of refinement in the lowest level is 7.5% of the turbine diameter in all directions. To analyse the numerical configuration, domain extents not being analysed are far from the wind farm while the changing variable is systematically altered.The following chapter will provide the results of the implementation of the simulation setup laid out in this chapter.

4

RANS simulation results and analysis

This chapter discusses the results of the experimental simulations as they pertain to the research questions. Each section covers the general setup of the simulations being analysed to provide context for a discussion of the results. Simulations are divided into sections based on the domain extent being analyzed to compare results and derive conclusions. First, the impact of domain height on the flow behaviour through the domain is covered, especially as it relates to upstream flow blockage. A similar analysis and discussion is carried out in regards to changes in the lateral extent of the domain for a finite wind farm. Analyses of inlet and outlet distance impacts on upstream flow blockage are then executed. Finally, the power production effects of each simulation suite related to upstream flow blockage is analysed. In this manor, the research questions are answered in the order they are presented in section 1.3. A discussion of the main findings and recommendations based on the results are available at the end of each section and a main summary of the chapter findings is available in the last section. Supplementary figures are available in Appendix A.

4.1. Domain height

As discussed in chapters 1 and 2, the height of the ABL is an important environmental characteristic in predicting the flow behaviour in and around a wind farm. As such, the domain height in CFD simulations is an interesting variable as it can be used to represent the ABL height. This section discusses the impact of changing the domain height of an infinite wind farm with large upstream and downstream extents on the resultant global blockage. An initial analysis of general flow behaviour in the simulation results is discussed first to ensure expected physical flow characteristics are observed. This is followed by a more in depth discussion and analysis of the upstream flow blockage and flow through and around the wind farm.

To ensure minimal influence from the domain boundaries not being investigated in this section, large extents are chosen for upstream and downstream boundaries. Moreover, cyclic BCs imposed upon the lateral extents to create an infinite wind farm. The environmental characteristics are chosen to ensure a neutral ABL with no veer or Coriolis effect, a flat terrain, and include a domain height independent shear-stress at the top BC to ensure proper homogeneous flow behaviour. As the domain height is often equated to the ABL height in this paper, that can vary from approximately a few hundred meters to several kilometers. The shortest domain height tested in this study is equal to 5D (630 m) from the bottom boundary, and the tallest test is 25D (3150 m) from the bottom. In total 5 domain heights are tested and analysed for global blockage. As such, Isolation simulations are carried out for each respective domain height simulation.

4.1.1. Initial analysis of general flow behaviour

A preliminary check of the results is carried out to ensure the velocity flow through the domain makes physical sense and to check for initial trends in flow behaviour. Slices depicting the streamwise velocity (U_x) in the domain are shown in figures 4.1, 4.2, and 4.3 for several different domain height simulations. As interpreting the colors of a simulation is subjective, these primary checks are used as a way to assess the bulk behaviour of the model and provide insight on what the behaviour of the fluid will show under more rigorous analysis.

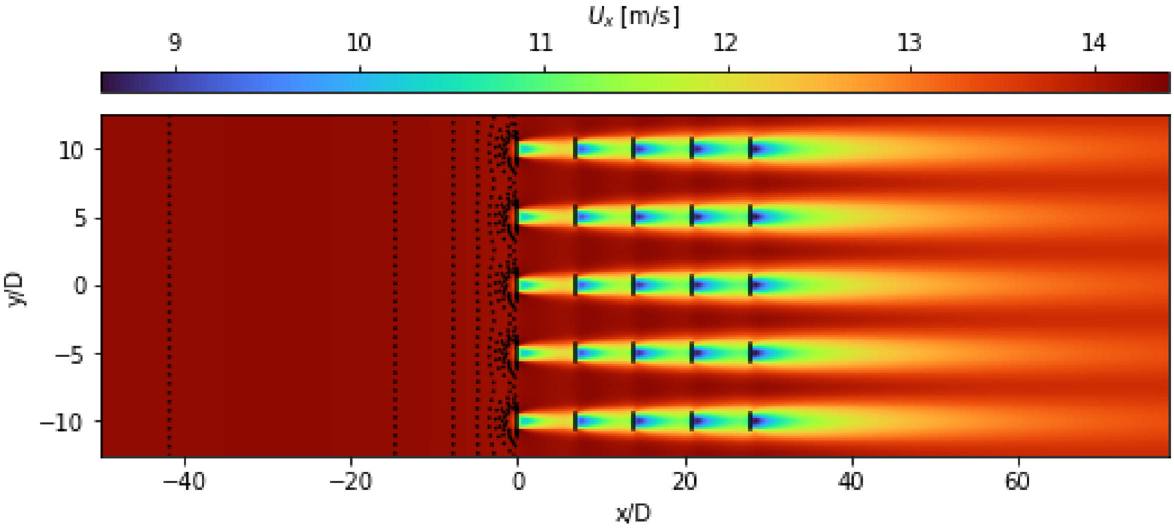

Figure 4.1: U_x field and contour lines at hub height for an laterally infinite wind farm for dh-25. Wind turbines shown as black bars.

The results show expected streamwise velocity behaviour throughout the domain. In figure 4.1 the velocity displays an observable decrease approximately upon approaching the wind turbines which can be seen by the contour lines. Wakes then form after the first row, which increase in intensity after each subsequent row of turbines. There is a slight increase in U_x between the columns of turbines. The wakes then slowly recover towards the end of the domain.

In figure 4.2, there is a developing boundary layer following the first row of turbines due to the thrust exerted by the turbines and the subsequent decrease of velocity in the wake. As the flow encounters additional rows of turbines, the boundary layer grows in height until it slowly reaches a maximum, at which point it begins to recover due to the turbulent nature of the flow. The contour lines shown for U_z give some indication that the effects of the wind farm are felt close to the top of the domain height.

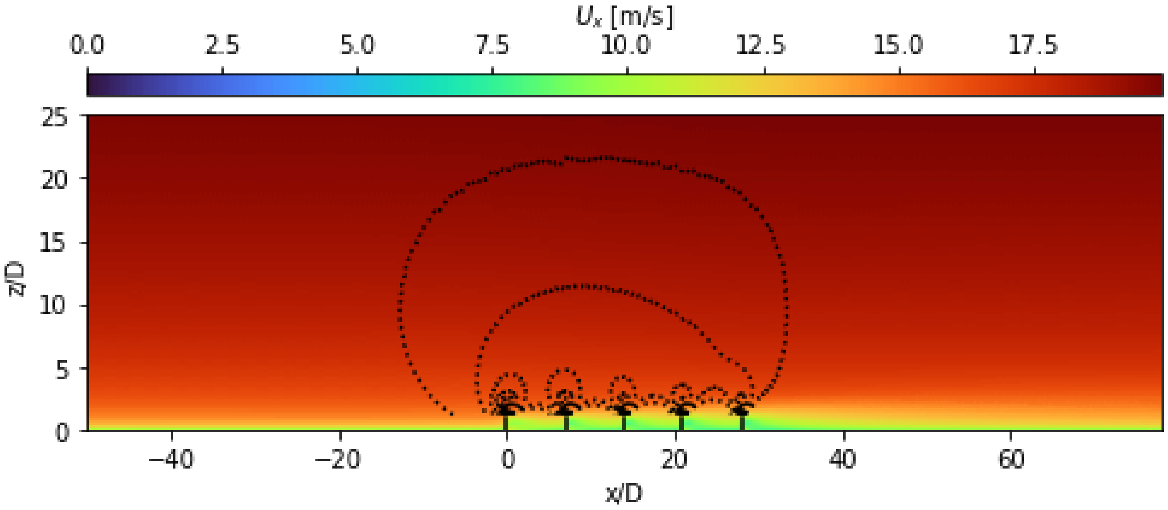

Figure 4.2: U_x field through column of turbines for dh-25. Wind turbine locations shown as black bars. Contour lines show U_z in increments of 0.03 m/s.

As the AD acts as a porous disc, much of the flow in the streamwise direction will move through the discs, however, some of the airflow will be diverted in the spanwise and vertical directions. Looking at the first row of turbines in figure 4.3, the spanwise and vertical velocity components demonstrate an increase in velocity around the discs. This brief visual assessment shows that the expected behaviour of the fluid is present and upstream blockage is observed.

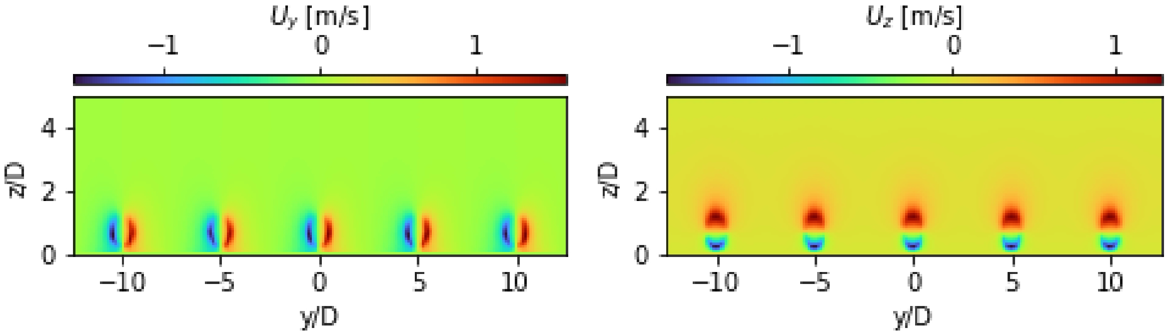

Figure 4.3: Lateral and vertical velocity at first row of turbines for dh-5.

In a addition to these visual checks, samples of velocity, pressure, and TKE are graphed through the center of the domain at hub height to analyse the flow through the fetch. Initial inspection of the velocity, pressure, and TKE sample through the domain shows similar behaviour in all simulations through the length of the domain, with differences in magnitude.

As discussed in chapter 1, as the flow approaches the wind farm, there is an expected decrease in velocity due to the force exerted by the rotor on the flow. The first graph in figure 4.4 shows the flow does indeed decrease with each respective turbine it encounters, and slowly recovers in the wake of the wind farm. Between the different domain height simulations, upon initial inspection, it appears that U_x is higher in shorter domain heights throughout the domain, with the difference increasing towards the end of the domain.

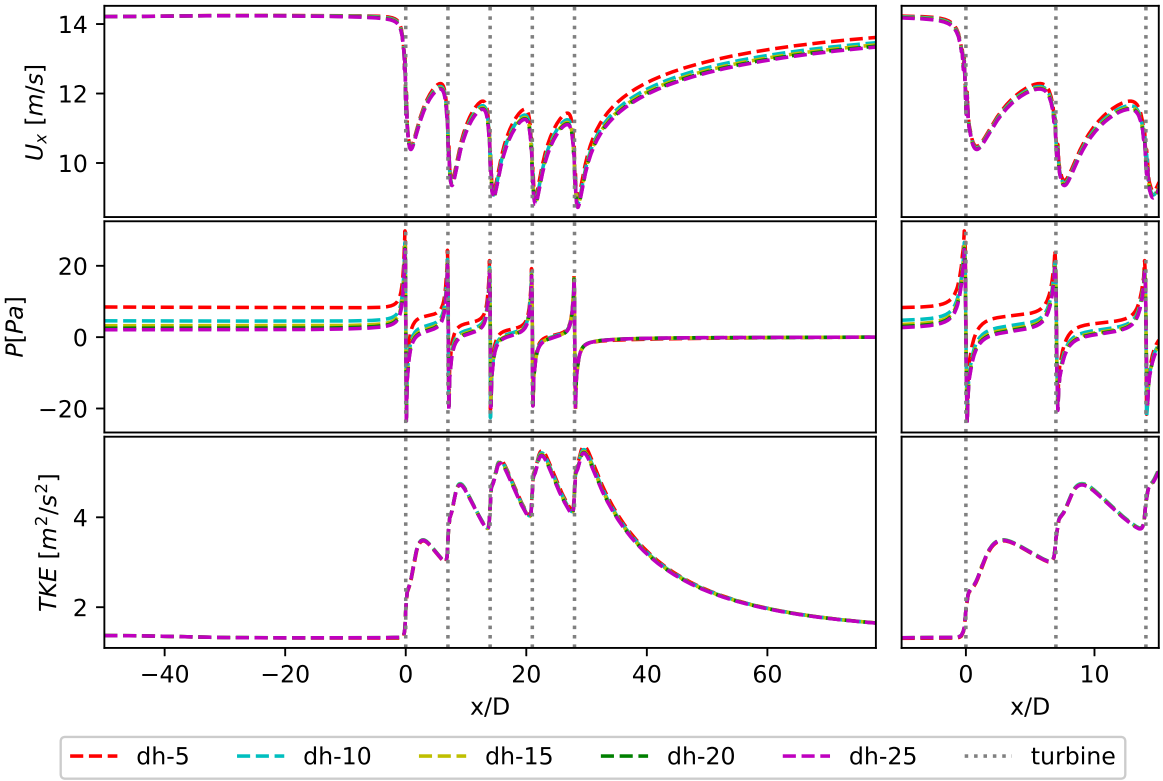

Figure 4.4: Streamwise velocity, pressure, and TKE through the center of the domain in the streamwise direction at hub height.

In regards to pressure, there is an obvious difference in magnitude between the simulations upstream of the wind farm. The shorter domain height simulations have a relatively higher pressure along the upstream area. As the air flows further along the x direction the differences in pressure between the simulations decreases. Immediately prior to the first row of turbines there is a spike in pressure followed by a drop, which is then repeated after each row of turbines. The differences in magnitude decreases after each row until the simulations converge to a constant pressure.

The TKE plot shows there is little to no difference between the domain height simulations in turbulent mixing throughout the entire domain, with an increase in turbulent energy following each interaction with a row of wind turbines as the wakes increase.

The general flow characteristics of the domain in all of the simulations fit the expected behaviour of flow through an infinite wind farm. To further investigate the difference between the numerical configuration i.e. the domain height, the flow will be more closely investigated upstream of the wind farm, as well as through and above the farm.

4.1.2. Behaviour of flow upstream of wind farm

As the main research question is to better understand how the numerical configuration affects the upstream flow blockage, the analysis of the domain height simulations will focus on the zone upstream of the first row of turbines. To identify the presence of upstream blockage the area from 0D to 20D upstream of the first row of turbines was investigated. Figure 4.5 shows the streamwise velocity at the spanwise center of the domain leading up to the first row of turbines for the different domain heights.

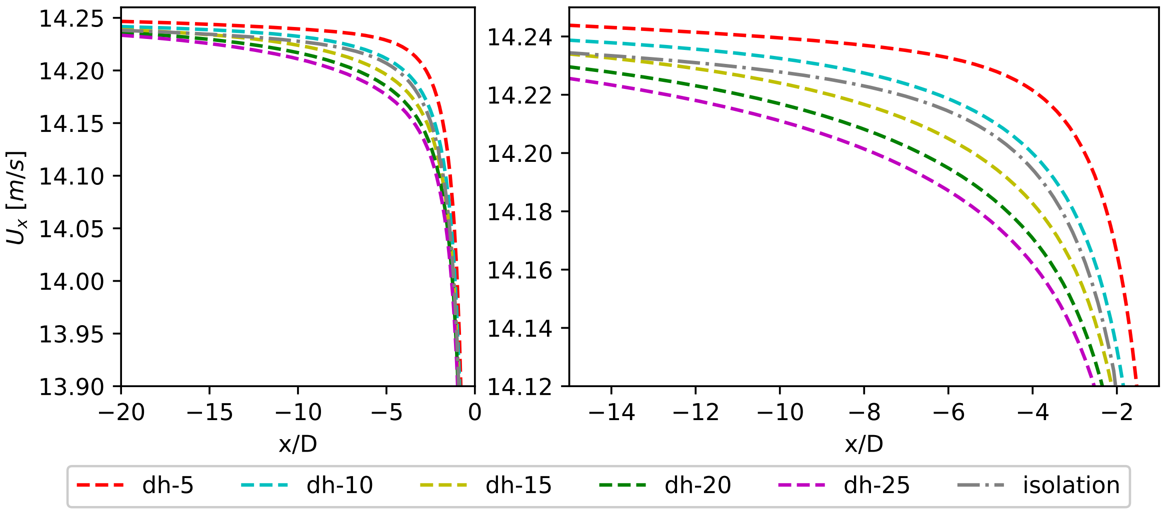

Figure 4.5: U_x upstream of first row of turbines for different domain height simulations. Shown isolation simulation is for a 25D domain height.

The figure on the right displays a smaller section of the upstream velocity to better show the difference in behaviour between the different domain height simulations. The induction of a single turbine with a simulated domain height of 25D is also graphed in order to compare the global blockage. It can be seen that upstream of the first row of turbines U_x is indeed decreased, i.e. blocked by the presence of the wind farm, confirming global blockage is present in the simulation.

Additionally, as can be seen from the figure on the right, as the flow approaches the turbines, it starts to behave closer to the normal expected induction. This leads to the idea that at some value close to the first row of turbines, induction has a higher impact on the flow behaviour than the combined blockage effect of the wind farm. When looking at how domain height changes the magnitude of the global blockage, it is apparent that as the vertical extent of the domain is increased, so is the blockage effect. Comparing inflow U_x between the turbine in isolation and the respective domain height simulations results in an increase in U_x of 0.18% for dh-5 and reduction of 0.23% for dh-25.

As RANS simulations must satisfy the conservation of mass and momentum equations discussed in chapter 3, if one component of the velocity is decreased then another must increase. To better understand the upstream blockage differences based on domain height, the remaining velocity components are investigated. Figures 4.6 and 4.7 displays the spanwise and vertical velocity components upstream of the first row of turbines.

Figure 4.6 shows expected flow behaviour upstream of the turbines close to the center of the turbine rotor. Relatively no impact on spanwise velocity component is observed until approximately 2.5D to 4D upstream of the turbine, where induction effects take effect. The flow is also virtually independent of domain height in comparison to the strong connection

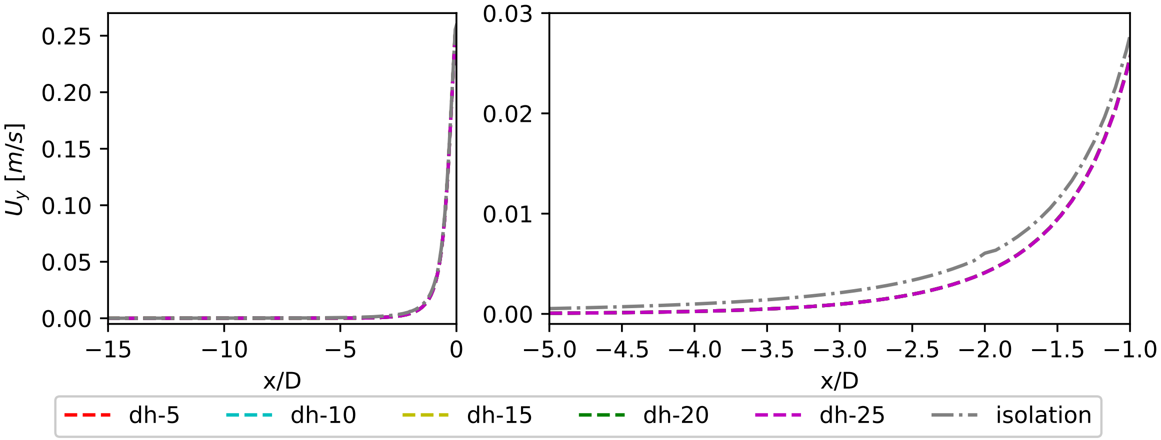

Figure 4.6: U_y upstream at the near center of the center turbine of the first row at various domain heights. Shown isolation is for 25D domain height.

observed in the streamwise velocity component. Additionally, the flow more closely follows the behaviour under the conditions of a turbine operating in isolation. As the wind farm is configured to be laterally infinite, this behaviour is expected as flow will be symmetrical along the y axis. If U_y is not greatly impacted by global blockage, the velocity changes demonstrated for U_x remain unaccounted for, which leads to the analysis of U_z.

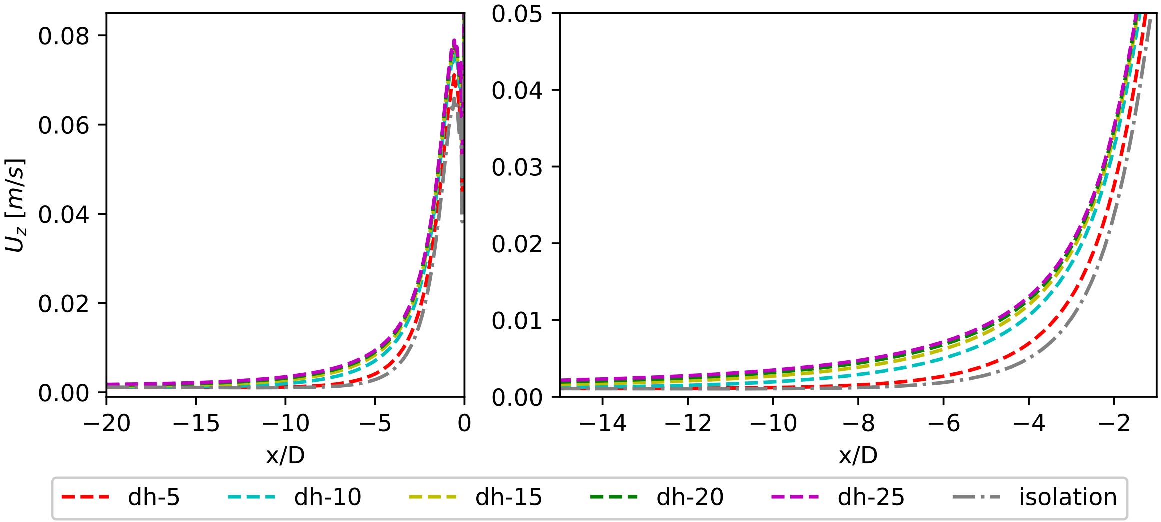

Figure 4.7: U_z upstream of the center turbine of the first row at various domain heights and theoretical induction. Shown isolation simulation is for 5D domain height.

A look at figure 4.7 shows behaviour more similar to that shown in figure 4.5, as there is a clear trend between the behaviour of U_z leading up to the first row of turbines and the domain height of the simulation. Firstly, looking at a turbine operating in isolation, the expected increase in vertical velocity is shown a few diameters ahead of the turbine. The general behaviour of the infinite wind farm simulations is similar, however, as domain height is increased, the increase in U_z is more drastic. The dh-5 simulation exhibits behaviour more similar to that of a turbine in isolation, with a relatively large jump to the dh-10 simulation, thereafter the vertical velocity component lines appear to converge as the domain height is increased. This increase in U_z implies that the momentum and mass transfer due to global blockage on the streamwise velocity is accounted for in the vertical velocity component. However, as this set of simulations utilizes the concept of an infinite wind farm in the lateral direction, this will be further investigated in the case there is a finite wind farm with varying domains in section 4.2.

It can be seen from the left hand graph of figure 4.5 that the velocity, begins to converge for the different domain heights further upstream. This raised the question as to where the domain height and blockage become independent from one another. To investigate this, several graphs were produced at various distances upstream from the wind farm, showing U_x across the spanwise direction.

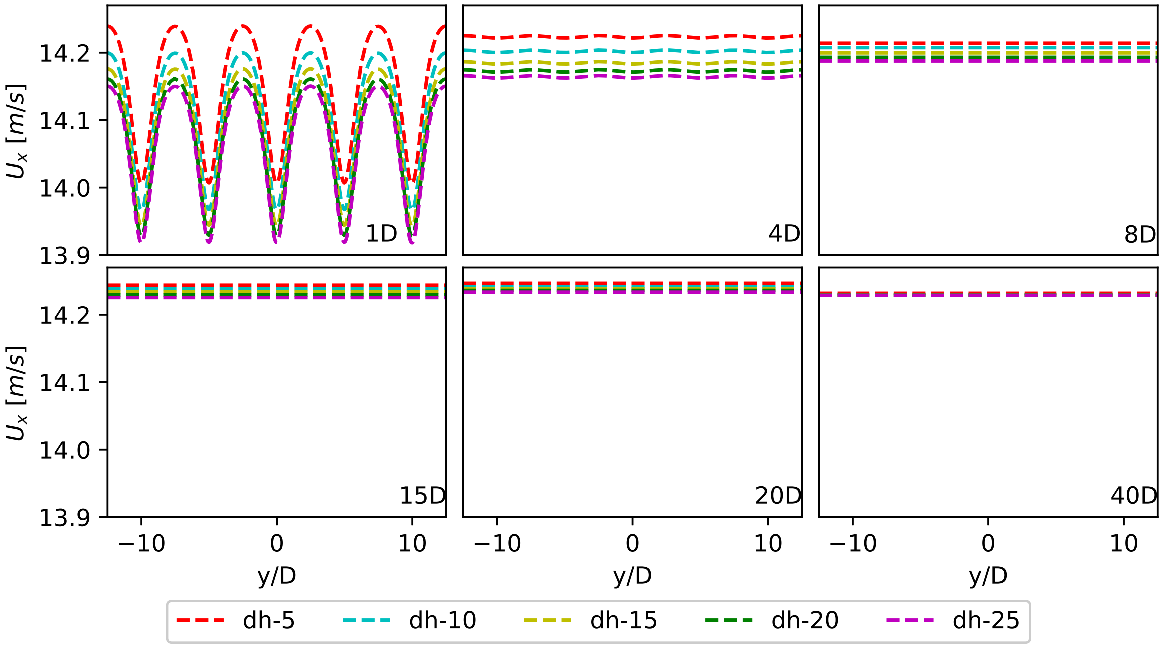

Figure 4.8: U_x at various distances upstream (indicated by label) of the wind farm for different domain heights.

Figure 4.8 provides some insight into the point where the blockage effect and chosen domain height become coupled. In regards to these sets of simulations, at some distance between 20D and 40D upstream, spanwise velocity is not impacted by the domain height, nor the existence of the wind farm. This result will be further analysed and discussed in section 4.3, where simulations with varying inlet distances are analysed for changes in upstream blockage.

4.1.3. Flow characteristics through and above wind farm

As there is an apparent link in upstream blockage and the domain height of a simulation, the flow of momentum through the wind farm and above it are investigated. To investigate whether higher domain heights allow for movement of energy above the wind farm, while lower domain heights restrict energy to flow through the wind farm, flow through and above the wind farm are analyzed. Figure 4.9 shows U_z above the wind farm for several domain heights. Through all the subplots, it is evident that the general shape of U_z is relatively the same, regardless of the domain height of the simulation.

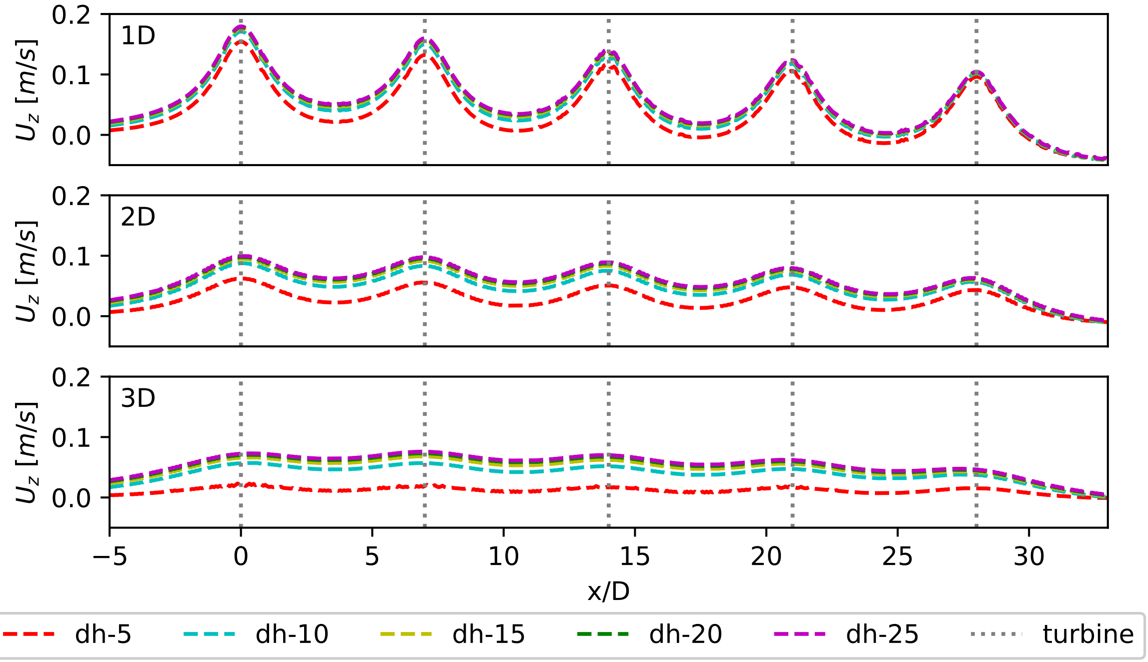

Figure 4.9: U_z at various heights above a laterally infinite wind farm (indicated by the label) for domain height simulations above center column of turbines.

Figure 4.9 shows that closer to the wind farm, the magnitude of the difference in U_z is quite small between different domain height simulations, as the sample point is moved further above the wind farm, to 2D and 3D above the farm, the difference in magnitude becomes more apparent. This leads to several conclusions. Firstly, that the larger domain heights do indeed allow for energy transfer to move in a more vertical fashion, above the wind farm, as opposed to a stricter horizontal flow. Conversely, at a low domain height, the flow is constricted to the wind farm area and there is less freedom in vertical movement.

As previously mentioned, there appears to be an increase in spanwise velocity between the wind turbines as shown in figure 4.1. Building upon this observation, several plots of U_x at various distances between two rows of turbines, shown in figure 4.10 are graphed in figure 4.11.

It can be seen that between the turbine rotors (1.25D and 2.5D) the streamwise velocities of the various domain height simulations increase as they encounter a row of turbines, then slowly reduce to a net decrease which grows after each subsequent row. This behaviour is expected as there is an initial constriction of flow between the columns of turbines which accelerates the flow, after which the velocities decrease due to turbulent interactions. At each sample line it is shown that as the flow moves through the wind farm the magnitude of the difference in U_x between domain height simulations increases. The largest difference can be seen in the zoomed in graphs on the left hand side. The differences are of similar magnitude, approximately 0.5 m/s between dh-5 and dh-25, regardless of the sample line chosen. This insinuates that the differences between streamwise velocities are constant throughout the span of the wind farm.

As previously mentioned and shown, it is suspected a shorter domain height confines the flow of mass and momentum to travel through the wind farm rather than over it. This is in accordance to what is shown in figure 4.11. As the streamwise velocity at the dh-5 and dh-10 domain heights experience the largest U_x values throughout the span of the wind farm. As the height of the domain increase, the streamwise velocities decrease, and the simulation results begin to converge.

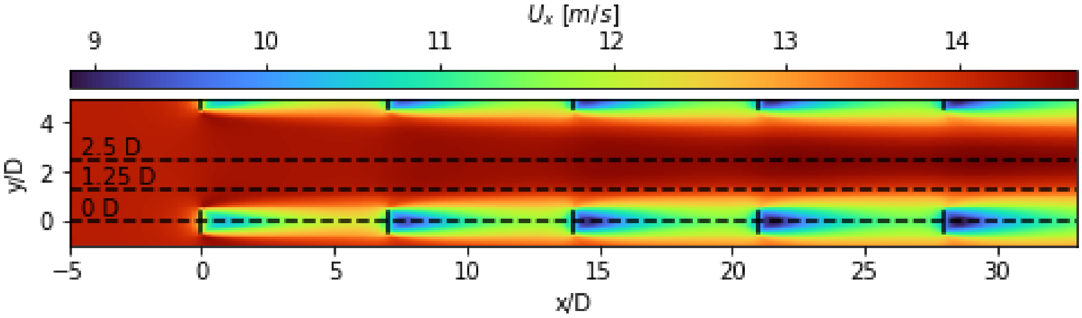

Figure 4.10: U_x sample locations between turbines columns for infinite lateral wind farms.

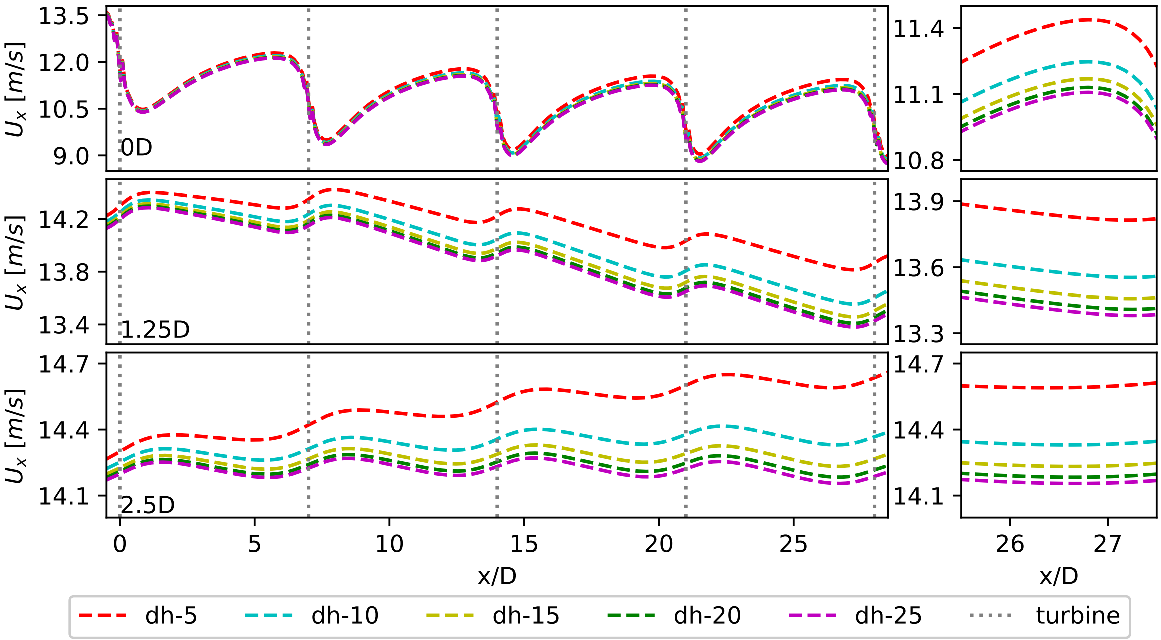

Figure 4.11: U_x between turbines at hub height for different domain height simulations. Graphs on the right are zoomed in versions of graphs on the left.

As the flow of momentum through the domain has been identified for the different domain height simulations it is clear that domain height as a clear impact on the flow field and resulting upstream blockage. These impacts are further discussed in the following subsection especially as they relate to the research questions.

4.1.4. Discussion of main results

There are several important conclusions that can be drawn from these results. Firstly, the domain height of a simulation can have a large impact on the resultant upstream flow blockage. As seen in section 4.1.2, the inflow spanwise velocity decreases more drastically for simulations with higher domain heights. The differences in upstream blockage between larger domain heights is smaller than when comparing to the shortest domain heights. Therefore, it is thought that at some domain height, global blockage will become decoupled from domain height. Additionally, that for shorter domain heights (less than 15D), blockage is not evident as the inflow velocity is greater than the respective velocity of a turbine operating in isolation. The magnitude of the change in U_x ranges from an increase of 0.18% for dh-5 to a decrease of 0.23% for dh-25.

There is a clear difference in magnitude between upstream blockage and domain height. However, the general behaviour of the velocity components over space are relatively consistent and well matched between results. This leads to the conclusion that the domain height of the simulation does not observably impact the shape of upstream flow blockage in a laterally infinite wind farm. Due to these observations a domain height of at least 15D is recommended to ensure the capture of upstream blockage.

To understand how the mass and momentum of flow are conserved between the different simulations an analysis of the other velocity components and look at prior knowledge is important. Comparing figures 4.5 and 4.7, it is deduced that having a larger vertical domain allows for the flow of energy to circumvent the wind farm. This concurs with the ideas covered in chapter 1 that wind farm interactions can cause the farm to act as a single blockage entity. As there is an expansion of flow in the wakes, there is opportunity for wake interactions between adjacent wind turbines to perhaps have compounding effects on the surrounding flow. This is supported by figure 4.11 as the difference in streamwise velocity between domain height simulations increases with each subsequent turbine row interaction. Therefore, the inherit momentum deficit in wind turbine wakes which recoups momentum from surrounding flow is highest for the larger domain height simulations, which also have the highest simulated upstream blockage.

4.2. Lateral extents of domain

When modeling a finite wind farm the lateral extent are often set far from the farm to reduce interference in the simulation. The lateral distance from the wind farm, does not represent real physical bounds and therefore should not impact the flow. It is not quite known at what distance from the finite wind farm, the sides should be located to produce proper blockage results. Additionally, as discussed in chapter 2, there is some conflicting opinions on whether global blockage is an energy loss or simply an energy distribution. Modelling a finite wind farm with varying lateral extents provides insight into this discussion.

This section covers the impact the distance from a wind farm to spanwise domain boundaries has upon the flow field, specifically as it relates to upstream blockage and the possible redistribution of energy through the farm. The general flow behaviour is analysed and broken down to understand the flow of energy through the domain. A general discussion of the main results concludes this section.

In testing the impact of lateral extent on the flow field, the other domain boundaries are set far away from the finite wind farm reduce distortion of results. The BCs chosen follow those given in chapter 3, as such the lateral boundaries which are set as symmetric BCs and provide a impermeable, frictionless, zero gradient boundary for the flow. The narrowest lateral extent is set to 2.5D from the farm and the widest domain is set to 20D from the wind farm with 3 additional domain extents in between. These domains are set in order to analyse how the flow behaves with very little space for spanwise flow around the farm to a large expanse for lateral flow. A total of 25 wind turbines make up the finite wind farm, with a laterally symmetric 5x5 array with 5D spanwise spacing and 7D streamwise spacing.

4.2.1. General flow behaviour through the fetch

The initial analysis of the flow behaviour is intended to identify changes in the behaviour in the domain at various lateral extents. The general flow behaviour is consistent with the baseline physical behaviour of airflow through a wind farm, as discussed in chapter 1. Figure 4.12 demonstrates the z-plane view at hub height for the widest lateral extent simulation. There is observable growing wakes after each row of turbines which slowly recovers towards the end of the domain. Additionally, there is clear interactions at each of the 25 turbines. Measurable upstream blockage is also shown, far exceeding the typical induction extent. Finally, there is no major changes in flow at the end of the lateral extents which are far from the finite wind farm.

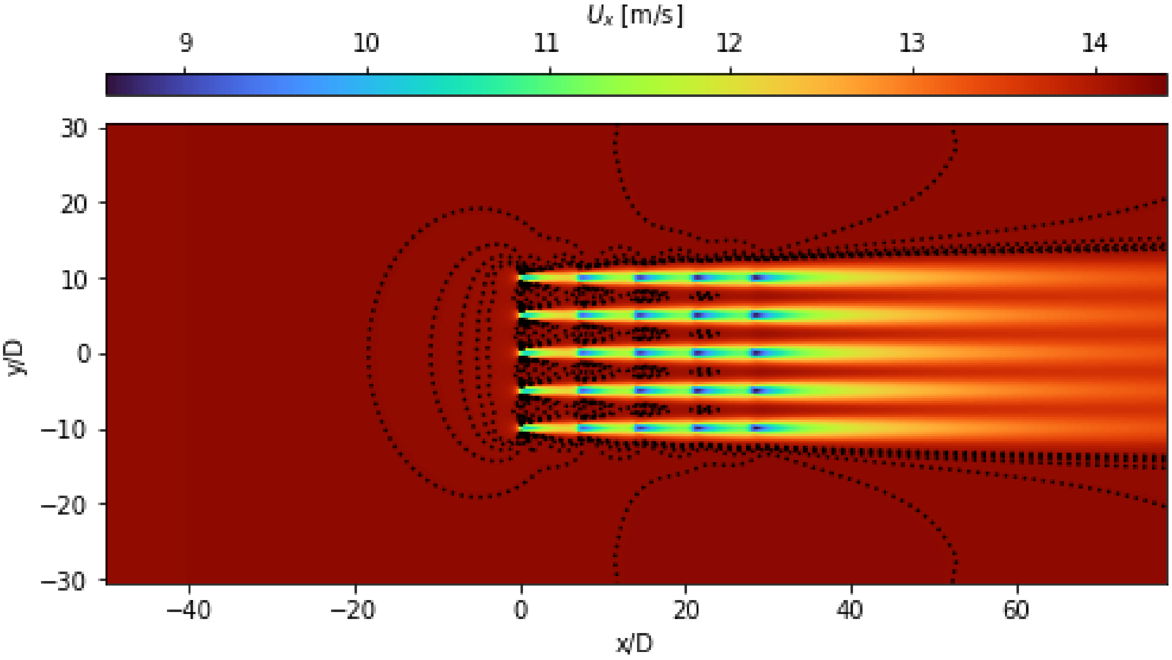

Figure 4.12: U_x at hub height for le-20. Contour lines show lines of equal U_x in increments of 0.02 $[m/s]$

The contour lines show lines of equal U_x through the domain with U_x decreasing upon approaching the wind farm. Upstream blockage is observed as the lines preceding the wind farm from approximately 4D to 30D upstream of the wind farm. The line upstream and closest to the first row of turbines appears to demonstrate the induction extent of about 4D preceding the wind farm as there is still identifiable interaction with each individual turbine.

Additionally, the contour lines show curvature in the upstream blockage which shows a peak at the center column. The blockage shows some overflow to the outer columns of the wind farm which then slightly oscillates at the outer column to the end of the wind farm. The outermost upstream blockage contour line for le-20 connects directly to the first row of turbines. The oscillations at the outer columns of turbines appear larger on the wider domain, hinting at increased velocities around the outer row.

As previously stated, there is some contention in whether upstream blockage is an energy loss or redistribution. Looking at figure 4.12 the contour lines show increasing velocity along the outer columns of turbines as well as between the individual turbines. This will be further analysed in subsection 4.2.3.

Similarly to in section 4.1, a vertical slice of the velocity in the streamwise direction was taken of the domain to ensure proper boundary layer development for the various wind simulations. The results showed no differences in the boundary layer development between the different simulations. Similar graphs for U_x, P, and TKE were also graphed through the center turbine as an initial check of proper flow behaviour and to determine where the simulations may differ. Figure A.10 shows that there is little to no change in the values for each variable through the center column of the finite wind farm and demonstrates expected flow interactions at each wind turbine with the fluid.

A visual check of the first row of turbines (figure A.13), shows the spanwise and vertical velocities for two lateral extents. Although there are no apparent differences between the lateral extents, the magnitude of the velocity changes is quite small as mentioned in subsections 4.1.2 and 4.1.3. As the simulations are of a finite wind farm, there is expected differences in all velocities from turbine to turbine due to the nature of global blockage. As such, the first row of turbines is analysed in depth in section 4.2.2 to identify these differences.

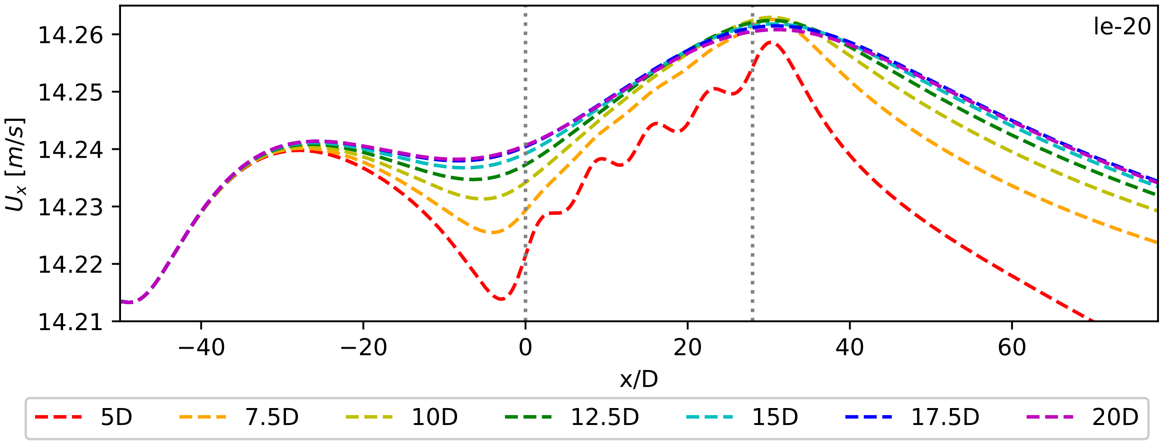

Figure 4.13: U_x sampled at hub height at various lateral distances from the center of the outside column of le-20.

Figure 4.13 demonstrates the streamwise velocity flow behaviour along the open space between the wind farm and lateral boundaries. It can be seen that the wind farm impacts the airflow along the sides throughout the entire domain. The streamwise flow is decreased as the flow approaches the wind farm and recovers momentum along the length of the farm, until it begins to decelerate in the outlet area. As the wind turbines operate as momentum sinks, the decrease in velocity upstream of the flow indicates blockage extending to the entire lateral extent, starting at approximately 30D upstream. However, as the flow accelerates along the lateral extents of the domain even though the wakes should be pulling in momentum along the extent of the farm to fully recover. This indicates that a large lateral extent may produce flow which directs airflow out of the wind farm to the lateral extents. The reduction in streamwise velocity is seen in the area following the farm, where turbulent wakes are expected to recover through interactions with the free flow. This is further investigated and analysed in the following subsections.

4.2.2. Behaviour of flow upstream of wind farm

The upstream blockage of the lateral extent simulations is of interest in analysing how the lateral boundaries may impact the magnitude and shape of the inflow velocity. Additionally, as the simulations contain finite wind farms, the difference in behaviour for each turbine in the front row is of interest in helping determine if upstream blockage is indeed energy redistribution or energy loss.

Looking first at the difference in magnitude of upstream blockage between the various lateral extents, velocity lines through the outside column of turbines are graphed in figures 4.14. The outside column of turbines is chosen, as this is where the differences between simulations should be most apparent. The isolation simulation represented in figure 4.14 is for a domain with lateral extents of 20D on each side of the turbine.

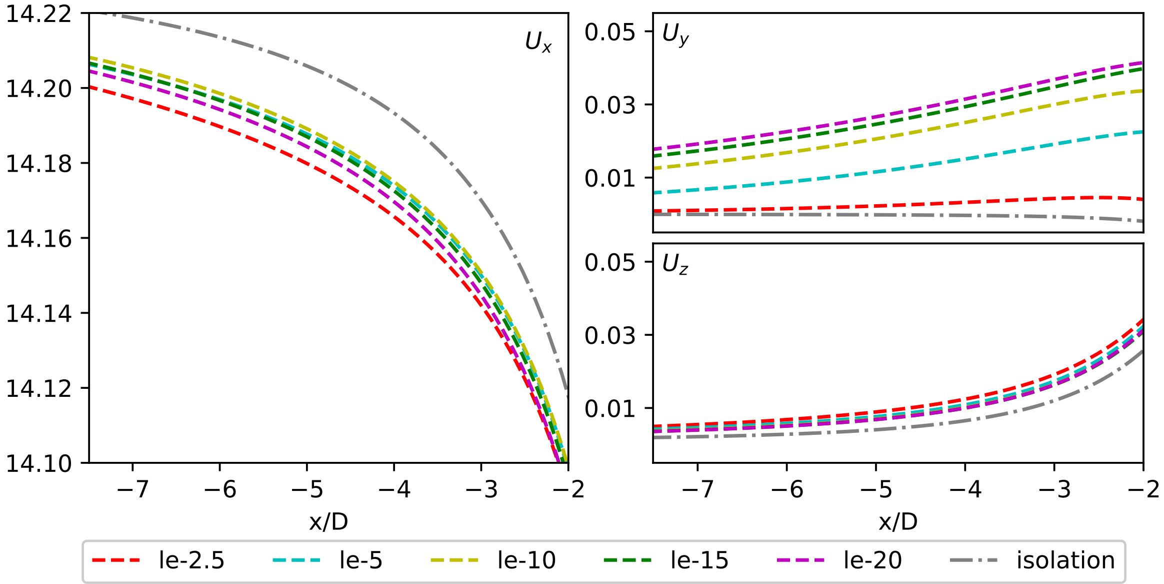

Figure 4.14: Velocity components (in m/s) upstream of outer column of turbines for lateral extent simulations. Components indicated by labels in upper corners. Scaling is approximate.

From figure 4.14, it can be seen that blockage is present at all lateral extent simulations as the streamwise velocity component is lesser than that of a turbine in isolation. Almost all the simulations follow the trend of increasing blockage with increasing lateral extent, however, le-2.5 demonstrates the largest blockage at the outer column of turbines. The total difference in U_x between simulations is relatively small, on the order 0.0085 m/s at 2.5D upstream of the wind farm. At the same location, in comparison to the turbine operating in isolation, streamwise velocity is decreased by $0.13 - 0.19\%$ between the lateral extent simulations.

Turning to the spanwise velocity component shown in figure 4.14, it is clear the narrower the domain the slower U_y is upon approaching the first row of turbines. The total difference between simulations for U_y 2.5D upstream is approximately 0.0334 m/s. This is contrary to the results seen in section 4.1, which saw no identifiable changes in lateral velocity. As finite wind farms are being used for these simulations, it is assumed this is due to the velocity being able to move more freely in the lateral direction, as there is unimpeded channels on each side of the wind farm.

Finally, analysing the vertical velocity component upstream of the finite wind farm in figure 4.14, it is shown that all finite wind farm simulations have an increased vertical velocity compared to a turbine operating in isolation. The results for all of the simulations are relatively well matched with a very slight increase in U_z as the domain lateral bounds are narrowed. A total change in U_z at 2.5D upstream of 0.0028 m/s is observed between simulations. This may be due to the constriction of flow along the sides of the wind farm which force the flow up and over the wind farm.

As global blockage is generally increased with lateral extent, the kinetic energy must be transferred to either the spanwise or vertical velocity components. The results of figure 4.14 show that for wider domains, there is more kinetic energy transferred to the lateral velocity component. However, to better understand the shape and magnitude of the upstream blockage, the velocities preceding each turbine in the first row are shown in figure 4.15.

It can be seen that the streamwise velocity for le-2.5 behaves close to that of an infinite wind farm such as those presented in section 4.1. There is relatively no change in velocity components between the turbines and the flow exhibits the most upstream blockage and highest values for U_z, although still relatively small. The remaining lateral extent simulations demonstrate the greatest blockage (i.e. decrease in U_x) at the center turbine which is expected. The maximum reduction in U_x of 0.31% is located at the center column of turbines for le-20.

Additionally, it can be seen that towards the outer columns U_x and U_y increase. However, the rate of increase is lower for U_x and higher for U_y as lateral extent is increased. U_x reaches a maximum at the outer columns of the first row, as all simulations demonstrated blockage at the outer column (figure 4.14), it is expected that blockage will be deemed a net loss of energy rather than energy distribution. This will be evaluated in subsection 4.5.2.

Through these results it is implied that upstream blockage is linked to the lateral extent of a simulated domain. The wider the domain the more blockage will be observed, however, the general shape in velocities across the first row is highly similar between all simulations except

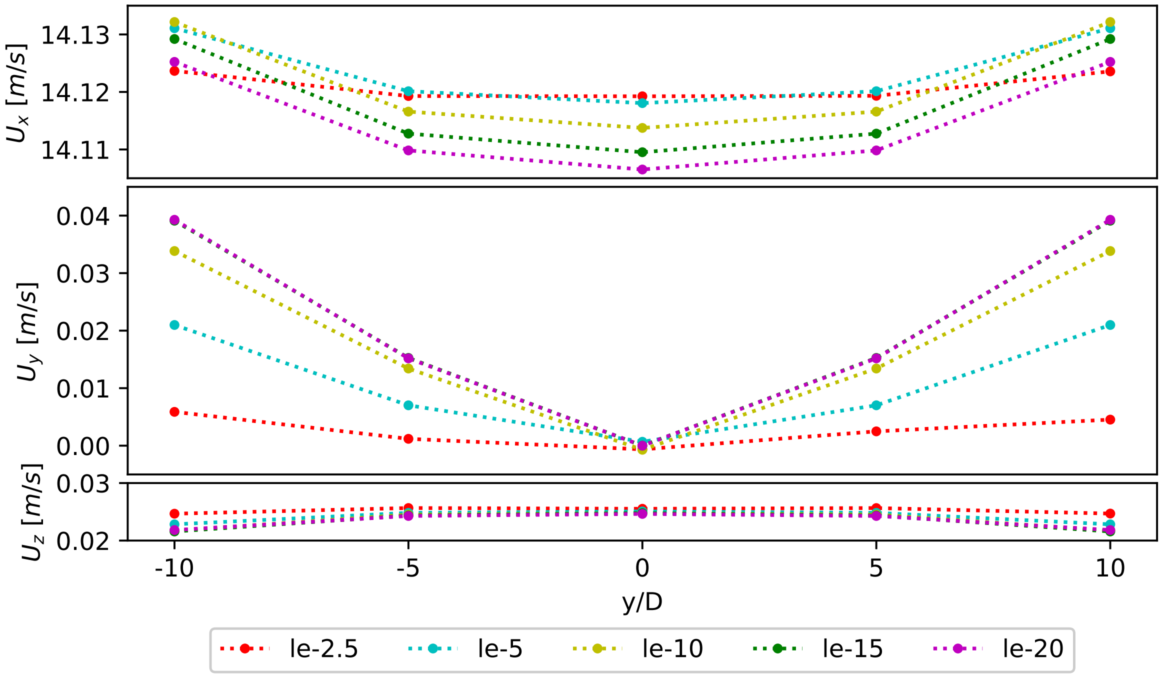

Figure 4.15: Velocity components 2.5D in front of first row of turbines. U_y is taken as the absolute value to account for directional sign. Scaling is approximately even between sub-figures.

le-2.5. As such, an extremely narrow (domain such as used in le-2.5) will exhibit behaviour reminiscent of a laterally infinite wind farm, consistent flow across the first row of turbines and and affinity for flow to be diverted in the vertical direction. To further investigate the flow field and links to upstream blockage and lateral extent, the flow behaviour in the remainder of the fetch is investigated.

4.2.3. Flow characteristics through and above wind farm

Firstly looking at the flow through the finite wind farm provides insight into the differences between lateral extent simulations. To investigate the difference between flow behaviour between columns of turbines, figure 4.17 shows the velocity at hub height for the lateral extent simulations for locations shown in figure 4.16.

As was seen in the inlet flow, the airflow behaviour within the central columns of turbines are relatively well matched for streamwise velocity. U_x between the turbine rows in figure 4.17 shows a similar pattern and magnitude throughout the length of the wind farm. The same distance along the outer row of turbines demonstrates quicker velocities which coincides with what is seen in figure 4.15. Comparing the behaviour between lateral extent simulations, it is seen that wider domains have relatively slower streamwise velocities between turbine columns and along the outside column.

The spanwise and vertical velocity components between the turbines provide further insight into the fluid motion. The further from the center of the wind farm, the faster and more varied U_y and U_z are between different domain sizes. For spanwise velocity, the narrower the domain the slower the velocity component, insinuating the constriction of flow to the vertical and

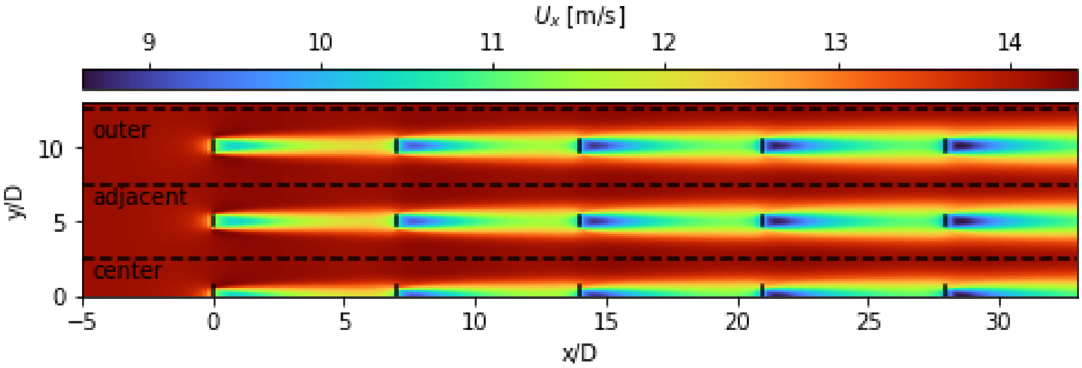

Figure 4.16: Sample locations between turbines columns for finite wind farm.

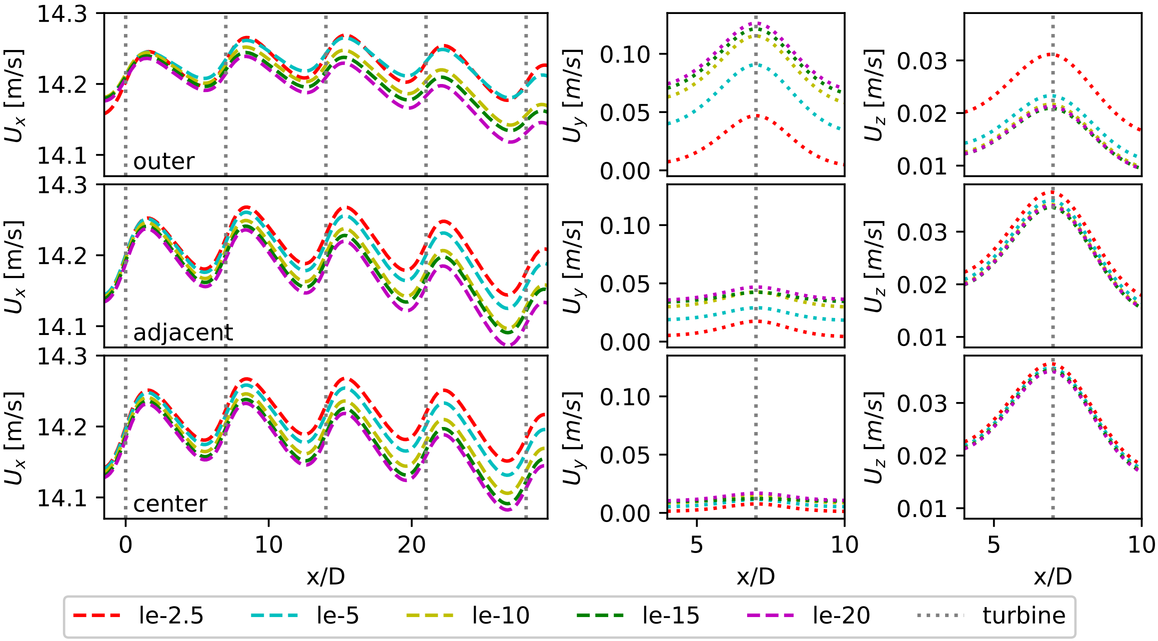

Figure 4.17: U_x, U_y, and U_z between columns of turbines at hub height for finite wind farms.

streamwise components. This is supported by the U_z components which shown the narrowest domain has the highest vertical velocity between columns, especially so at the outside of the wind farm.

Moving to the area above the wind farm, figure 4.18 shows the spanwise and vertical velocities above the wind farm at the center row of turbines. Coinciding with previous figures, the narrow domains continue to display increased vertical velocity and lower spanwise velocity. However, the behaviour of the vertical velocity is relatively well match and consistent through the width of the wind farm for all simulations. Additionally, at both sample heights, U_y demonstrates a gradual increase for all simulations (excluding le-2.5), towards the outside of the farm which agrees with the upstream flow behaviour as shown in figure 4.15.

Looking to the area between the wind farm and lateral boundaries, U_x for all domains shows a minimum at the start of the wind farm and general increase over the span, indicating a transfer

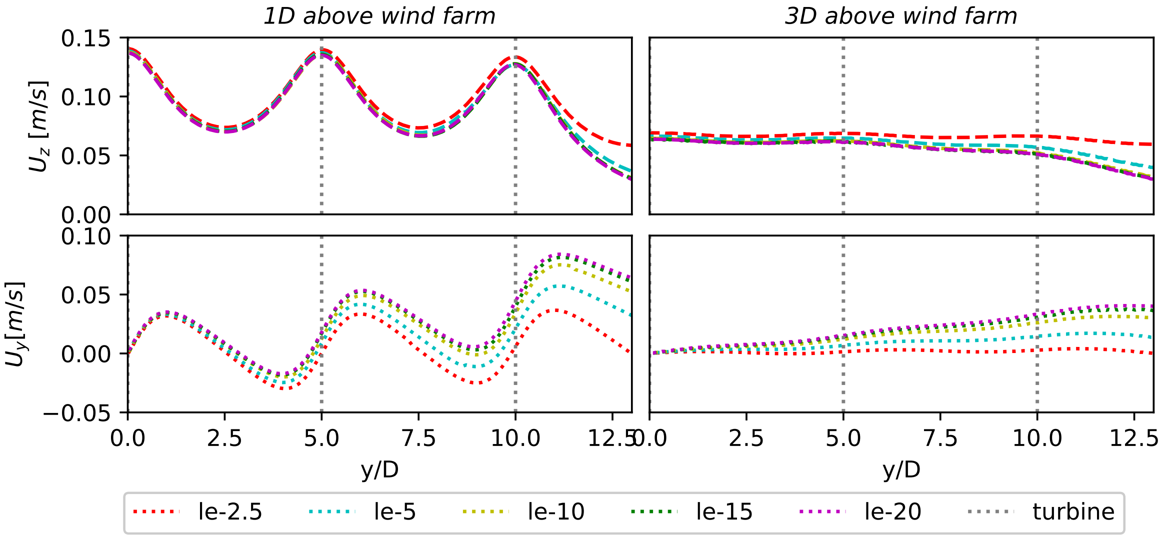

Figure 4.18: U_z and U_y at various heights above the center row of turbines for lateral extent simulations.

of momentum to the space between the wind farm and side boundaries. Again the narrowest domain exhibits very low U_y values in comparison to the wider domains, as seen in figure 4.19. Meanwhile, the wider domains have higher lateral velocities which steadily decrease along the length of the wind farm. Vertical velocity is highest for the narrow domain, but also decreases along the wind farm. Generally, the figure shows that for wider lateral extents the flow of momentum is in the lateral direction rather than vertical, with the opposite being true for the narrower domains.

Analysing the flow through, around, and above the finite wind farm gives insight into how constricting lateral extents can impact preferential pathways for the flow of momentum. Wider domains result in more lateral movement through the wind farm and towards the sides of the domain. Meanwhile, narrower domains constrict the flow to streamwise and vertical movement, both through and above the wind farm. The general results of the changes in lateral extents as they pertain to the upstream blockage and flow field in the domain are discussed in the following subsection.

4.2.4. Discussion of main results

In regards to the lateral extent of a simulation, there are some main points to highlight. Firstly, all simulations resulted in decreasing U_x in the upstream area of the domain. The scale of the upstream flow blockage is relatively consistent with expected values, as a minimum of 0.13% and maximum 0.31% reduction of U_x, in comparison to a turbine in isolation, is observed. Generally, at wider domains the reduction in upstream streamwise velocity is higher, i.e. more blockage is observed. However, at le-5 and le-2.5, this trend breaks down, especially along the outer row of turbines.

Excluding le-2.5, the general shape of the velocity components is consistent between simulations, with highest blockage at the center column and lowest blockage at the outer columns. This indicates that the shape of upstream blockage is independent of lateral extents at values

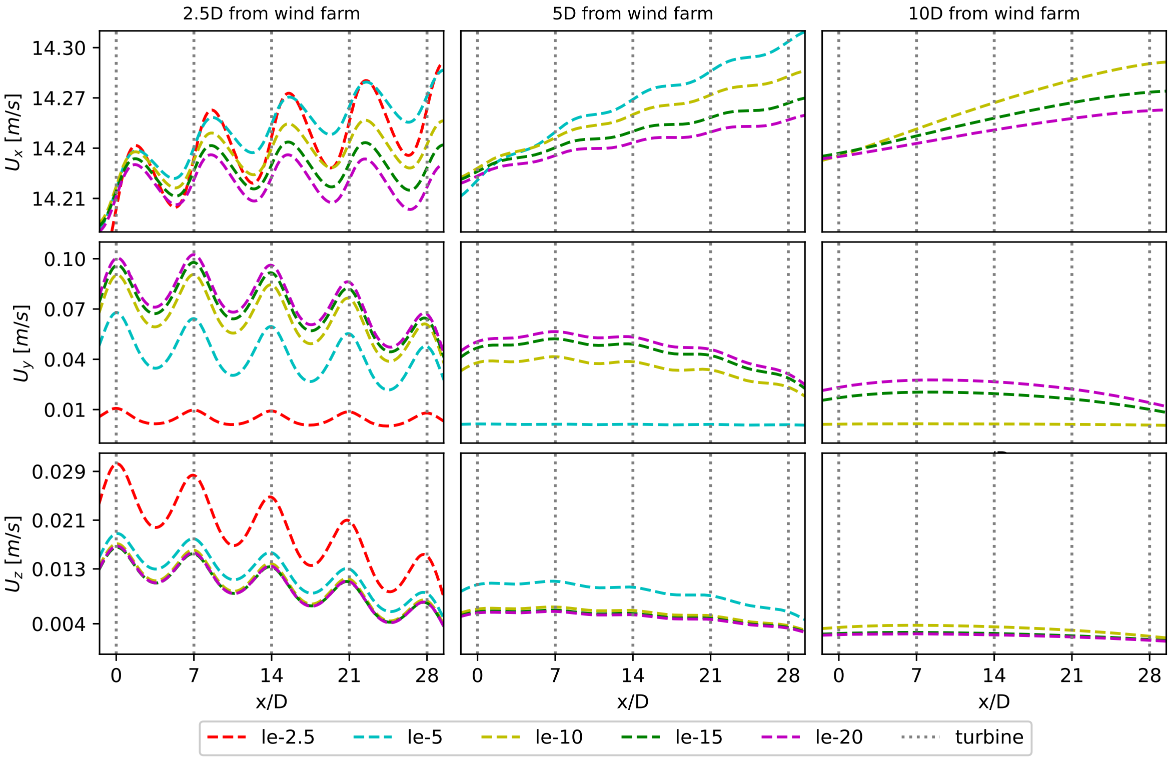

Figure 4.19: U_x U_y, and U_z at various lateral distances from the wind farm.

at and wider to 5D. At narrower lateral widths, the flow field behaves similarly to that of an infinite wind farm and the shape of upstream blockage is relatively linear across the spanwise direction.

Additionally, under very narrow simulation widths, flow to be confined to the wind farm and above it, resulting in higher streamwise velocities through the farm. As the lateral extent is widened, flow of momentum will prefer lateral movement around and out of the wind farm. This lateral movement is most evident at the outer column of wind turbines.

Due to general trends in the flow behaviour, a lateral extent of at least 10D on each side of the finite wind farm is suggested in modelling upstream blockage and flow through a finite wind farm.

4.3. Inlet distance

As global blockage is a backward looking impact of wind farms on the upstream flow, setting a proper inlet distance is important to ensure adequate representation and space for the development of blockage. Additionally, as it is not yet known how far upstream blockage extends, there is not an appropriate gauge to determine the sizing of the inlet distance. Choosing an inlet distance that is too short could distort the flow behaviour through the entire domain by not allowing for proper formation of upstream blockage. Additionally, modelling a superfluously large inlet distance could add unnecessary computational and time costs.

In order to investigate the impact of inlet distance on upstream flow blockage, a laterally infinite wind farm is simulated with 5 rows of turbines spaced 7D behind the preceding row, with cyclic lateral BCs. A laterally infinite wind farm is utilized in the same manor and reasoning as in section 4.1. The domain dimensions are set to a height of 25D, lateral distance of 2.5D from the center of the rotor to the cyclic lateral BC, and outlet distance of 50D. Inlet distance in the range of 15D to 100D from the first row of turbines are tested in this manner, with a total of 5 distances simulated.

An initial analysis of the general flow through the domain to check for errors and trends is discussed first. This is then followed by an in depth discussion of the upstream area for global blockage trends and to determine the impact of the inlet distance. An analysis of the flow through the wind farm is then carried out to better understand the impact on flow behaviour of inlet distance. Finally, a discussion of the main findings of the simulations are discussed.

It should be noted that although the log-law is set at the inlet BC through the Richards and Hoxey, 1993 BCs, there is still a slight error in the area upstream of the wind farm which was discussed in section 3.2.2. This error especially impacts this investigation as the simulations will have varying error due to the differing inlet distances. To remove this error and properly investigate the upstream blockage, empty domains with the same dimensions and BCs were run for the same convergence criteria. The flow through the wind farm domains were then normalized against this empty domain and the inlet profile imposed upon the domain. In this manner, the small increase in inlet velocity is removed and the correct log-law profile is imposed upon the velocity profile.

4.3.1. Initial analysis of flow through the fetch

The initial analysis first looks to determine that proper flow behaviour is exhibited through the domain as discussed in chapters 1 and 2. General flow behaviour through the fetch is consistent with expected flow behaviour such as decreasing velocity and increasing pressure at each turbine. All domains exhibit proper wake development and dissipation, increasing velocities between turbine columns, and laterally symmetric contour lines associated with a laterally infinite wind farm.

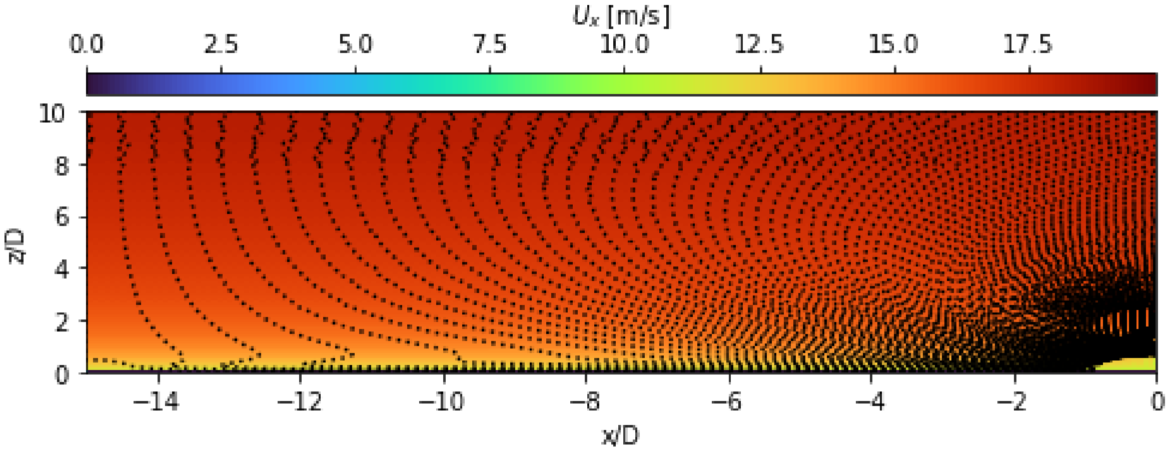

Figure 4.20: U_x slice of up-15 through center row of turbines with U_z contour lines.

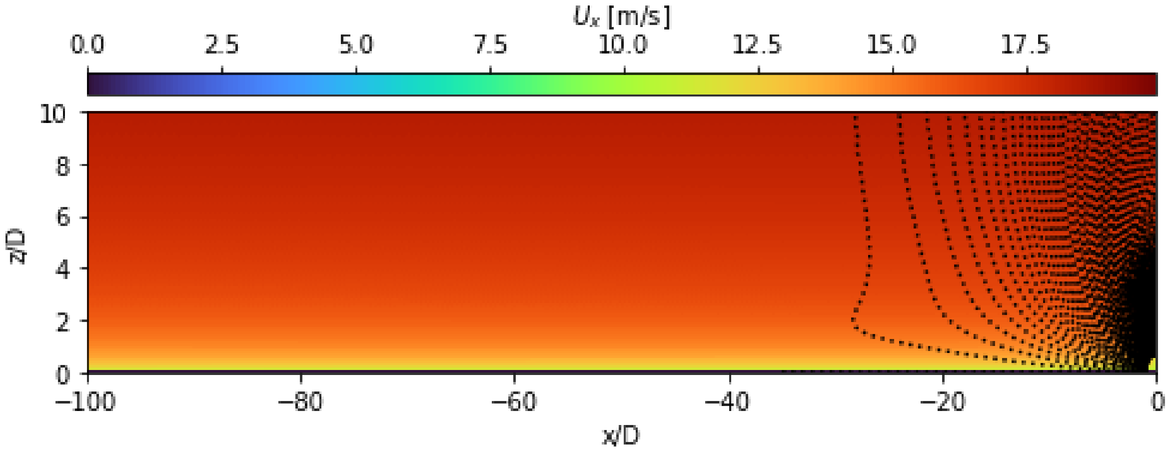

Figure 4.21: U_x slice of up-100 through center row of turbines with U_z contour lines.

Figures 4.20 and 4.21 provide some context into the flow behaviour upstream of the wind farm. The contour lines show the vertical velocity lines at intervals of 0.001 m/s, increasing in the positive x direction. In up-15 the velocity lines extend through the domain, while in up-100, these lines extend to approximately 28D upstream of the wind farm. As was seen in the domain height simulations, with a vertical extent of 25D, the flow of mass and momentum are generally above the wind farm through the vertical velocity component. From figure 4.21 it appears that this effect is present at between 20D to 40D upstream of the wind farm. In simulations with less than 50D inlet distance, such as in figure 4.20, the contour lines extend through the entire expanse of the upstream area. Domains with higher than 50D inlet distance show an area upstream at which U_z increases, insinuating the start of upstream blockage.

To further investigate the extent of upstream blockage and the impact varying inlet distance has on the blockage magnitude, the flow in the area upstream of the wind farm is further analysed in the proceeding subsection.

4.3.2. Upstream flow

As is seen in figures 4.20 and 4.21, the upstream blockage may have an impact through around 40D upstream of the fetch. In order to better understand the distance upstream blockage extends from the wind farm, it is important to separate it from induction effects defined here as the velocity upstream of a turbine in isolation. For the purposes of this investigation, upstream blockage will be *detected* when the difference between the induction velocity and laterally infinite wind farm velocity is greater in magnitude than 0.01% of the inlet velocity. This value is set to ensure early detection of upstream blockage without overestimating the extent upstream.

Figure 4.22 shows that for inlet distance simulations with extents greater than or equal to 50D, the upstream blockage extends from approximately 30D to 31D. Up-15 and up-25 simulations with less than 50D inlet distances result in upstream blockage within 5D of the inlet boundary as can be seen in figure 4.22. From these results, it is apparent that global blockage extends to approximately 30D upstream under the specified wind farm configuration.

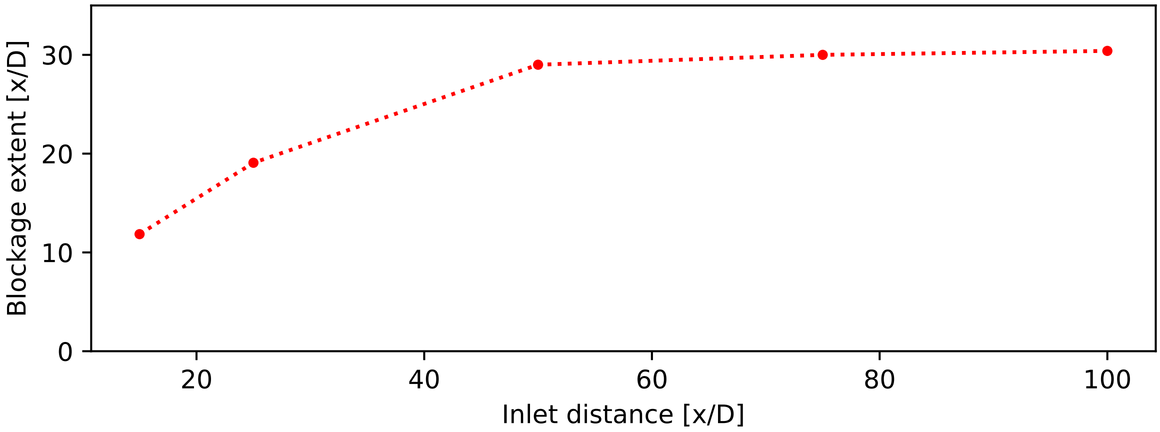

Figure 4.22: Upstream extent of global blockage from various inlet distance simulations.

Moving closer to the wind farm to understand the impact of inlet distances, figures 4.23 and 4.24 provide a closer look at the upstream blockage. It can be seen that for up-15 and up-25, U_x exhibits less global blockage in comparison to the larger inlet distance domains. For up-15 the reduction in U_x is approximately 0.01 $[m/s]$ or 0.12%, compared to a turbine in isolation. Meanwhile, up-50, up-75, and up-100 demonstrate extremely close behaviour approaching the first row of turbines in regards to the streamwise velocity. The reduction in U_x compared to a turbine in isolation for up-50 is 0.03 $[m/s]$ or 0.22%. All simulations do demonstrate blockage in comparison to the inlet velocity of a turbine in isolation, however, the difference between simulations is an order of magnitude in regards to velocity reduction. The isolation simulation shown in figures 4.23 and 4.24 is for a 50D inlet distance.

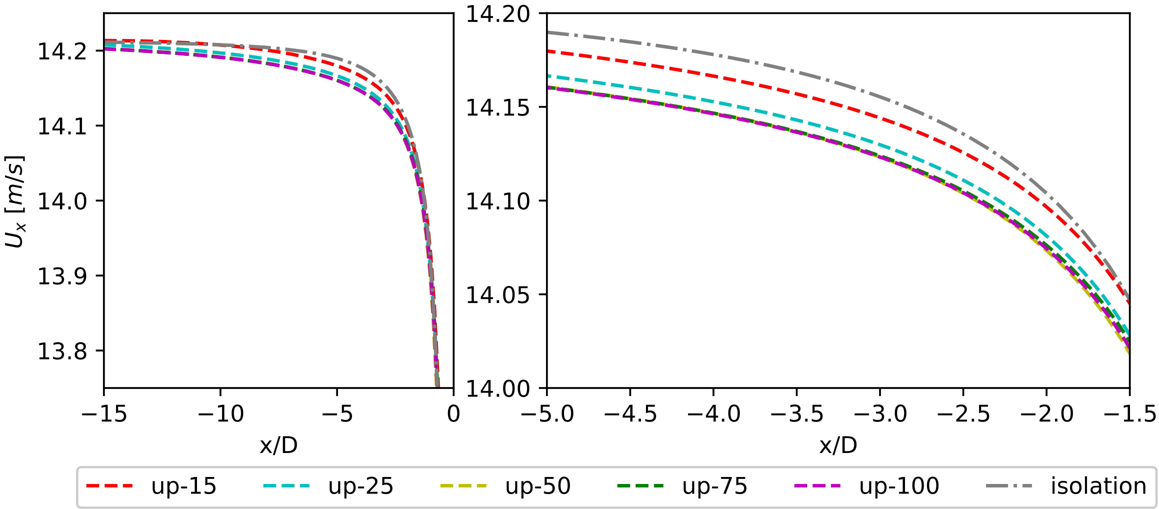

Figure 4.23: U_x upstream of infinite wind farm for inlet distance simulations.

In contrast to U_x, U_y for all the simulations are well matched, which is also seen in subsection 4.1.2, as this behaviour is expected for a laterally infinite wind farm. As the flow of mass and momentum must be conserved, the varying velocity seen in U_x upon approaching the wind farm must be accounted for in the remaining velocity component, U_z.

Figure 4.24 shows the vertical velocity component for all inlet distance domains. There is varying magnitude between all domains, which is in conflict with the results figure 4.23 which showed only differences between the shortest two versus the longer domains. There is a general trend between the length of the inlet and the vertical velocity, with U_z increasing as inlet distance increases. Up-15 and up-25 demonstrate quite low vertical velocities which is expected when accounting for the conservation of mass and momentum.

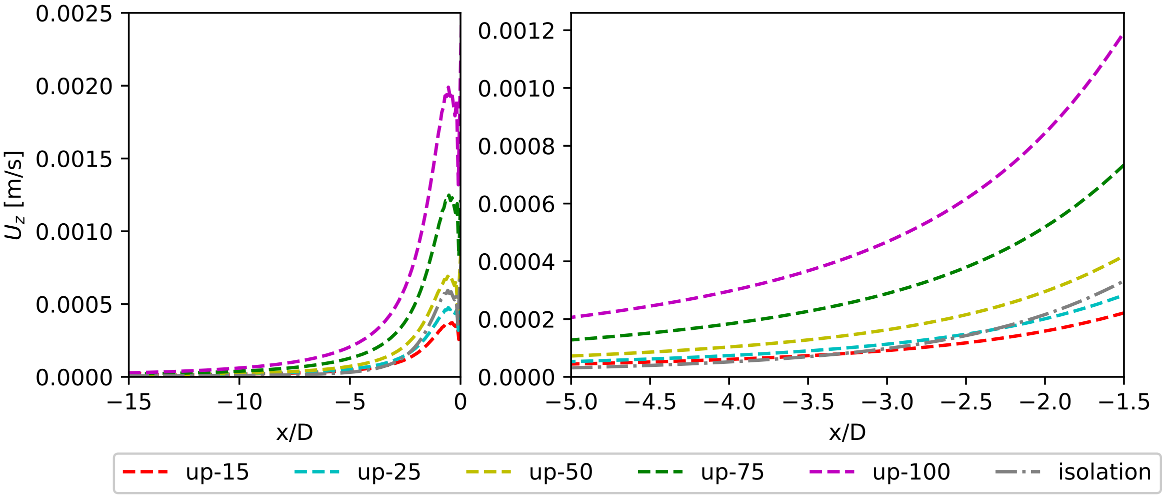

Figure 4.24: U_z upstream of infinite wind farm for inlet distance simulations.

It can be seen that leading up to the wind farm all upstream simulations exhibit some reliance on the vertical velocity component to account for the mass and momentum of the airflow. In order to further investigate the effect of inlet distance on flow behaviour, the area through and around the wind turbines is analysed in more depth.

4.3.3. Flow through and around turbines

As it was observed in the preceding section that as inlet distance increases, U_x decreases and U_z increases. It is expected for U_x to be slightly higher through the wind farm for up-15 and up-25 due to the large difference observed in the upstream flow. This can be seen in figure 4.25 which shows the streamwise and vertical velocity components at hub height for various distances between the turbine columns Sample locations for figure 4.25 are taken as a section of those shown in figure 4.10.

A closer examination of the figure shows that the behaviour of flow through the wind farm is relatively well matched for all domains. There is an observable trend of increasing streamwise velocity with decrease in inlet distance. However, the difference between the simulations is quite small, on the order of 0.03 $[m/s]$ between up-15 and up-100.

In regards to the vertical velocity component, there is little to no observable differences between the simulations through the wind farm. Due to the inconsequential differences in velocity components between the upstream simulations, it can be determined that the impact of the inlet distance of a simulation does not impact the flow within the wind farm in a meaningful way. The flow of all the simulations therefore circumvent the farm and flow through it in

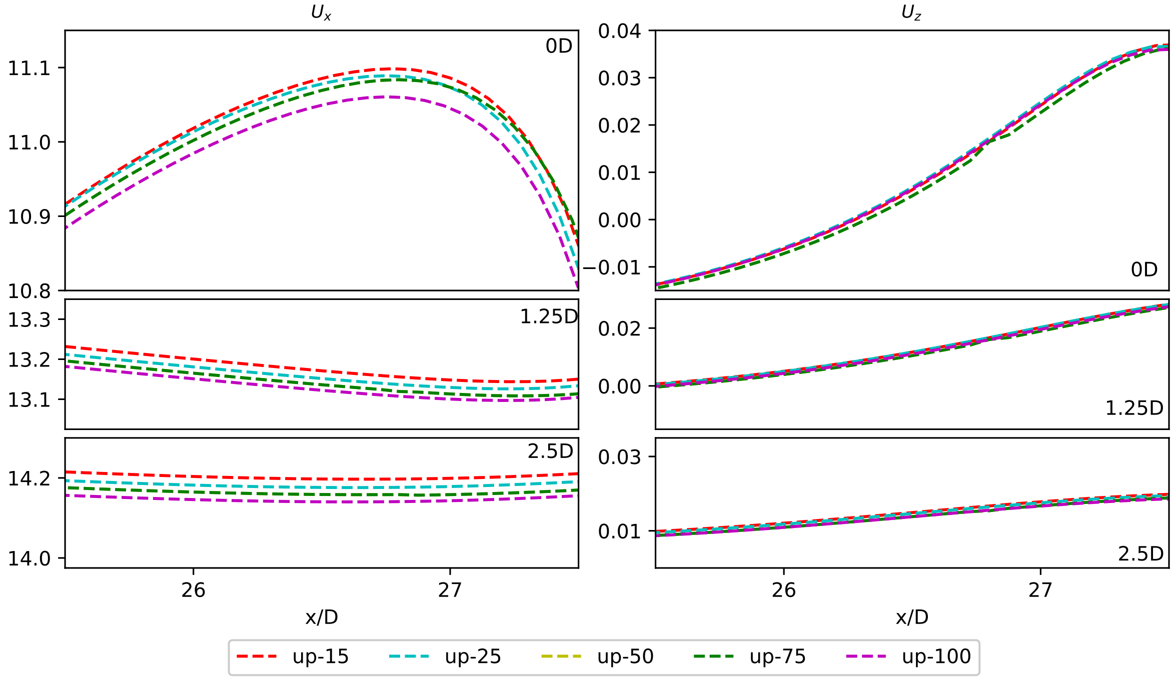

Figure 4.25: U_x and U_z velocity components in m/s and between turbine columns of infinite wind farm at hub height for inlet distance simulations.

similar fashions, and inlet distance does not impact the flow field past the first row of turbines.

4.3.4. Discussion of main findings

The inlet distance simulations provide some interesting insight into correctly modelling upstream flow blockage of infinite wind farms. Firstly, that the upstream flow blockage extends to approximately 30D upstream of the first row of wind turbines. Secondly, that an adequate inlet distance of 50D or longer will cause a reduction in streamwise velocity of approximately 0.03 $[m/s]$ or 0.22% compared to a turbine in isolation. A shorter inlet distances results in upstream blockage within 5D of the inlet boundary and in the case of up-15, the reduction in velocity is 0.01 $[m/s]$ or 0.12% compared to a turbine in isolation. Therefore, the magnitude and extent of the upstream blockage is artificially reduced due to the inadequate inlet distance.

As blockage is still not fully understood, a comparison to existing literature can lend insight into the results obtained in this section. In regards to the extent of upstream blockage, the results of this study concluded that for a wind farm of this size, blockage extends approximately 30D upstream. A wind tunnel experiment carried out by Ebenhoch et al., 2017 found that blockage effects can be detected up to 30D upstream of the wind farm. Conversely, Sanchez Gomez et al., 2021 found that upstream blockage extents to approximately 15D through an LES study with a stable atmosphere. However, Sanchez Gomez et al., 2021 modelled a stable ABL which could impact the results of the upstream blockage, amongst other differences between the simulation configurations.

4.4. Outlet distance

As wakes are thought to be intrinsically linked to upstream blockage, the outflow distance, i.e. the space allowed for dissipation is a possible factor in the projected upstream blockage. This section will outline the impact that a varying outlet distance has on upstream blockage of a laterally infinite wind farm.

As in sections 4.1 and 4.3, a laterally infinite wind farm consisting of 5 rows with turbines spaced 7D streamwise and 5D spanwise is simulated. The domain height, upstream distance, and lateral distances are set as 25D, 50D, and 2.5D, respectively. The BCs are consistent with that of a log-law wind profile, fully developed flow at the outlet, cyclic conditions on the sides, and a shear-stress at the top boundary. A total of 5 outlet distances are simulated, ranging from 15D to 100D from the last row of turbines, consistent with table 3.2.

A general analysis of the flow behaviour through the entire domain for the various outlet distances is done to check for errors and initial trends. This is followed by a more in depth analysis of the upstream flow and flow through and above the wind farm. Followed by a brief discussion of the main findings of the study.

4.4.1. Initial flow analysis

To obtain an initial gauge of the flow through the domain and the possible effects of outlet distance, streamwise velocity at hub height is analysed first. Figure 4.26 and figure 4.27 show that the general behaviour through the wind farm for all of the outlet distance simulations is consistent with expected behaviour as described in chapters 1 and 2.

The figures show proper wake development and dissipation following each subsequent encounter with a turbine, as well as symmetry between the columns of turbines expected for a laterally infinite wind farm. The largest outlet distance simulation is shown to show the almost full dissipation of the wind farm wakes.

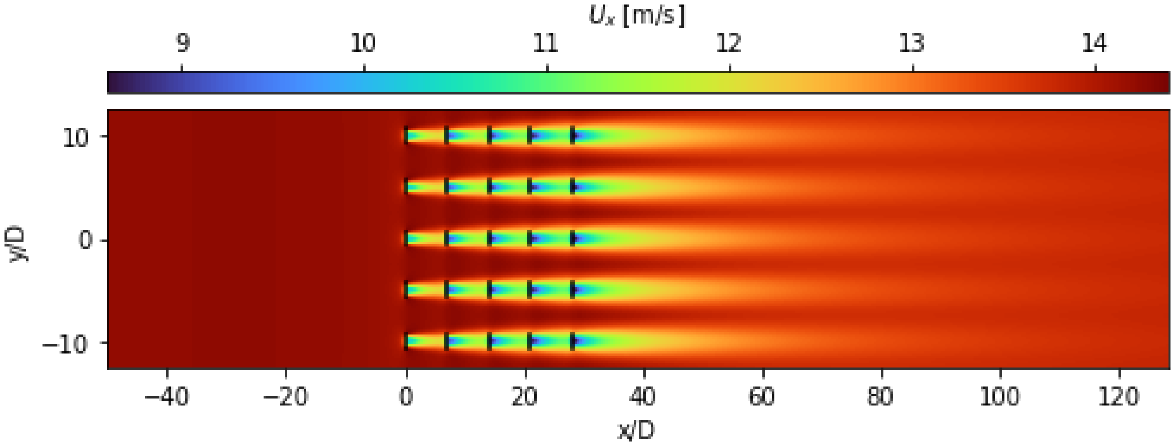

Figure 4.26: U_x at hub height for 100D outlet distance simulation.

Additionally, the streamwise velocity for all outlet distance simulations through the center column of turbines at hub height is consistent with expected behaviour. All of the outlet

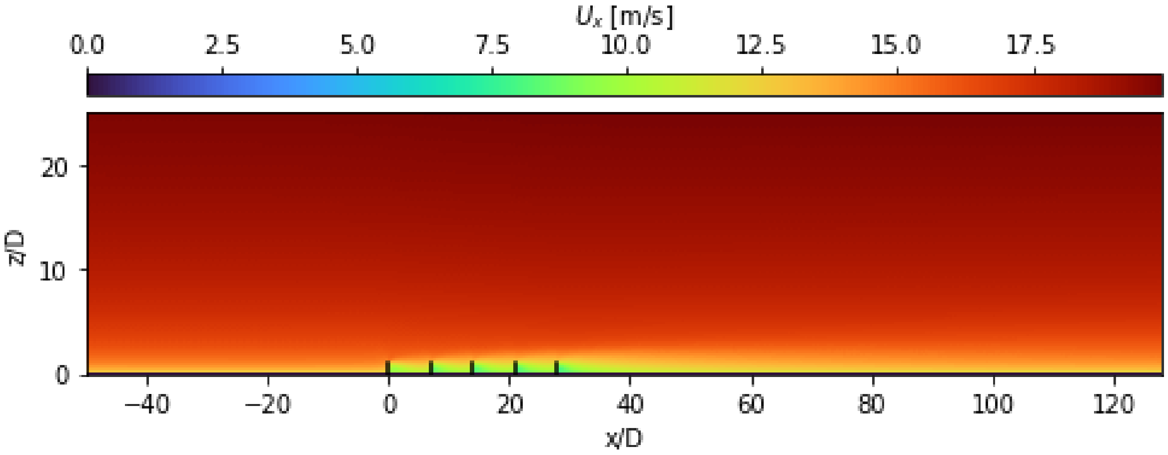

Figure 4.27: U_x at center row of turbines for 100D outlet distance simulation.

distance simulations appear to be extremely well matched through the entirety of the domains. Each outlet simulation has the same reaction upon reaching a wind turbine, as well as recovery over the length of the outlet distance. The longer outlet distances show higher streamwise velocity recovery, however, at each respective outlet distance, all simulations have the same magnitude of streamwise velocity.

The initial analysis does not show any clear indication that there is a difference between the outlet distance simulations in terms of upstream blockage and general flow behaviour through the fetch. As there is so far no obvious difference between the outlet distance simulations or an indication as to how the outlet distance affects the upstream blockage, further investigation is needed.

4.4.2. Upstream flow

A closer look at the upstream blockage present in the outlet distance simulations is done through analysing the velocity components for each simulation upon approaching the wind wind farm. Figure 4.28 shows the three velocity components at hub height approaching the center row of turbines. It is shown that all simulations exhibit upstream blockage in very close magnitudes to one another. The magnitude of the reduction in U_x is approximately 0.03 $[m/s]$ or 0.23% for all simulations.

In comparison to the turbine operating in isolation, the outlet distances have a decreased U_x which shows the global blockage. Due to all of the outlet distance simulations having equal streamwise velocity upon approaching the first row of turbines, it appears that upstream blockage is independent of outlet distance. Turbine in isolation in figure 4.28 has the same domain size as dw-50.

Moving to the remaining velocity components, figure 4.28 shows no divergence in spanwise velocity for the simulations. This lack of difference is similar to that exhibited in the other simulation suites in subsections 4.1.2 and 4.3.2 which modelled laterally infinite wind farms.

There is a difference between the condition of a turbine operating in isolation which is expected

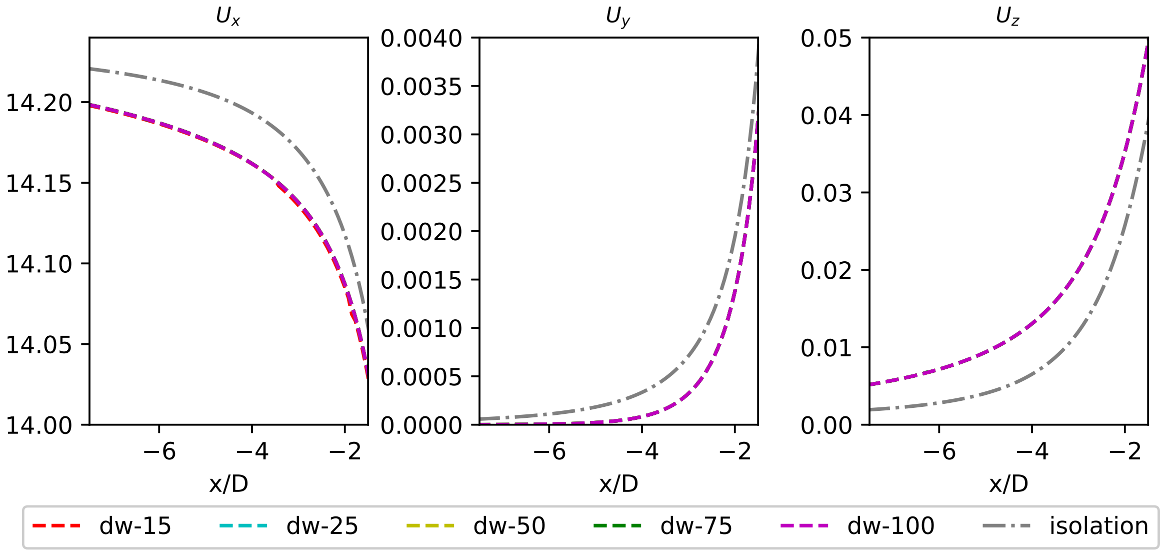

Figure 4.28: Velocity components in m/s indicated in subtitles for outlet distance simulations at near center of a column of turbines.

due to the presence of additional wind turbines impacting the flow. The turbine operating in isolation shows increased lateral velocity in comparison to the outlet distance simulations which is expected as the flow is able to freely move around the single turbine without interference of additional turbines.

Figure 4.28 also demonstrates no apparent change in vertical velocity component between the outlet distance simulations. As there was no difference in the streamwise and spanwise velocity components, this lack of change between vertical velocity against outlet distance simulation is expected.

There is an increase in vertical velocity between the simulations and a turbine operating in isolation, which is expected due to conservation of mass and momentum. As the wind farm simulations have lower streamwise and spanwise velocities, there must be an increase in velocity in the vertical direction and vice-versa for the turbine in isolation.

Due to the behaviour of flow preceding the wind farm it is apparent that upstream flow blockage is independent of outlet distance of a simulation. Additionally, that the flow approaching a laterally infinite wind farm is deflected and circumvents the wind farm in the vertical direction as opposed to in the spanwise direction. Conversely, a turbine operating in isolation has a higher affinity for lateral movement as opposed to vertical.

4.4.3. Flow through and around turbines

In order to determine if there is other unintended consequences of the outlet distance of a laterally infinite wind farm, the flow behaviour through and above the wind farm is analysed. As is true in the upstream area of the farm, the behaviour through the farm for all outlet distance simulations are well matched. In opposition to the trends seen in subsections 4.1.3 and 4.3.3, there is no change between the simulations between the turbines which can be seen in figure 4.29.

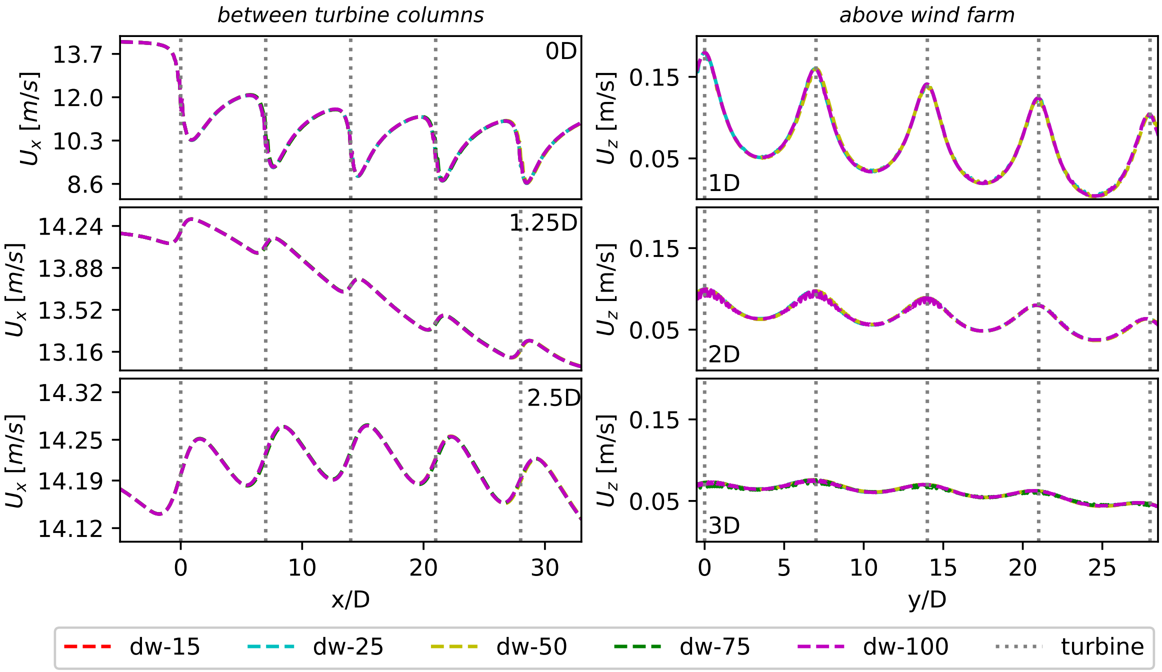

Figure 4.29: Velocities through and above wind farm for outlet distance simulations. Labels indicate distance from center of turbine or distance above wind farm.

Looking to the area above the wind farm, figure 4.29 shows the vertical velocity component of the outlet simulations at various distances above the wind farm. At all vertical distances above the wind farm, the vertical velocity between the outlet distance simulations is well matched. As with all other areas of the domain, this similarity between the velocities shows outlet distance has no identifiable impact on the flow ahead of the downstream area.

4.4.4. Discussion of main findings

The overwhelming result of this suite of simulations is that upstream blockage is independent of outlet distance. The magnitude of the blockage reduction in streamwise velocity was shown to be approximately 0.03 $[m/s]$ or 0.23% for all simulations. As no differences between flow behaviour was shown throughout the entire domain, it is recommended that the outlet distance be at 15D. As this provided results agreeing with larger domains and reduces unnecessary computational time.

4.5. Impact on power production

As discussed in chapter 1, a large motivating factor in investigating upstream blockage is to better understand the effect on power production for improved financial understanding of prospective wind farm installations. In order to investigate the impact of the various numerical configurations on power production, each simulation suite is individually analysed for the associated power loss of the first row of turbines against a respective turbine operating in isolation. For the finite wind farm simulations in section 4.2 power loss associated with the entire wind farm compared to that of a single column of turbines is also analysed. A comparison between the simulations and attempt at generalisation of the prospective upstream blockage losses due to domain sizing is executed. All calculations utilize sample points 2.5D upstream of the respective turbine being analysed.

4.5.1. Domain height effect on power production

As the domain height simulations consist of laterally infinite wind farms, to assess losses against a turbine in isolation, only power production at the center front turbine and respective isolation simulation are required to analyse changes in power. Equation 4.1, derived from Sommer, 2021 is utilized to quantify this impact in regards to the domain height and subsequent blockage. This equation is used as it is a measure of the difference between the inherit induction losses against global blockage losses that are produced due to additional turbines.

$$P_{loss} = \frac{P(U_i) - P(U_{ct})}{P(U_i)} * 100\% \tag{4.1}$$

Where P_{loss} is the loss of power in the center turbine in the first row due to wind farm interactions, $P(U_{ct})$ is the available power from the center turbine (ct) in an infinite wind farm simulation, and $P(U_i)$ is the power produced from a turbine in isolation. The power was calculated using equation 1.1 and results can be seen in figure 4.30.

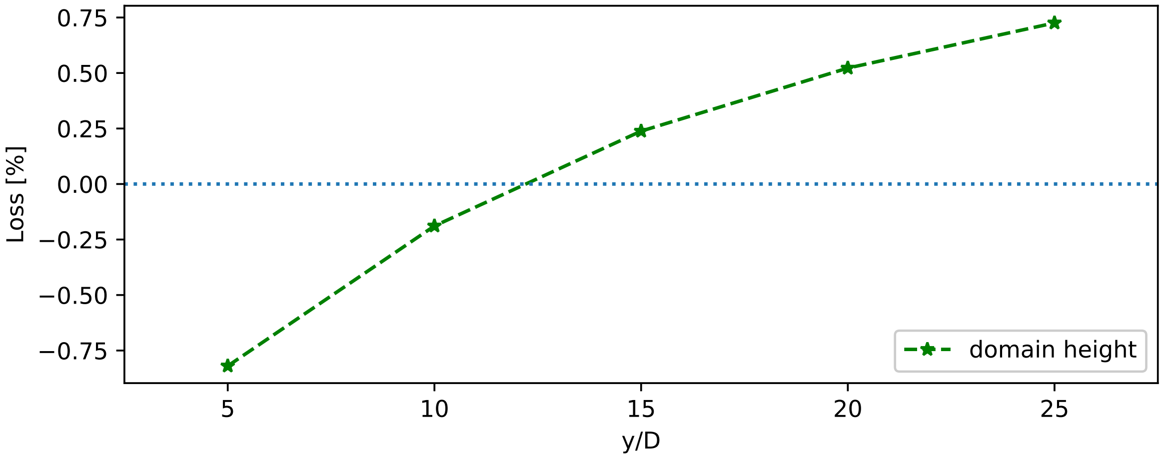

Figure 4.30: Power production loss associated with changes in domain height

Taking a closer look at figure 4.30, it shows that at the smaller domain heights (dh-5 and dh-10) there is a negative power loss, which means an actual gain in power in comparison to a turbine operating in isolation under the same domain size. For all other domain heights, the presence of the wind farm creates a net power loss when compared to a turbine operating in isolation. This result provides some insight on the importance of adequately sizing domain heights to correctly determine global blockage and flow behaviour.

In comparison to prior studies, the results of the domain height simulations is somewhat varied. Bleeg and Montavon, 2022 found that for a single row of turbines with a symmetric bounds (i.e. created a laterally infinite row) and vertical extents of 7.4D and 125D resulted in power gains of 3.3% and 0.5%, respectively. Conversely, the results of section 4.5.1 demonstrated power gains of approximately 0.75% for dh-5 and 0.15% for dh-10. The difference in results can perhaps be attributed to the presence of additional rows of wind turbines. As Bleeg and Montavon, 2022 simulated a single row of turbines, additional turbine wake interactions in the spanwise direction are not present. As was seen in figure 4.11, the difference in velocity of different domain height simulations increases at each respective turbine row. This could support the claim that additional wind turbine rows increases global blockage and therefore the power gains are limited to lower domain height simulations.

4.5.2. Lateral extent impact on power production of finite wind farm

As some hypothesize that upstream blockage is a redistribution of energy through the wind farm rather than a net loss, looking at the theoretical power loss of the finite wind farm can provide insight into this discussion. Subsection 4.2.2 showed that there is a higher velocity, i.e. less upstream blockage, approaching the outer turbines as opposed to inner turbines. Using a method similar to in equation 4.1, the power loss of the first row is looked at first in comparison to a turbine in isolation. Equation 4.2 gives the generalized equation where N is the number of turbines in the first row (5) and n is the respective turbine number. The results of the equation for each lateral extent domain are shown in figure 4.31.

$$P_{loss,row} = \frac{N * P(U_i) - \sum_{n=1}^{5} P(U_n)}{N * P(U_i)} * 100\% \tag{4.2}$$

Additionally, the power loss of the entire wind farm is calculated in respect to a single column of wind turbines to account for wake effects. A similar approach to in equation 4.2 is used, with adjustments made to account for the power of each turbine in the column as shown in equation 4.3, with c as the turbine number in the column, and N as the number of columns in the wind farm. The results of equation 4.3 are given in figure 4.31.

$$P_{loss,windfarm} = \frac{N * \sum_{c=1}^{5} P(U_c) - \sum_{n=1}^{25} P(U_n)}{N * \sum_{c=1}^{5} P(U_c)} * 100\% \tag{4.3}$$

Upstream blockage of the first row, regardless of lateral extent is generally around 0.7%. It is shown that for the narrowest domain, there is a higher loss in the first row in comparison to a slightly wider domain. After the initial drop in loss, there is steady increase in calculated loss as the domain is widened, insinuating higher blockage. This drop may be due to a change in preferential pathway from the narrowest domain, which generally flows up and over the wind farm, in comparison to a slightly wider domain which has a higher affinity for streamwise and lateral movement. This higher lateral extent allows for higher velocities along the outer column of turbines and increases power. However, as the lateral extent is widened further, the momentum exhibits more lateral movement around the wind farm which causes an increase in power loss as the flow is not as confined.

The losses exhibited against the entire wind farm in comparison to a single column of turbines is

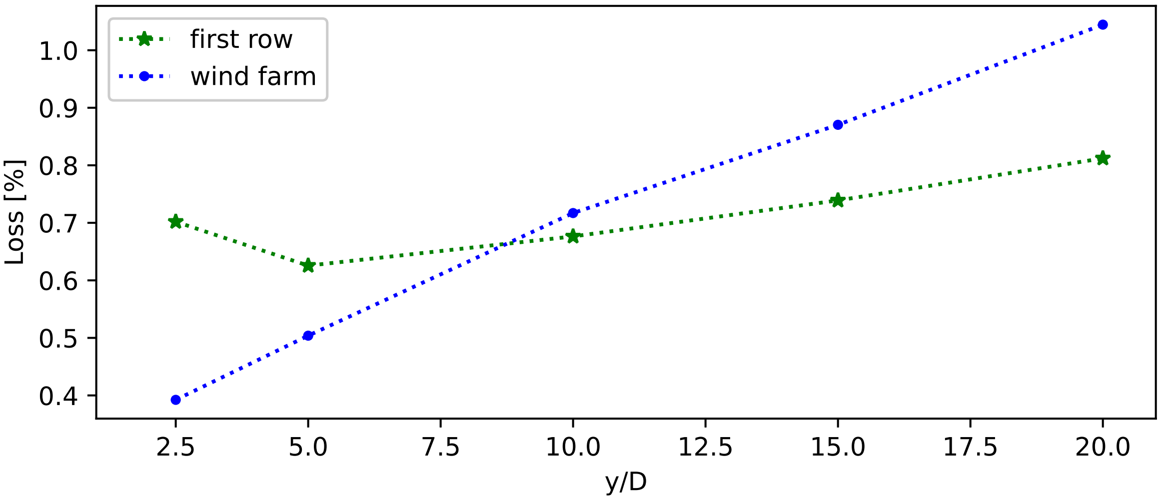

Figure 4.31: Global blockage losses of a single row of turbines compared to isolation and 5x5 wind farm compared to a column of turbines. Lateral extent from wind farm to boundary shown on x axis.

near linear in relation to lateral extent. Interestingly, le-2.5 and le-5 have a smaller percentage of loss in the entire farm as opposed to in the first row calculations. This indicates that energy is being constricted to flow within the narrower domains and is somewhat recouped in the subsequent turbine rows. Conversely, the wider domains exhibit losses for the farm greater than for the first row. Based on the rudimentary calculation and assumptions implemented in equation 4.3 and figure 4.31, it can be hypothesized that upstream flow blockage is inherently an energy loss as all simulations exhibited reduced power production.

Bleeg and Montavon, 2022 assessed the blockage of a single row of turbines under physical conditions. For a domain consisting of lateral extents of about 16D and 130D on each side of the wind turbine row, with domain heights of 25D, and 7.4D (and 125D) respectively. Power gains for these simulations ranging from 0.1% to 1.0% were observed. This is in contradiction to the results of this study which found that all lateral extent simulations exhibited power losses. Some possible differences between the work done by Bleeg and Montavon, 2022 and this study which could account for the change in blockage could be the narrower streamwise spacing, single row of turbines, disc-based C_T, or lack of a shear stress top BC used in Bleeg and Montavon, 2022. However, there are countless possible configurations which could alter the results.

4.5.3. Inlet distance power effects

Using equation 4.1, the power loss for each inlet distance simulation is calculated and the results shown in figure 4.32. The power loss is based on comparing the potential power in the streamwise velocity component of the wind for the laterally infinite wind farm with 5 rows against a single turbine operating in isolation under the same domain bounds. The values for U_x are taken 2.5D upstream of the wind turbine at hub height.

There is an apparent plateau at up-50 with a value of 0.69% loss in power which continues for up-75 (0.71% loss) and up-100 (0.68% loss). Power loss for up-15, the shortest inlet distance, is

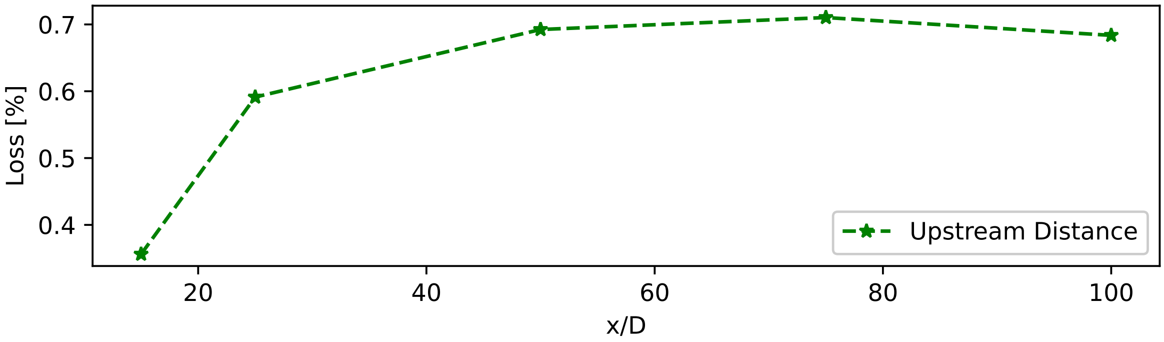

Figure 4.32: Power loss associated with upstream blockage for inlet distance simulations.

approximately 0.34% less than the average plateau value, or a 49% drop in projected upstream blockage power loss. Up-25 has a power loss of 0.59% or 15% less projected power loss than the plateau value.

Figure 4.32 leads to the assertion that at an inlet distance of 50D and above the associated power loss of a laterally infinite wind farm due to upstream flow blockage is approximately 0.69%. Additionally, that domains with shorter inlet distances may drastically under represent the upstream flow blockage of the wind farm.

4.5.4. Outlet distance impact on power loss

Due to no differences between the outlet distance simulations in regards to flow through the wind farm there is no expected change in power loss between the outlet distance simulations. Equation 4.1 is used to determine the power loss due to upstream blockage of the outlet distance simulations in comparison to a turbine operating in isolation. Figure 4.33 shows the results of these calculations vary slightly between the outlet distance simulations.

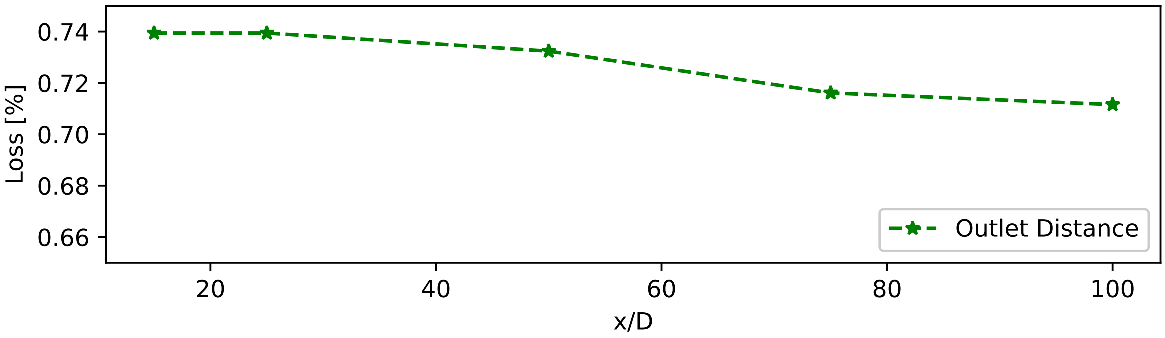

Figure 4.33: Power loss associated with upstream blockage for outlet distance simulations

Dw-15 and dw-25 are exactly matched in project upstream blockage with a loss of 0.739%. The largest three domains, dw-50, dw-75, and dw-100 have a projected loss of 0.724% 0.716% and 0.712% respectively. Overall, the difference in projected loss between the outlet distance simulations is 0.028% which is relatively negligible.

4.5.5. Comparison between simulations

In order to compare the blockage effects on power production between turbine simulations the results must be standardized to account for changes in numerical configuration. Therefore, as all simulations related power loss to a single row of turbines against a turbine in isolation, this area will be utilized to compare results. Firstly, the ratio (R_A [%]) between the cross-sectional area (CS) of the domain and surface area of the AD (SA) normal to the flow direction is described in equation 4.4. Both domain height and lateral extents have a variable CS while inlet and outlet distances have a constant CS. As such, only the values for up-50 and dw-50 are analysed to ensure other sizing factors do not influence results.

$$R_A = \frac{SA}{CS} * 100\% \tag{4.4}$$

A trendline is fit to the data following a third order polynomial and has the form of equation 4.5 with an RES value of 0.03983987.

$$P_{loss} = 0.23720218 * R_A^3 - 1.05224986 * R_A^2 + 0.47863479 * R_A + 0.70838428 \tag{4.5}$$

The results of plotting power loss developed in the preceding subsections against the ratio of areas between the turbine and domain are shown in figure 4.34.

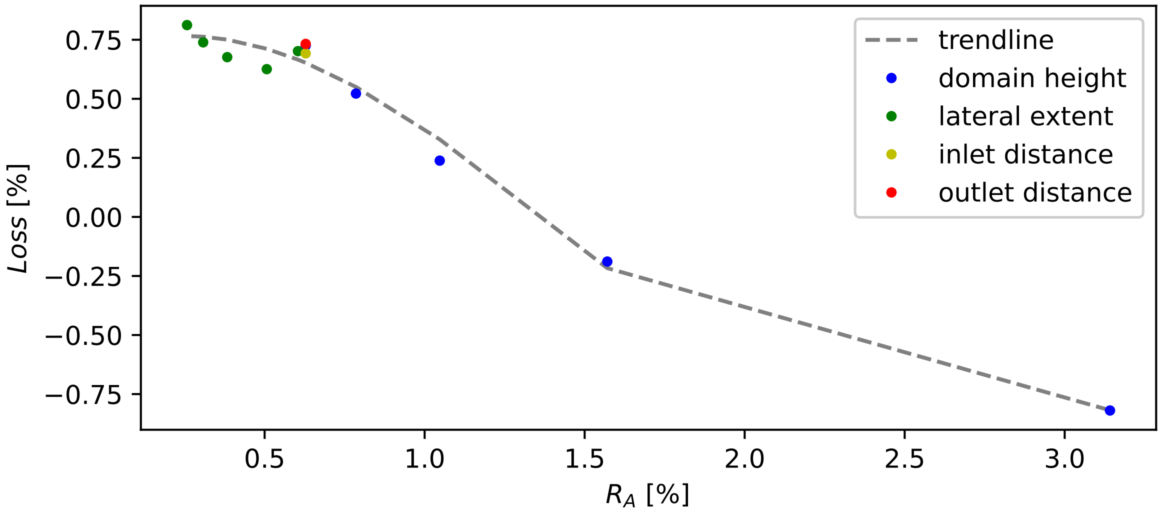

Figure 4.34: Comparison of power loss in a single row of turbines with the ratio of turbine SA and domain CS.

From the figure it is evident that there is a strong correlation between the upstream blockage loss in the first row to the ratio between the domain CS and turbine SA. Additionally, the losses from simulations with equal R_A are very well matched which increase confidence in the results. There is an identifiable trend of increasing losses with decreasing R_A, i.e. as the CS. The trendline also indicates losses may level off at 0.75% and R_A of 0.4. There is some discrepancy with these trends at an R_A of about 0.4%. There is still too much uncertainty in the the correlation between R_A and upstream losses in the first row. Further investigation of R_A values would be needed to improve confidence in the loss estimation given in equation 4.5.

4.6. Summary

This chapter laid out the execution of four simulation suites of changing domain extents for simulating upstream blockage. Domain height, lateral extent, inlet distance, and outlet distance were systematically adjusted to analyse respective impacts on upstream blockage as well as general flow behaviour through and above wind farms. The power loss associated with upstream blockage was then calculated and compared amongst simulations to determine possible trends in domain sizing and associated upstream blockage power loss.

It was found that the domain height has a large impact on the validity of model results. In the case of a relatively small domain height (dh-5 and dh-10) flow was forced through the wind farm and resulted in a power increase in the zone preceding the wind farm. At higher domain heights (dh-15, dh-20, and dh-25) flow circumvented the farm in the vertical direction and exhibited increasing blockage with height. Based on flow trends and behaviour, it is recommended that the domain height be at least 15D from the ground.

The lateral extent of the domain allowed for further investigation of a finite wind farm to observe the behaviour along the sides of the domain as well as upstream and within the wind farm. Narrow lateral extents (le-2.5 and le-5) resulted in flow being forced through and above the wind farm, while wider domains (le-10, le-15, and le-20) exhibited more lateral movement around the wind farm. Analysing the prospective power loss, for the first row of a wind turbine, all domains exhibited power loss, with le-5 having the lowest power loss possibly due to more area for the flow to move through the wind farm as opposed to in le-2.5. When analysing the power loss of the wind farm in comparison to a column in isolation, the domains exhibited a consistent, almost linear trend of increasing power loss with domain width. Based on these results, it is recommended that a domain have lateral extents of at least 10D on each side of the finite wind farm.

Analysis of inlet distance provided some insight on the extent upstream at which blockage is observed as well as the impact on the upstream blockage. It was found that upstream blockage extends approximately 30D upstream of the first row of wind farms for a laterally infinite wind farm with 5 rows of turbines. Additionally, the power loss of such blockage is approximately 0.69% when inlet distances are set far enough ahead to capture the entire upstream blockage. As such, it is recommended to have an inlet distance of at least 50D from the wind farm.

Finally, the outlet distance was altered and found little to no change in general flow behaviour. Although it is thought turbine wakes and upstream blockage are linked, there was no observable change in fluid behaviour when comparing the different outlet distance simulations. There was slight change in projected power loss, with a trend of decreasing loss with increasing outlet distance, however the change is considered negligible. As such it is recommended to have an outlet distance of 15D from the last row of wind turbines as this was the shortest domain tested.

5

Conclusion and recommendations

This chapter contains a summary of the main conclusions and recommendations based on the completed study. The first section discusses the answers to the research questions given in section 1.3 based on the results presented in the preceding chapter. Section 5.2 will cover recommendations for sizing domains for a wind farm simulation under the conditions discussed in chapter 3. Finally, an overview of suggestions for potential future work is laid out.

5.1. Main conclusions for research questions

In order to address the main research question, the sub questions will be discussed first. Each sub-question will be addressed separately with a final summary to address the main question.

What is the impact of domain height on the magnitude and shape of upstream flow blockage and how does it alter the wind farm flow field?

There is a general trend of increasing upstream flow blockage with increasing domain height. At low domain heights of 5D and 10D, the velocity is actually increased with respect to a turbine operating in isolation. Change in streamwise velocity 2.5D upstream of the wind farm ranged from an increase of 0.18% to a reduction of 0.23% for a domain height of 5D and 25D, respectively. However, the general shape of upstream blockage for all domain height configurations remained relatively unchanged, i.e. domain height does not impact the shape of upstream blockage.

Within the flow field of the wind farm, the domain height with upstream flow blockage demonstrated higher vertical velocities in comparison to shorter domain heights, which maintained higher streamwise and spanwise velocities. This leads to the conclusion that higher domain heights allow for flow to circumvent the wind farm while shorter domain heights are restricted to flow through the wind farm in the spanwise direction.

In what ways does the extent between a finite wind farm and lateral boundaries affect the upstream blockage and flow field within the domain?

Firstly, narrow lateral bounds of 2.5D on each side of the finite wind farm were found to restrict flow through and above the wind farm which resulted in decreased blockage. Wider wind farms of 5D to 20D displayed increasing blockage with increasing lateral extent. Regardless, all lateral simulations exhibited upstream blockage in comparison to a turbine in isolation. The magnitude of spanwise velocity reduction was largest at the center turbine and decreased towards the lateral bounds. U_x was found to decrease by a minimum of 0.13% for lateral bounds of 10D at the outer turbine column while a maximum reduction of 0.31% for lateral bounds of 20D at the center turbine column was determined. The general shape of the upstream blockage remained consistent through domains with lateral extents between 5D and 20D. However, at less than 5D, the shape of the upstream blockage was more similar to that of a laterally infinite wind farm.

Additionally, the narrowest domain had a high affinity to momentum flow above the wind farm, whereas the next narrowest domain displayed some preference for lateral velocity flow as well. As the domain is widened, this trend continues with increasing lateral velocity flow around the farm. This indicates that between lateral extents of 2.5D and 5D the preferential pathway for momentum changes from U_z to U_y. The wider domains consistently displayed increasing lateral velocity with increasing domain width.

How do the inlet and outlet distances change the resultant upstream flow blockage magnitude and extent?

At inlet distances of 50D and larger, upstream flow blockage is found to remain relatively consistent in magnitude and extent. The magnitude of the the reduction of streamwise velocity and extent of upstream blockage is approximately 0.22% and 30D, respectively, for simulations with adequate inlet distance. As inlet distance is decreased, the extent of upstream blockage is reduced to within 5D of the inlet boundary condition and the magnitude of upstream blockage is reduced to approximately 0.12%.

Outlet distance does not demonstrate a distinguishable impact on the upstream flow blockage magnitude and extent. Within the entire domain the outlet distance simulations display well matched upstream blockage. The magnitude of upstream blockage for simulations is approximately 0.23% and the extent is consistently around 30D upstream.

To what extent does wind farm flow blockage impact potential power production for various domain sizing?

For the domain height simulations, the two shortest domain heights of 5D and 10D showed an increase in power production of 0.82% and 0.19%, respectively. Conversely, the higher domain heights of 15D, 20D, and 25D showed losses of 0.24%, 0.52%, and 0.72% respectively. Inlet distances of 50D or higher had an upstream blockage power production loss of 0.69±0.02%. While shorter inlet distances displayed losses of 0.35% and 0.59% for the 15D and 25D inlet distance simulations, respectively. Finally, outlet distance simulations showed relatively close upstream blockage across all simulations with an average value of 0.72% for power production loss. Single rows of lateral extent simulations all showed power production losses with a minimum loss of 0.63% for a 5D lateral extent and a maximum loss of 0.81% for a 20D lateral extent.

Comparing the ratio of surface area between a turbine and the cross sectional area of the domain against the single row losses results in is clear correlation. The general trend conveys that as the ratio between areas decreases, the power production losses increase. A third order polynomial equation is somewhat able to fit the trend, which indicates a leveling off of losses around 0.75% and ratio of 0.4.

Finally in regards to the main research question:

"How does the numerical configuration of RANS simulations impact the upstream flow blockage of a theoretical wind farm?",

several points can be made. It can be generally seen that as the domain is constrained closer to the wind farm, upstream blockage will decrease. When this constraint is done in the vertical direction, it can lead to an absence of upstream blockage and increase in potential power production. Narrow lateral extents restrict flow through and above the wind farm which results in lower upstream blockage. Meanwhile, wider lateral extents allow for flow around the sides of the wind farm and increased upstream blockage. Closely constrained inlet distances result in a shorter extent of upstream blockage and reduced upstream blockage, while inlet bounds defined an adequate distance from the wind farm demonstrate an upstream extent of 30D and relatively consistent upstream blockage. Finally, outlet distance bounds show little to no impact on the upstream blockage, with near negligible impact on power production loss due to upstream blockage.

5.2. Recommendations

The boundaries of a simulation have a clear impact on the upstream flow blockage for a RANS simulation of a wind farm. Due to these effects, there are several recommendations of where to set domain bounds for studying upstream blockage which are covered in this section. These recommendations are summarized in table 5.1.

	Domain Height	Lateral Extent	Inlet Distance	Outlet Distance
Sizing	15D	10D	50D	15D

Table 5.1: Final recommendations for minimum domain sizing.

In regards to the height of a domain, a minimum height of 15D is recommended as the flow behaviour is generally well matched to higher domains. However, higher domain heights of 20D and 25D may provide better results and do not require excess computing time due to the multi block method used in this study. A minimum lateral extent of 10D on each side of a finite wind farm is suggested due to the convergence of flow behaviour between 10D and wider domains of 15D and 20D. An inlet distance of 50D is recommended as it provides near equal results to those of longer inlet distances without superfluous computational time and costs. Finally, an outlet distance of at 15D is recommended as there were little to no change in upstream blockage with outlet distance and therefore larger sizing is unnecessary.

5.2.1. Potential future work

Through completion of this work, several aspects were encountered that could provide further insight into upstream blockage of wind farms. One potential area for future work is to explore the relationship between wind farm spacing and configuration with upstream flow blockage. As this study focused on a symmetric wind farm layout and consistent sizing, investigating the effect of streamwise and spanwise spacing with resultant upstream blockage could provide interesting insight. In that regard, investigating the impact of how many rows of turbines are included in the model could provide insight into the scaling of upstream blockage with respect to wind farm size.

Additionally, implementing more complex methodology such as a disc-based C_T, ALM, or changing the turbulence model coefficients may improve the understanding the cause of upstream blockage. This may also provide insight on the sensitivity of the numerical configuration.

Finally, simulating more elaborate environmental setups by including atmospheric characteristics such as veer, Coriolis effect, and changing stability could provide results more applicable to a real world wind farm. As many of these parameters directly impact the governing equations and turbulence modelling, including them may provide drastically different results, but that align more closely to data.

References

Alfonsi, G. (2009). Reynolds-averaged navier-stokes equations for turbulence modeling. *Applied Mechanics Reviews - APPL MECH REV*, *62*. https://doi.org/10.1115/1.3124648

Allaerts, D. (2016). *Large-eddy simulation of wind farms in conventionally neutral and stable atmospheric boundary layers* (Doctoral dissertation). KU Leuven. Leuven, Belcium.

Allaerts, D., Broucke, S. V., van Lipzig, N., & Meyers, J. (2018). Annual impact of wind-farm gravity waves on the belgian–dutch offshore wind-farm cluster. *Journal of Physics: Conference Series*, *1037*, 072006. https://doi.org/10.1088/1742-6596/1037/7/072006

Allaerts, D., & Meyers, J. (2018). Gravity waves and wind-farm efficiency in neutral and stable conditions. *Boundary-Layer Meteorology*, *166*, 269–299. https://doi.org/10.1007/s10546-017-0307-5

Ammara, I., Leclerc, C., & Masson, C. (2002). A Viscous Three-Dimensional Differential/Actuator-Disk Method for the Aerodynamic Analysis of Wind Farms. *Journal of Solar Energy Engineering*, *124*(4), 345–356. https://doi.org/10.1115/1.1510870

Anjum, L. (2014). Wind resource estimation techniques-an overview. *International Journal of wind and Renewable Energy*, *Volume 3*, 26–38.

Avila, M., Gargallo-Peiró, A., & Folch, A. (2017). A CFD framework for offshore and onshore wind farm simulation. *Journal of Physics: Conference Series*, *854*, 012002. https://doi.org/10.1088/1742-6596/854/1/012002

Barber, S. (2017). *Annual energy production part 2 - aep estimations for investors*. https://www.windspire.ch/blog/2017/7/31/annual-energy-production-part-2

Besta, S. (2019). *Ns energy*. Retrieved December 24, 2020, from https://www.nsenergybusiness.com/features/worlds-biggest-onshore-wind-farms/

Bleeg, J., & Montavon, C. (2022). Blockage effects in a single row of wind turbines. *Journal of Physics: Conference Series*, *2265*(2), 022001. https://doi.org/10.1088/1742-6596/2265/2/022001

Bleeg, J., Purcell, M., Ruisi, R., & Traiger, E. (2018). Wind farm blockage and the consequences of neglecting its impact on energy production. *Energies*, *11*(6). https://doi.org/10.3390/en11061609

Blocken, B., Stathopoulos, T., & Carmeliet, J. (2007). Cfd simulation of the atmospheric boundary layer: Wall function problems. *Atmospheric Environment*, *41*(2), 238–252. https://doi.org/https://doi.org/10.1016/j.atmosenv.2006.08.019

Branlard, E., Quon, E., Forsting, A. R. M., King, J., & Moriarty, P. (2020). Wind farm blockage effects: Comparison of different engineering models. *Journal of Physics: Conference Series*, *1618*(6), 062036. https://doi.org/10.1088/1742-6596/1618/6/062036

Brune, W. (2020). *A day in the life of the boundary layer*. Retrieved May 5, 2022, from https://www.e-education.psu.edu/meteo300/node/712

Burton, T., Jenkins, N., Sharpe, D., & Bossanyi, E. (2011). Wind energy handbook. John Wiley & Sons, Ltd.

Caretto, L. S., Gosman, A. D., Patankar, S. V., & Spalding, D. B. (1973). Two calculation procedures for steady, three-dimensional flows with recirculation. In H. Cabannes & R. Temam (Eds.), *Proceedings of the third international conference on numerical methods in fluid mechanics* (pp. 60–68). Springer Berlin Heidelberg.

Centurelli, G., Vollmer, L., Schmidt, J., Dörenkämper, M., Schröder, M., Lukassen, L. J., & Peinke, J. (2021). Evaluating global blockage engineering parametrizations with LES. *Journal of Physics: Conference Series*, *1934*(1), 012021. https://doi.org/10.1088/1742-6596/1934/1/012021

Chamorro, L. P., & Porté-Agel, F. (2011). Turbulent flow inside and above a wind farm: A wind-tunnel study. *Energies*, *4*(11), 1916–1936. https://doi.org/10.3390/en4111916

Deskos, G., Abolghasemi, M. A., & Piggott, M. (2017). Wake predictions from two turbine models using mesh-optimisation techniques. *EWTEC 2017*.

Ebenhoch, R., Muro, B., Dahlberg, J.-Å., Berkesten Hägglund, P., & Segalini, A. (2017). A linearized numerical model of wind-farm flows. *Wind Energy*, *20*(5), 859–875. https://doi.org/https://doi.org/10.1002/we.2067

Fallis, R. (2010). Whitelee wind farm. https://www.flickr.com/photos/scottishgovernment/5285288002/in/photostream/

Forsting, A. M., Rathmann, O., van der Laan, M., Troldborg, N., Gribben, B., Hawkes, G., & Branlard, E. (2021). Verification of induction zone models for wind farm annual energy production estimation. *Journal of Physics: Conference Series*, *1934*(1), 012023. https://doi.org/10.1088/1742-6596/1934/1/012023

Frandsen, S. (1992). On the wind speed reduction in the center of large clusters of wind turbines. *Journal of Wind Engineering and Industrial Aerodynamics*, *39*(1), 251–265. https://doi.org/https://doi.org/10.1016/0167-6105(92)90551-K

Göçmen, T., van der Laan, M. P., Réthoré, P.-E., Diaz, A., Larsen, G., & Ott, S. (2016). Wind turbine wake models developed at the technical university of denmark: A review. *Renewable and Sustainable Energy Reviews*, *60*, 752–769. https://doi.org/10.1016/j.rser.2016.01.113

Hansen, M. (2000). *Aerodynamics of wind turbines: Rotors, loads and structure*. James & James. https://books.google.com/books?id=d%5C_REBCyBuKkC

Hargreaves, D., & Wright, N. (2007). On the use of the k– model in commercial cfd software to model the neutral atmospheric boundary layer. *Journal of Wind Engineering and Industrial Aerodynamics*, *95*(5), 355–369. https://doi.org/https://doi.org/10.1016/j.jweia.2006.08.002

IRENA. (2019). Future of wind: Deployment, investment, technology, grid integration and socio-economic aspects (a global energy transformation paper).

Jonkman, J., Butterfield, S., Musial, W., & Scott, G. (2009). *Definition of a 5-me reference wind turbine for offshore system development*. Retrieved September 26, 2022, from https://www.nrel.gov/docs/fy09osti/38060.pdf

Launder, B., & Spalding, D. (1974). The numerical computation of turbulent flows. *Computer Methods in Applied Mechanics and Engineering*, *3*(2), 269–289. https://doi.org/https://doi.org/10.1016/0045-7825(74)90029-2

Martínez-Tossas, L. A., Churchfield, M. J., & Leonardi, S. (2015). Large eddy simulations of the flow past wind turbines: Actuator line and disk modeling. *Wind Energy*, *18*(6), 1047–1060. https://doi.org/https://doi.org/10.1002/we.1747

Medici, D., Ivanell, S., Dahlberg, J.-Å., & Alfredsson, P. H. (2011). The upstream flow of a wind turbine: Blockage effect. *Wind Energy*, *14*(5), 691–697. https://doi.org/https://doi.org/10.1002/we.451

Menter, F., Kuntz, M., & Langtry, R. (2003). Ten years of industrial experience with the sst turbulence model. *Heat and Mass Transfer*, *4*.

Menter, F. R. (1993). Zonal two equation k-w turbulence models for aerodynamic flows.

Meyer Forsting, A., Troldborg, N., & Gaunaa, M. (2017). The flow upstream of a row of aligned wind turbine rotors and its effect on power production. *Wind Energy*, *20*(1), 63–77. https://doi.org/10.1002/we.1991

Mikkelsen, R. (2004). *Actuator disc methods applied to wind turbines* (Doctoral dissertation No. 2003-02). Technical University of Denmark.

Montavon, C. (2022). *Dnv*. Retrieved May 2, 2022, from https://www.dnv.com/article/wind-farm-scale-blockage-loss-or-redistribution--191488

Nishino, T., & Draper, S. (2015). Local blockage effect for wind turbines. *Journal of Physics: Conference Series*, *625*, 012010. https://doi.org/10.1088/1742-6596/625/1/012010

Nygaard, N. G., Steen, S. T., Poulsen, L., & Pedersen, J. G. (2020). Modelling cluster wakes and wind farm blockage. *Journal of Physics: Conference Series*, *1618*(6), 062072. https://doi.org/10.1088/1742-6596/1618/6/062072

Parente, A., Gorlé, C., Beeck, J., & Benocci, C. (2011). A comprehensive modelling approach for the neutral atmospheric boundary layer: Consistent inflow conditions, wall function and turbulence model. *Boundary-Layer Meteorology*, *140*, 411–428. https://doi.org/10.1007/s10546-011-9621-5

Popescu, M., & Flåtten, T. (2021). A study of blockage effects at the wind turbine and wind farm scales. *Energies*, *14*(19). https://doi.org/10.3390/en14196124

Porté-Agel, F., Bastankhah, M., & Shamsoddin, S. (2020). Wind-turbine and wind-farm flows: A review. *Boundary-Layer Meteorology*, *174*. https://doi.org/10.1007/s10546-019-00473-0

Richards, P., & Hoxey, R. (1993). Appropriate boundary conditions for computational wind engineering models using the k- turbulence model [Proceedings of the 1st International on Computational Wind Engineering]. *Journal of Wind Engineering and Industrial Aerodynamics*, *46-47*, 145–153. https://doi.org/https://doi.org/10.1016/0167-6105(93)90124-7

Rodriguez, S. (2019). Les and dns turbulence modeling. *Applied computational fluid dynamics and turbulence modeling: Practical tools, tips and techniques* (pp. 197–223). Springer International Publishing. https://doi.org/10.1007/978-3-030-28691-0_5

Sanchez Gomez, M., Lundquist, J. K., Mirocha, J. D., Arthur, R. S., & Muñoz-Esparza, D. (2021). Quantifying wind plant blockage under stable atmospheric conditions. *Wind Energy Science Discussions*, *2021*, 1–21. https://doi.org/10.5194/wes-2021-57

Schneemann, J., Theuer, F., Rott, A., Dörenkämper, M., & Kühn, M. (2021). Offshore wind farm global blockage measured with scanning lidar. *Wind Energy Science*, *6*(2), 521–538. https://doi.org/10.5194/wes-6-521-2021

Sebastiani, A., Castellani, F., Crasto, G., & Segalini, A. (2021). Data analysis and simulation of the lillgrund wind farm. *Wind Energy*, *24*(6), 634–648. https://doi.org/https://doi.org/10.1002/we.2594

Segalini, A., & Dahlberg, J.-Å. (2020). Blockage effects in wind farms. *Wind Energy*, *23*(2), 120–128. https://doi.org/https://doi.org/10.1002/we.2413

Shah, J. (2016). *Optimizing energy production: Addressing rotor wakes at wind farms.* Retrieved August 11, 2016, from https://www.windpowerengineering.com/optimizing-energy-production-addressing-rotor-wakes-wind-farms/

Shahan, Z. (2014). *Renewable energy world.* Retrieved April 25, 2022, from https://www.renewableenergyworld.com/storage/history-of-wind-turbines/#gref

Simisiroglou, N., Polatidis, H., & Ivanell, S. (2019). Wind farm power production assessment: Introduction of a new actuator disc method and comparison with existing models in the context of a case study. *Applied Sciences*, *9*(3). https://doi.org/10.3390/app9030431

Sivanandan, H. (2021). *Numerical study on the impact of self induced gravity waves on offshore wind farms* (Master's thesis). Delft University of Technology. Delft, The Netherlands.

Sommer, A. Ø. (2021). *A numerical study of blockage effects in wind farms for different atmospheric conditions* (Master's thesis). Technical University of Denmark. Roskilde, Denmark.

Stergiannis, N., Lacor, C., Beeck, J. V., & Donnelly, R. (2016). CFD modelling approaches against single wind turbine wake measurements using RANS. *Journal of Physics: Conference Series*, *753*, 032062. https://doi.org/10.1088/1742-6596/753/3/032062

Stull, R. (2011). Meteorology for scientists & engineers. *3*, 938. https://www.eoas.ubc.ca/books/Practical_Meteorology/

Troldborg, N., & Meyer Forsting, A. (2017). A simple model of the wind turbine induction zone derived from numerical simulations. *Wind Energy*, *20*(12), 2011–2020. https://doi.org/10.1002/we.2137

van der Laan, M. P., Sørensen, N. N., Réthoré, P.-E., Mann, J., Kelly, M. C., & Troldborg, N. (2015). The k- -fp model applied to double wind turbine wakes using different actuator disk force methods. *Wind Energy*, *18*(12), 2223–2240. https://doi.org/https://doi.org/10.1002/we.1816

Venditti, B. (2022). *Animation: The world's biggest wind turbines.* https://www.visualcapitalist.com/visualizing-the-worlds-biggest-wind-turbines/ (accessed: 06.09.2022)

Wagner, H.-J. (2013). Introduction to wind energy systems. *EPJ Web of Conferences*, *54*, 01011–. https://doi.org/10.1051/epjconf/20135401011

Wu, K. L., & Porté-Agel, F. (2017). Flow adjustment inside and around large finite-size wind farms. *Energies*, *10*(12). https://doi.org/10.3390/en10122164

Yan, B. W., Li, Q. S., He, Y. C., & Chan, P. W. (2016). Rans simulation of neutral atmospheric boundary layer flows over complex terrain by proper imposition of boundary conditions and modification on the k- model. *Environmental Fluid Mechanics*, *16*. https://doi.org/10.1007/s10652-015-9408-1

Zaaijer, M., & Viré, A. (2020). Introduction to wind turbines: Physics and technology.

Zhang, X. (2009). Cfd simulations of neutral abl flows.

A

Additional results

A.1. Domain height simulations

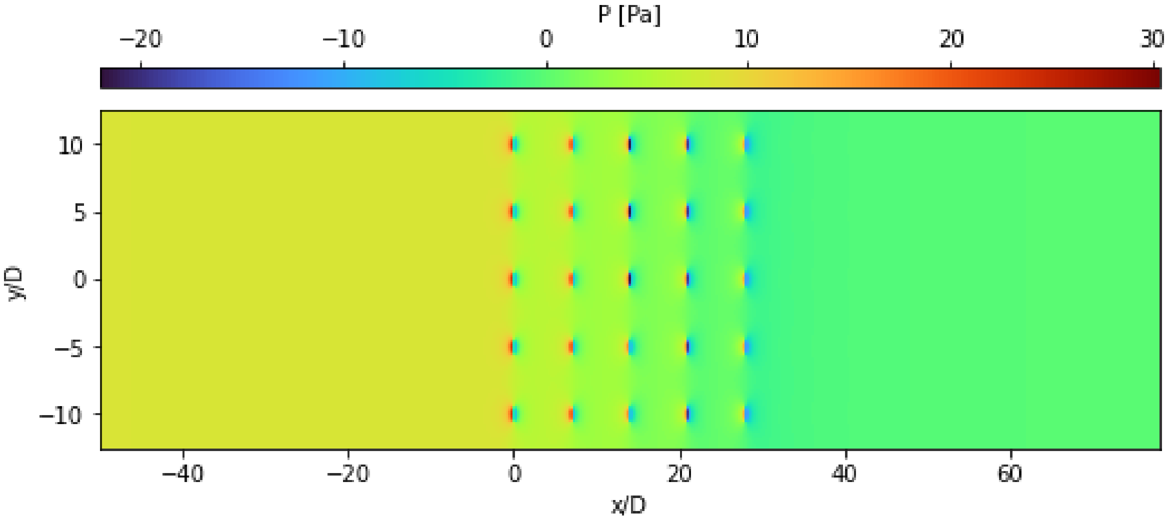

Figure A.1: Pressure at hub height for dh-5.

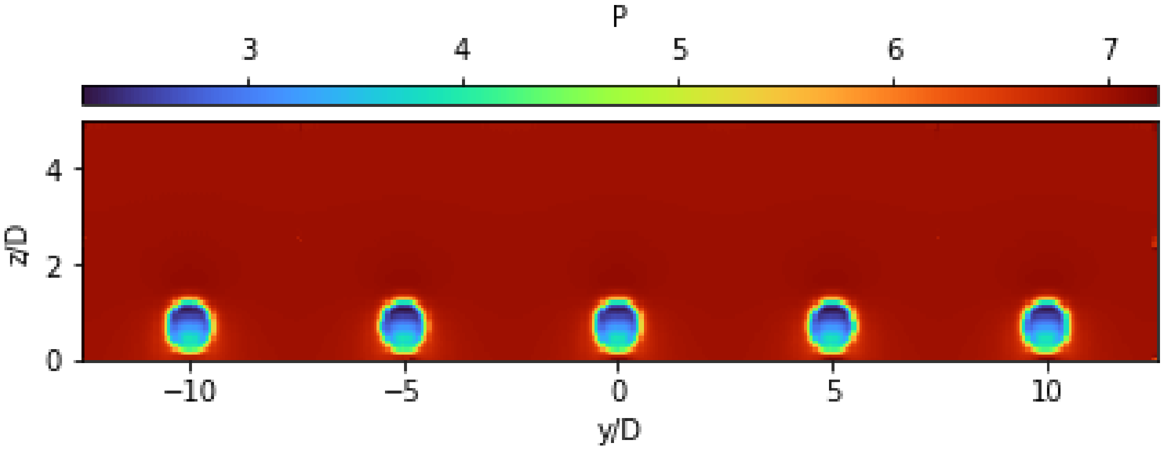

Figure A.2: Pressure at first row of turbines for dh-5.

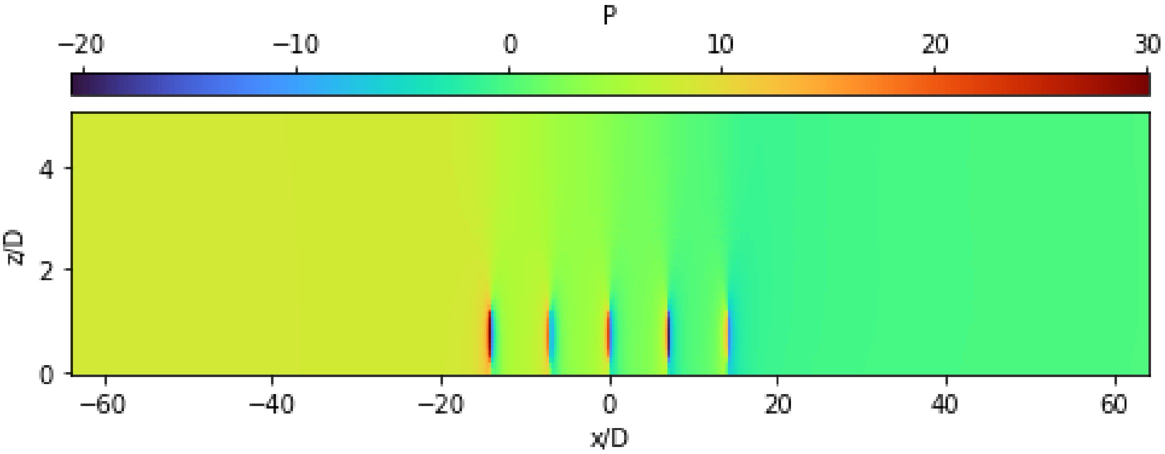

Figure A.3: Pressure through center column of turbines for dh-5.

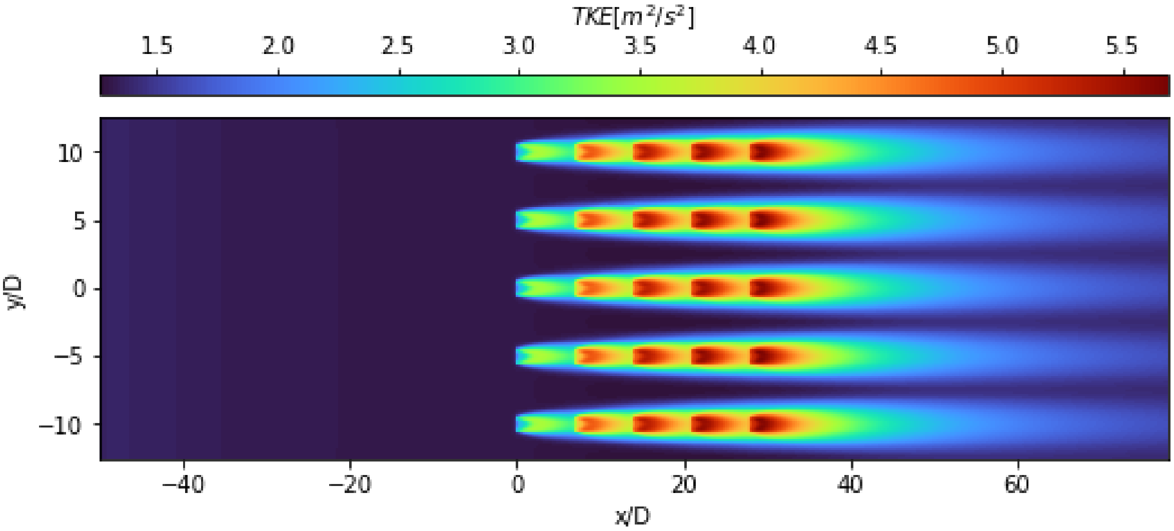

Figure A.4: TKE at hub height for dh-5.

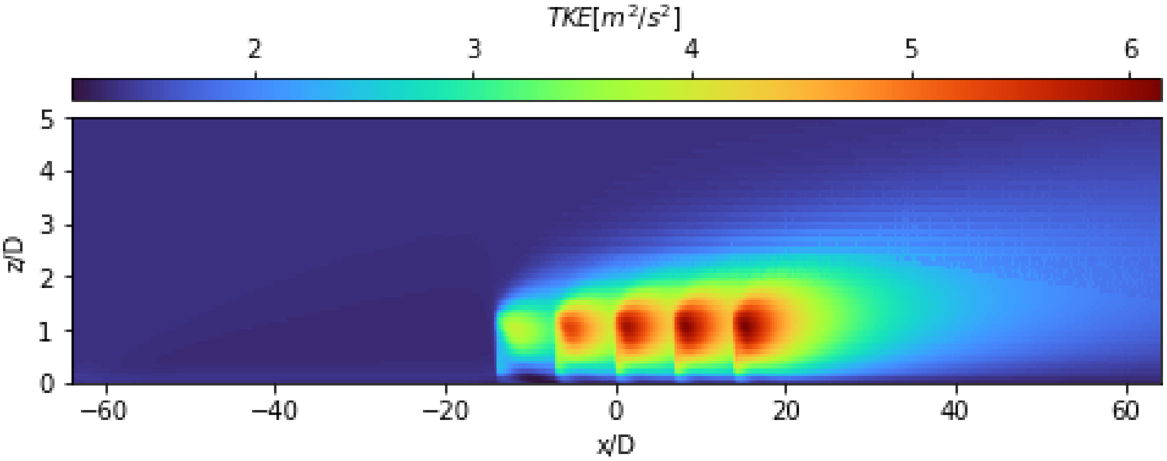

Figure A.5: TKE through center column of turbines for dh-25.

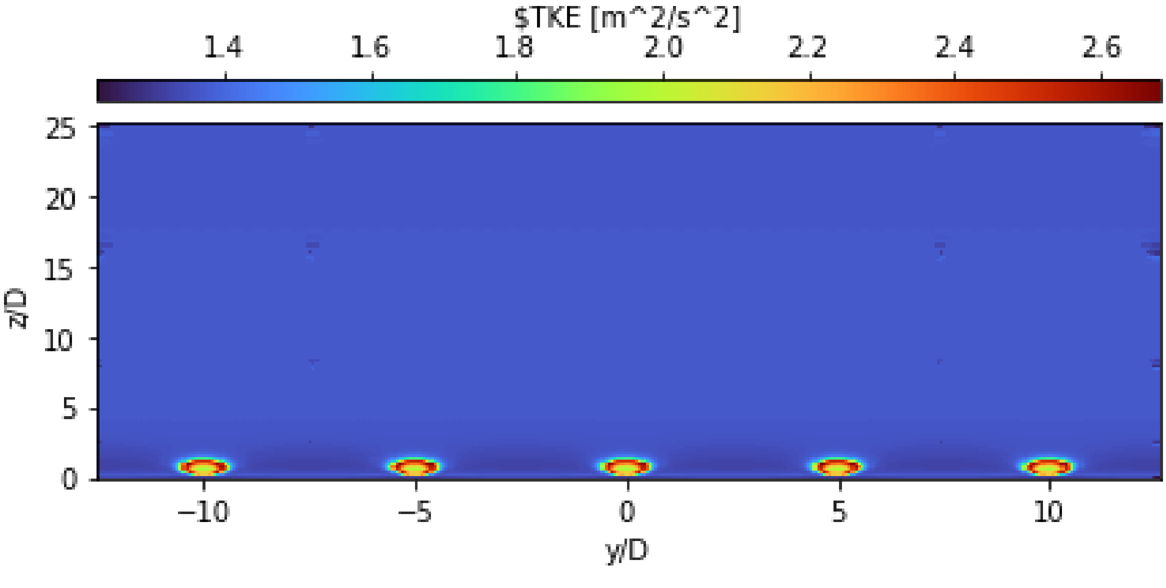

Figure A.6: TKE at first row of turbines for dh-25.

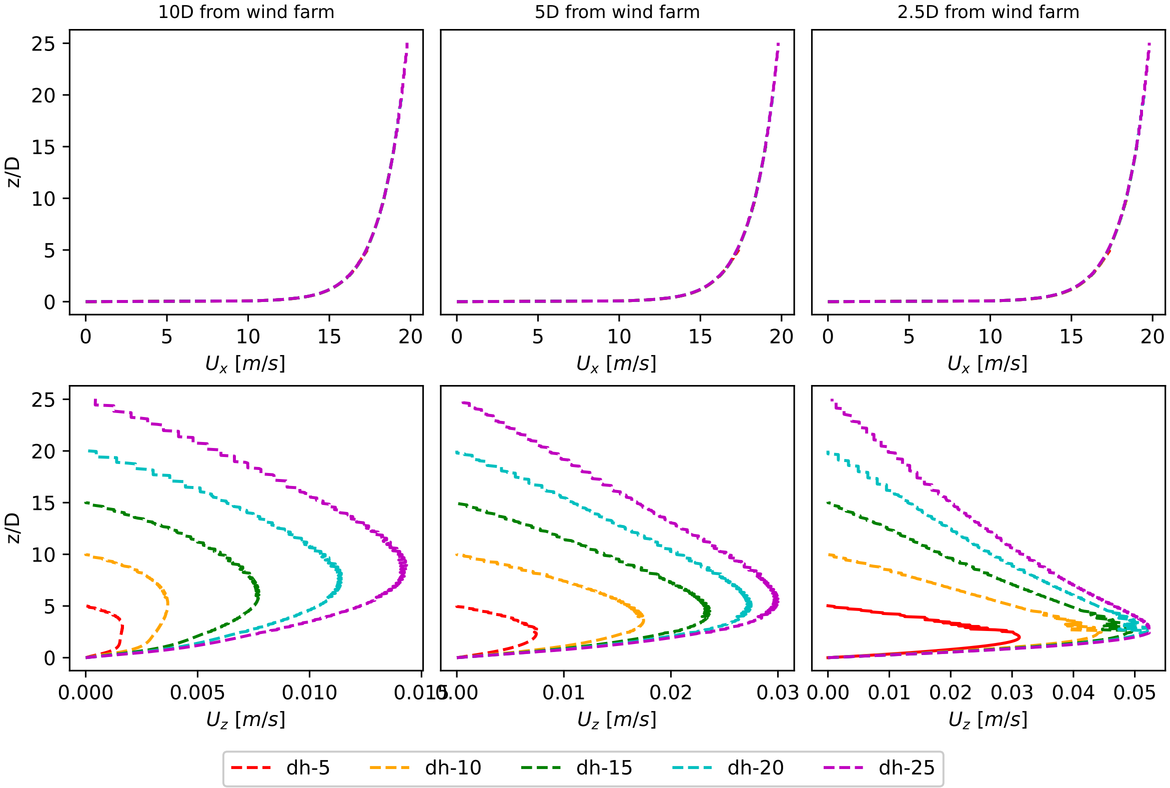

Figure A.7: U_x and U_z upstream of center column of turbines for domain heights.

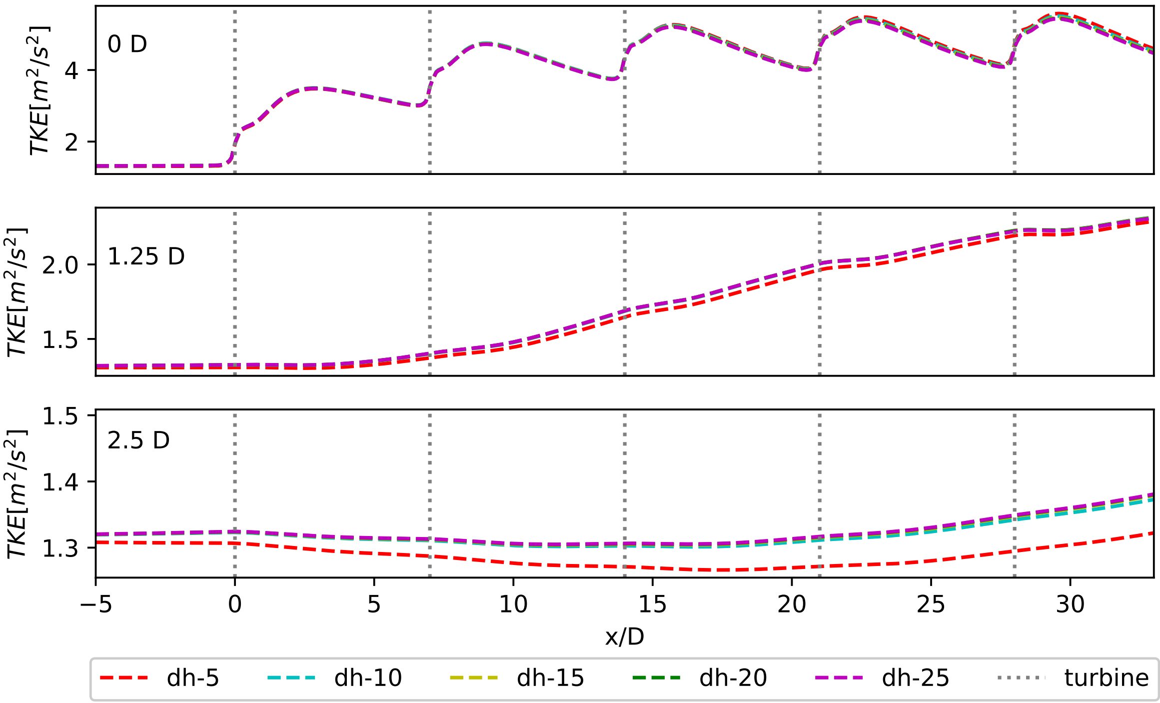

Figure A.8: TKE at sample locations between turbine columns given by labels

A.2. Lateral extent simulations

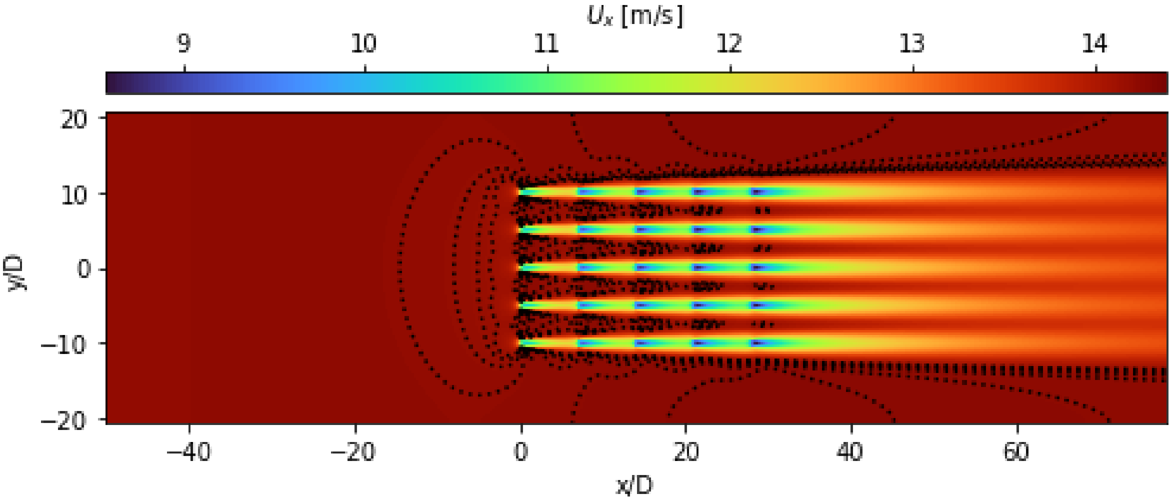

Figure A.9: U_x at hub height for le-10 and contour lines in increments of 0.025 m/s

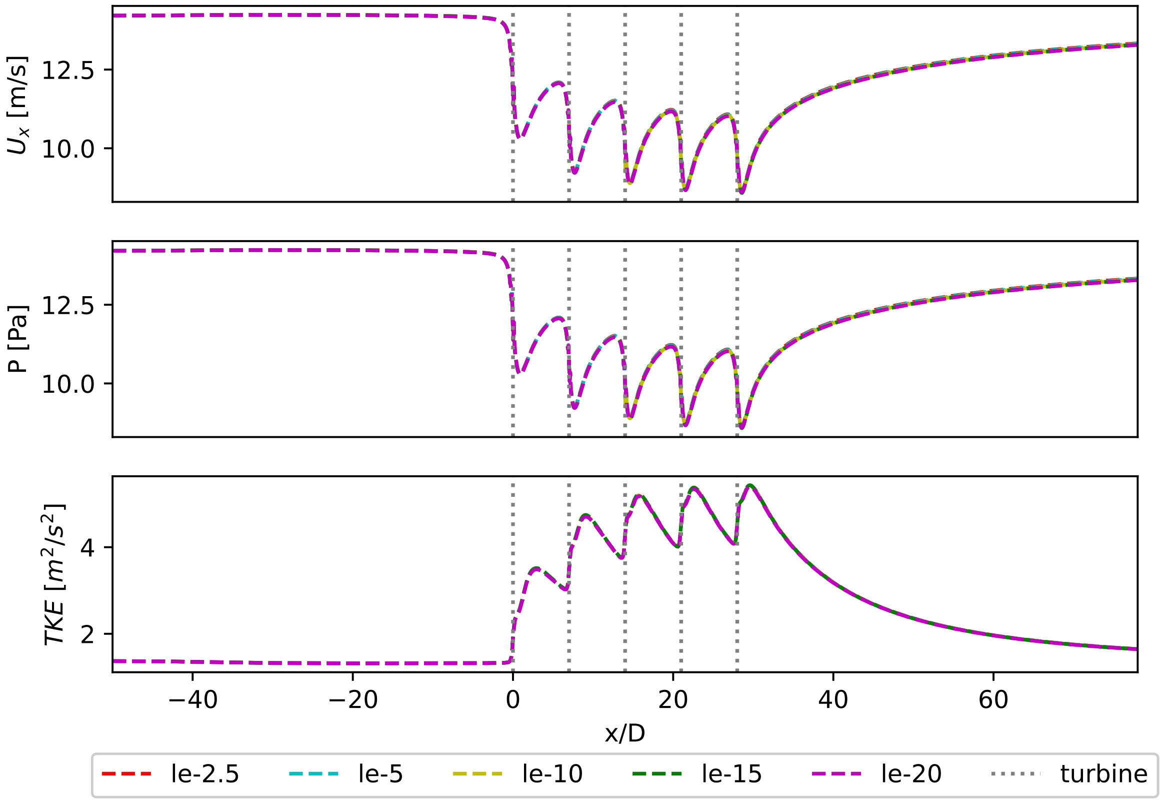

Figure A.10: U_x, pressure, and TKE at hub height for lateral extent simulations through center turbine for lateral extent simulations

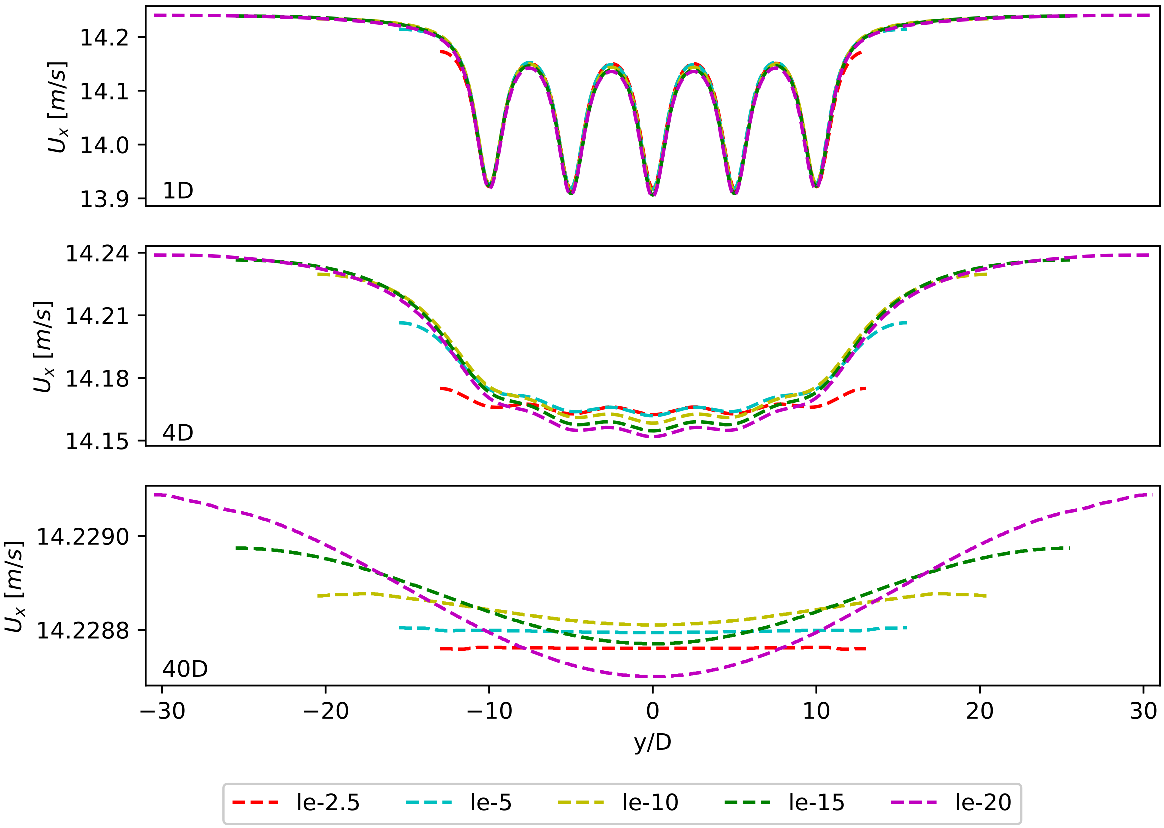

Figure A.11: U_x at hub height and at various distances upstream for lateral extent simulations.

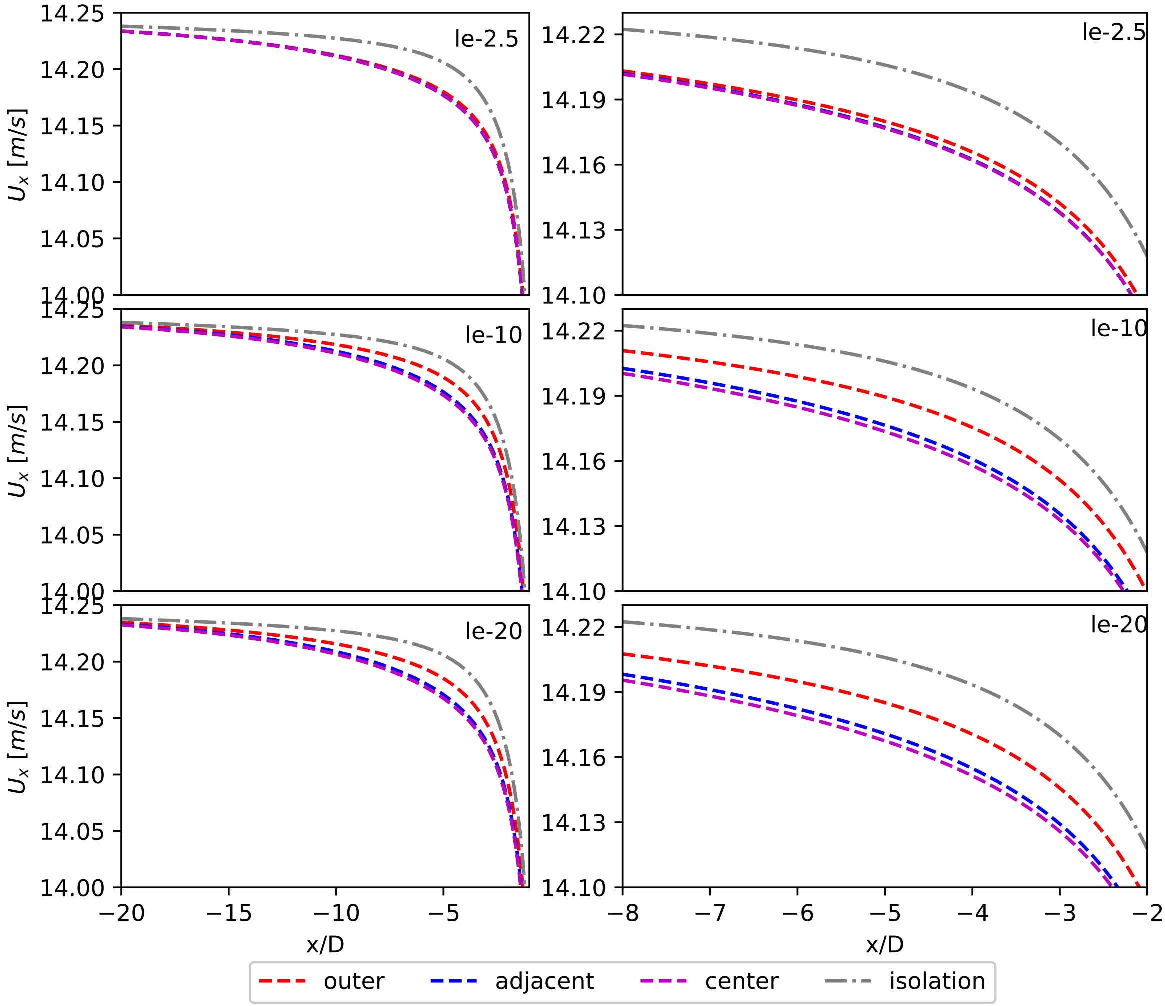

Figure A.12: U_x at hub height at center, adjacent, and outer column of turbines upstream of finite wind farm.

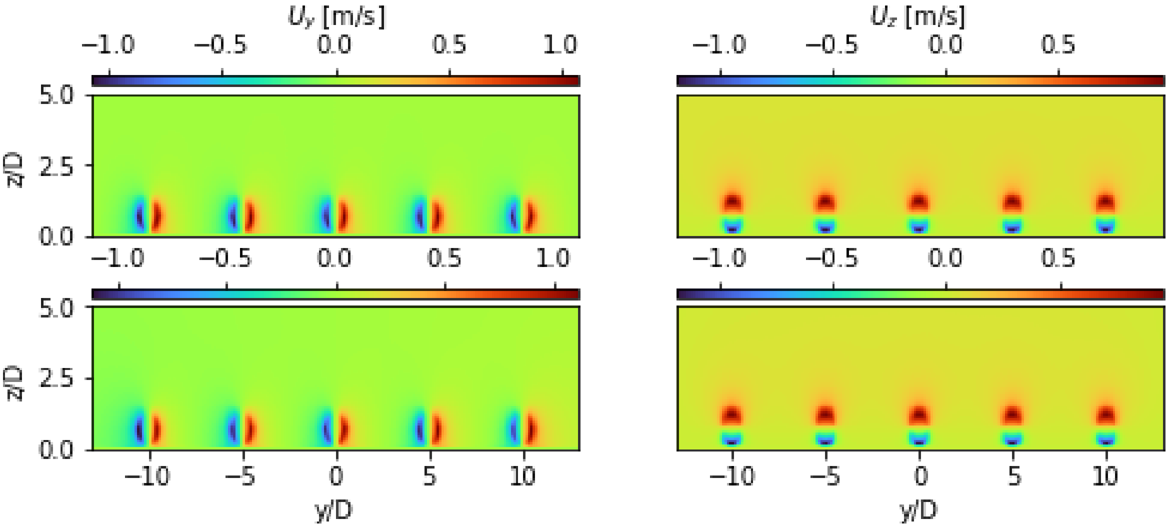

Figure A.13: U_y and U_z at the first row of turbines for a le-2.5 lateral extent (top figures) and le-20 lateral extent (bottom figures). Figures are zoomed into the width of the wind farm and from the ground to 5D in the vertical direction.

A.3. Inlet distance simulations

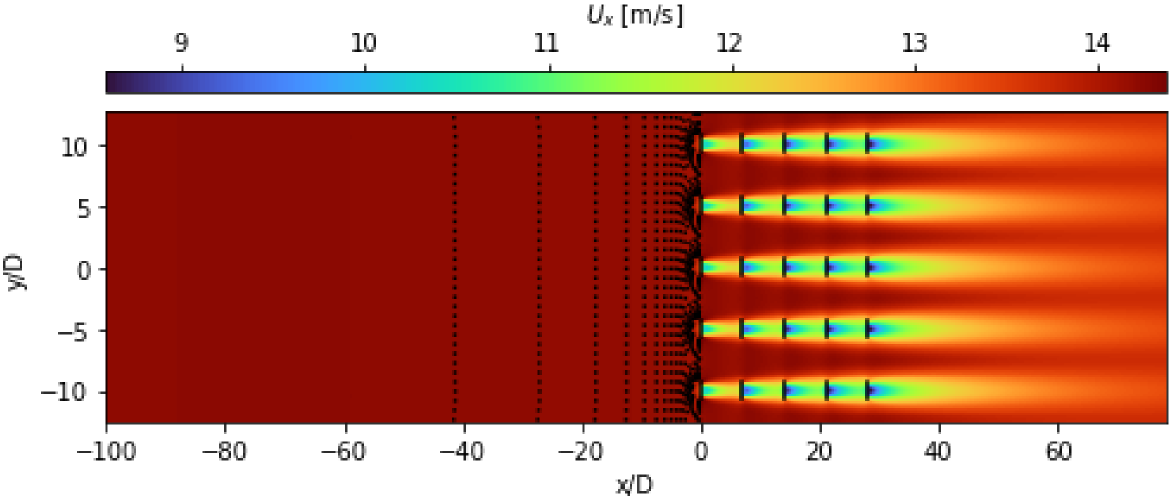

Figure A.14: U_x at hub height for up-100 inlet distance simulation.

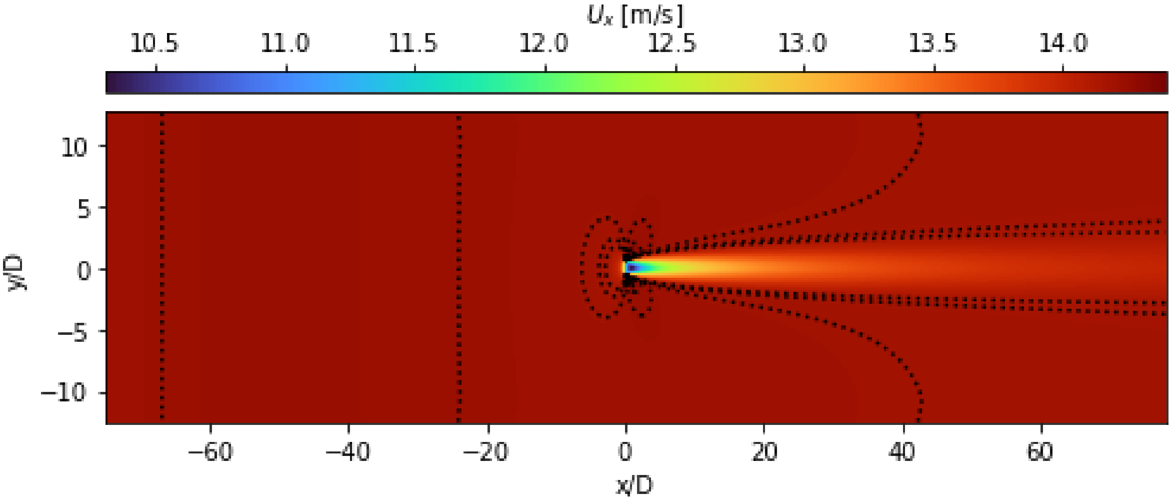

Figure A.15: U_x for turbine operating in isolation for up-100 domain size.

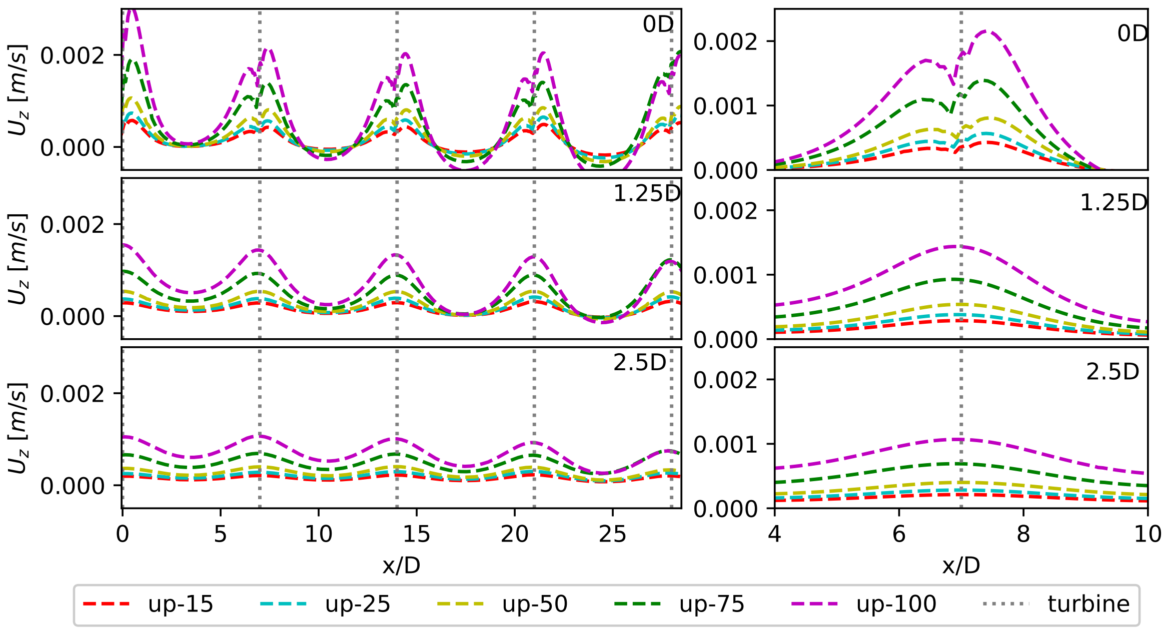

Figure A.16: U_z between columns of turbines for inlet distance simulations. Sample points consistent with figure 4.25.

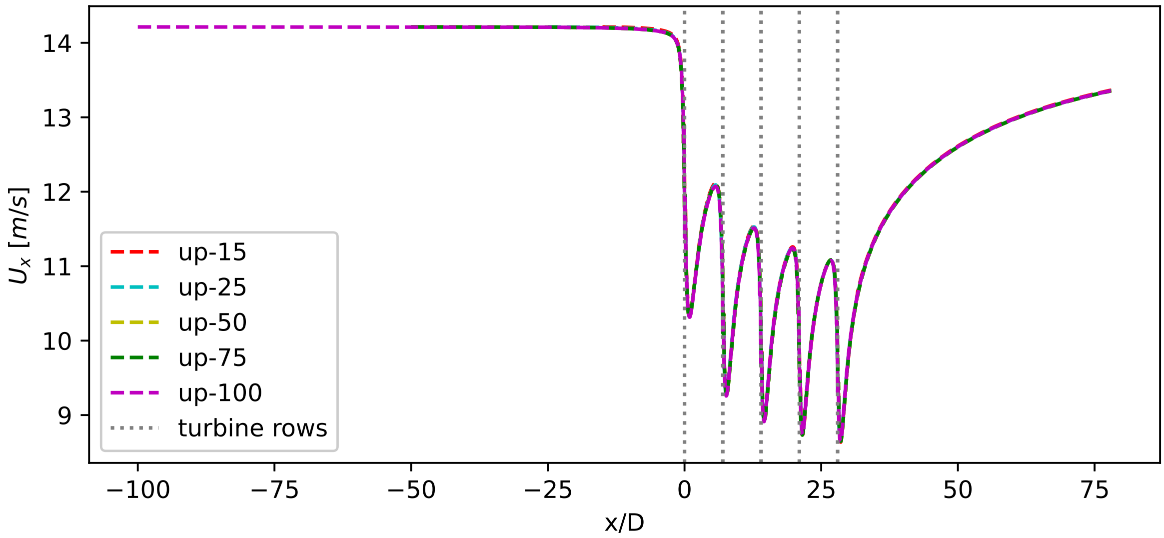

Figure A.17: U_x at hub height through the fetch for inlet distance simulations

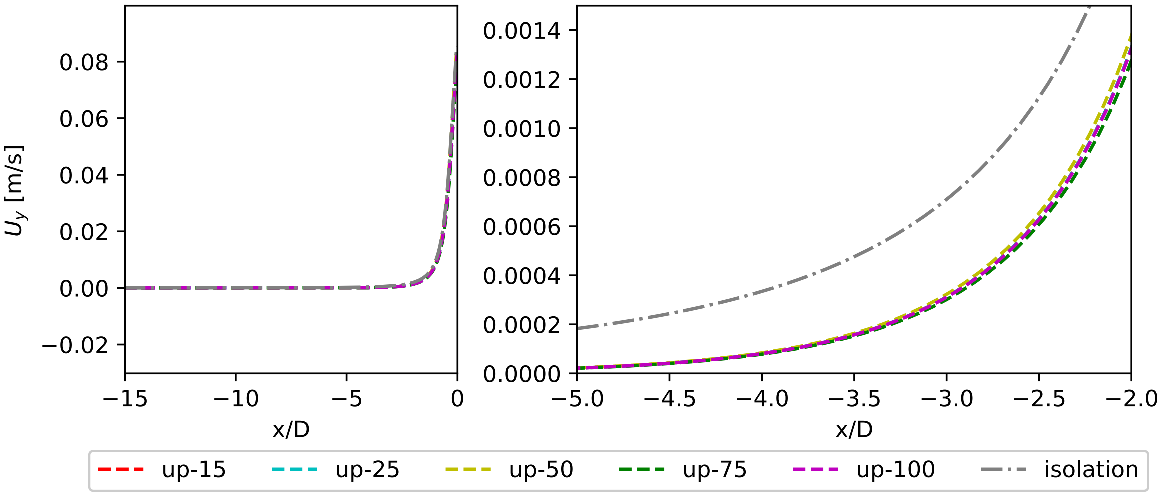

Figure A.18: U_y at hub height approaching wind farm for inlet distance simulations

A.4. Outlet distance simulations

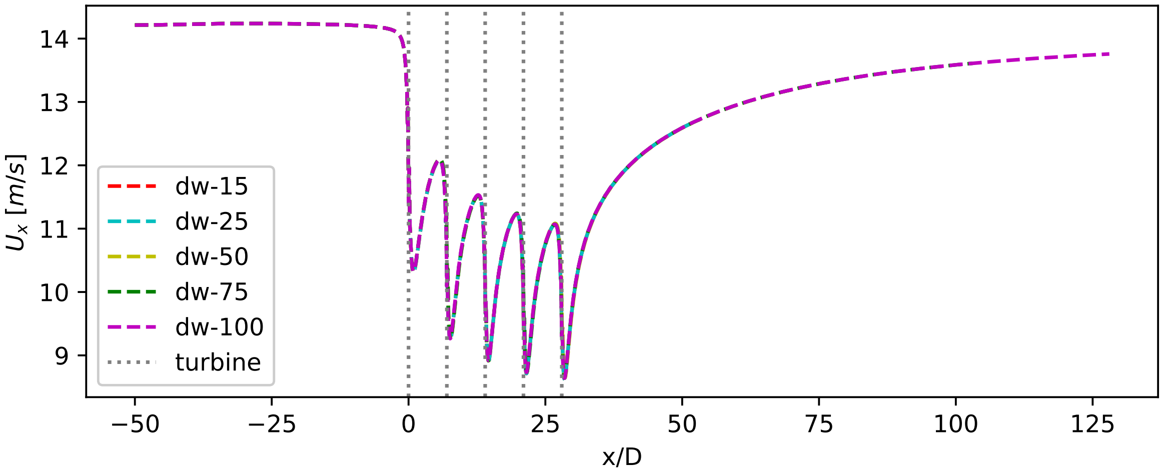

Figure A.19: U_x through center row of turbines at hub height for all turbine simulations.

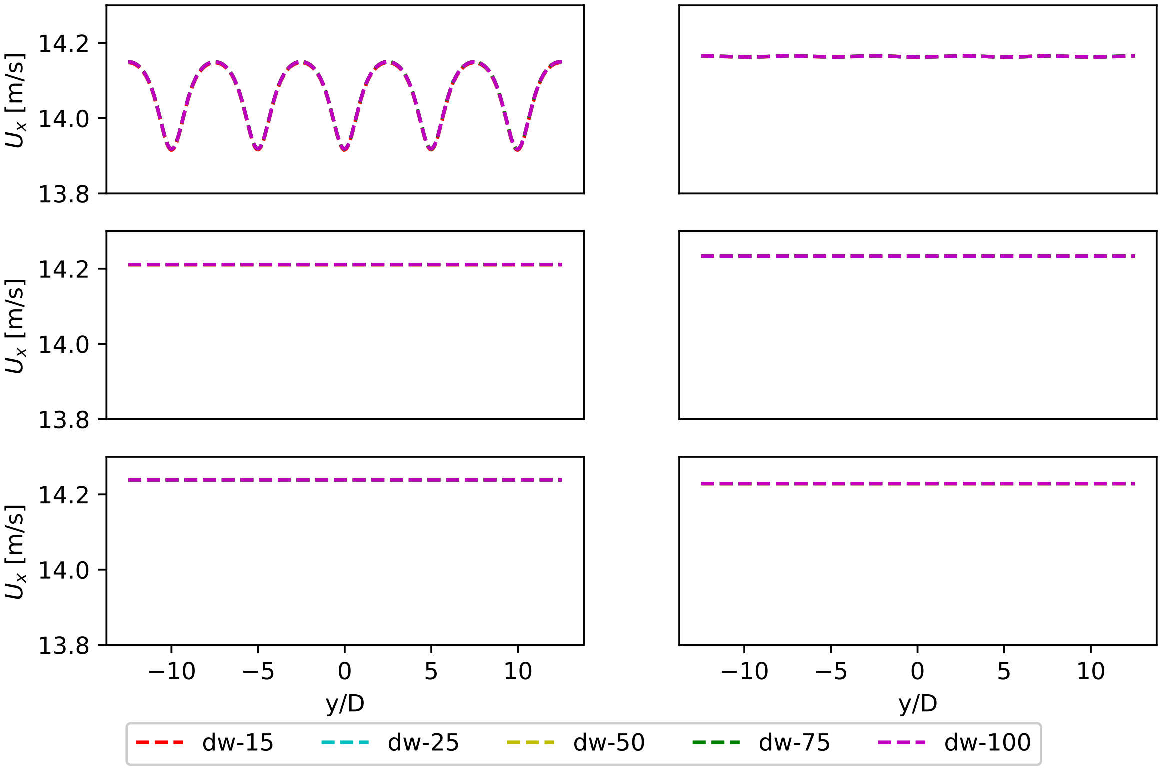

Figure A.20: U_x at locations upstream of wind farm. From left to right, top to bottom: 1D, 4D, 10D, 20D, 40D.